

10-27-2022

LC-MS Screening Assay for Abused Drug Exposure Based on Covalent Peptide/Protein Modification

Ludmyla Santos Tavares
ltava009@fiu.edu

Follow this and additional works at: <https://digitalcommons.fiu.edu/etd>



Part of the [Analytical Chemistry Commons](#), and the [Toxicology Commons](#)

Recommended Citation

Santos Tavares, Ludmyla, "LC-MS Screening Assay for Abused Drug Exposure Based on Covalent Peptide/Protein Modification" (2022). *FIU Electronic Theses and Dissertations*. 5177.
<https://digitalcommons.fiu.edu/etd/5177>

This work is brought to you for free and open access by the University Graduate School at FIU Digital Commons. It has been accepted for inclusion in FIU Electronic Theses and Dissertations by an authorized administrator of FIU Digital Commons. For more information, please contact dcc@fiu.edu.

FLORIDA INTERNATIONAL UNIVERSITY

Miami, Florida

LC-MS SCREENING ASSAY FOR ABUSED DRUG EXPOSURE BASED ON
COVALENT PEPTIDE/PROTEIN MODIFICATION

A dissertation submitted in partial fulfillment of

the requirements for the degree of

DOCTOR OF PHILOSOPHY

in

CHEMISTRY

by

Ludmyla Santos Tavares

2022

To: Dean Michael R. Heithaus
College of Arts, Sciences and Education

This dissertation, written by Ludmyla Santos Tavares, and entitled LC-MS Screening Assay for Abused Drug Exposure Based on Covalent Peptide/Protein Modification, having been approved in respect to style and intellectual content, is referred to you for judgment.

We have read this dissertation and recommend that it be approved.

Jose Almirall

David Becker

De Etta Kay Mills

Kevin O'Shea

Anthony De Caprio, Major Professor

Date of Defense: October 27, 2022

The dissertation of Ludmyla Santos Tavares is approved.

Dean Michael R. Heithaus
College of Arts, Sciences and Education

Andrés G. Gil
Vice President for Research and Economic Development
and Dean of the University Graduate School

Florida International University, 2022

© Copyright 2022 by Ludmyla Santos Tavares

All rights reserved by the author with the exception of Figures 2, 3, 6 and 7.

These figures have been included with the permission of the respective
publishers.

DEDICATION

This dissertation is dedicated to my parents, Enes and Rosângela, who have been there for me every step of the way and have always encouraged me to pursue my dreams no matter what. Your love has meant the world to me, and I will be eternally grateful to you.

ACKNOLEGMENTS

First, I would like to acknowledge my advisor, Dr. Anthony DeCaprio, for being my research advisor and welcoming me in his laboratory. I would like to also thank Dr. José Almirall, Dr. David Becker, Dr. De Etta Kay Mills and Dr. Kevin O'Shea for serving as my committee members. I appreciate your constructive criticism, feedback, and words of advice in helping me to become a better scientist. Thank you to Dr. Christopher Dares and Jeffrey McLachlan for all your help with my electrochemistry experiments and data analysis. Thank you, Dr. Anamary Tarifa, for your guidance and assistance during instrumentation roadblocks and all your words of encouragement.

I would like to thank the National Institute of Justice (NIJ) for funding my research and for covering my travel expenses to national conferences. I would also like to thank the Department of Chemistry and University Graduate School at Florida International University for funding provided through a teaching assistantship at the beginning of my Ph.D. studies.

I especial thank you to my father Enes, my mother Rosângela and my brother Vitor. You have supported me from the very beginning and helped me in the process of coming to the United States to do my Ph.D. I would not have gone this far without all your help and love. Thank you, Danny, for becoming my family away from home, for always being a supporting partner, and the love of my life.

I have to thank my friends Higor Moraes and Natália Moura who have started this academic journey with me more than 10 years ago. For still being our “biscoito, caramelo e chocolate” and for our three-way video chats that always

made my days. I huge thank you to Phuong Pham that has been my rock, the best roommate I could possibly have and a great friend. Thank you for all the gossip over the dinner table, for listening to all my venting about graduate school difficulties and thank you for keeping me sane. Thank you to Lilian Valadares for being my little piece of Brazil in Miami and for being an amazing friend. I big thank you to T.J. Dickson and Dr. Justin Carmel for being there for me and always inviting me to spend Thanksgiving in their home.

And finally, I would like to thank my lab-mates past and present. First, I would like to thank Dr. R. Allen Gilliland and Dr. Jenna Chenevert Aijala for welcoming me to the lab and helping me start my Ph.D. career. A big thank you to William Morrison for being by my side since the start, for being a great friend and fellow project mate. Thank you for all your insight, for talking over scientific ideas with me and pushing me to be a better researcher. Thank you to Meena Swaminathan for being there for me when I needed help, had concerns, and to discuss ideas. Also thank you for being my Zumba and workout companion. Lastly, thank you to Brianna Spear, Rebecca Smith, Leonardo Maya, and Kaylyn Keith for sharing the lab with me and listening to all my presentations.

ABSTRACT OF THE DISSERTATION
LC-MS SCREENING ASSAY FOR ABUSED DRUG EXPOSURE BASED ON
COVALENT PEPTIDE/PROTEIN MODIFICATION

by

Ludmyla Santos Tavares

Florida International University, 2022

Miami, Florida

Professor Anthony DeCaprio, Major Professor

In vitro metabolic assays are commonly used in forensic toxicology to assess the extent and rate of drug metabolism and to identify specific metabolites formed. Available *in vitro* systems include synthetic metalloporphyrins, HLM assays, and electrochemical assays. These assays also have utility in identifying reactive metabolites when a nucleophilic trapping molecule is included. While enzyme-based assays are widely employed for drug metabolite generation in forensic toxicology, alternative *in vitro* systems have not been extensively tested for identification of stable (SM) and reactive (RM) metabolites of drugs of abuse. The capability of reactive drug metabolites to form adducts with glutathione and a specific β -Hb tryptic peptide containing a highly reactive nucleophilic thiol moiety (i.e., GTFATLSELH⁹³CDK; β ⁹³Cys peptide) was also investigated.

Covalent binding of drugs to proteins and/or peptides is an alternative to hair analysis for long-term or retrospective assessment of drug abuse or exposure. Identification of such peptide or protein modifications (i.e., adducts) can offer

valuable information about exposure history. Protein adducts have the potential to survive throughout the life of the protein (e.g., 120 days in the case of human hemoglobin).

In this project, the comparison of the three *in vitro* assays systems revealed that the metabolites obtained exhibited a few common derivatives but also compounds unique to each system. In addition, major reported *in vivo* metabolites for each drug were also found with all three *in vitro* systems, *i.e.*, NAPQI, MDA, amphetamine, and 11-COOH-THC from acetaminophen, methamphetamine, MDMA, and Δ^9 -THC, respectively. The electrochemical oxidation and synthetic metalloporphyrin systems appeared to generate a wider variety of metabolites than encountered with human liver microsomes, including stable and potentially reactive derivatives such as HFA, HPA, an imine derivative, 11-CHO-THC, and methylidene-THC. These results indicate that use of all three *in vitro* systems may provide a more complete profile of potential Phase I oxidative SM and RM for a variety of drugs of abuse that may be targeted for analysis in forensic toxicological studies and that may reveal possible adduct forming species.

Results of the *in vitro* trapping assay studies with GSH and the $\beta^{93}\text{Cys}$ peptide demonstrated that the EC assay can be employed in the generation and trapping of RM by peptides containing reactive thiol moieties. The ability of abused drugs and/or metabolites to covalently modify the β -Hb peptide containing the reactive ^{93}Cys suggests that such modifications could be monitored as an alternative to clinical and forensic hair analysis and could be usefully applied in areas of drug testing and forensic toxicological analysis.

TABLE OF CONTENTS

CHAPTER	PAGE
1. INTRODUCTION.....	1
1.1. Statement of the Problem.....	1
1.2. Significance of Study.....	2
1.2.1. Task 1 – Generation and identification of SM and RM of selected drugs: 3	
1.2.2. Task 2 – Assessment of adduction potential of drug RM with model peptides:	3
1.2.3. Task 3 – Development of a predicted MRM assay for routine peptide adduct screening:	4
2. LITERATURE REVIEW.....	4
2.1. Drugs of abuse.....	4
2.2. Drug metabolism	7
2.3. <i>In vitro</i> metabolism assays.....	10
2.4. <i>In silico</i> prediction of drug metabolism	17
2.5. Retrospective monitoring of drug use or exposure.....	19
2.5.1. Hair analysis.....	20
2.5.2. Drug protein/peptide adduction	21
2.6. Liquid Chromatography - Mass Spectrometry	26
2.7. LC-MS protein and peptide analysis.....	30
2.8. Research objectives.....	32
3. METHODOLOGY.....	32
3.1. Instrumentation	33
3.2. Drug selection	34
3.3. Chemicals and reagents.....	34
3.4. HLM assay	35
3.4.1. Generation of drug metabolites.....	35
3.4.2. Adduction to selected peptides	37
3.5. Synthetic metalloporphyrins assay	38
3.6. Electrochemical assay.....	40
3.6.1. Optimization of EC assay.....	40
3.6.2. Generation of drug metabolites.....	40
3.6.3. Adduction to selected peptides	42
3.7. <i>In silico</i> methods	42
3.8. LC-QqQ-MS dMRM analysis.....	43
3.9. Peptide adducts analysis.....	44
4. RESULTS AND DISCUSSION.....	45
4.1. Task 1 – Generation of drug metabolites	45

4.1.1.	<i>In silico</i> generation of drug metabolites:.....	45
4.1.2.	Optimization of the synthetic MP assay:	47
4.1.3.	Optimization of EC assay:.....	50
4.1.4.	Full Scan MS analysis of the obtained metabolites:.....	51
4.1.5.	Targeted MS/MS analysis of the obtained metabolites	57
4.2.	Task 2 – Assessment of adduct potential with peptides	82
4.2.1.	GSH adduction studies	83
4.2.2.	Preliminary IAM adduction study.....	87
4.2.3.	Targeted MS/MS analysis of the drug-peptide adducts.....	88
4.3.	Task 3 – Development of an MRM method for adducted peptide screening	98
SUMMARY AND PROSPECT		101
REFERENCES		104
APPENDICES		113
VITA		128

LIST OF TABLES

TABLE	PAGE
Table 1: Drug schedule and their descriptions.....	6
Table 2: Drugs selected for this study.	7
Table 3: Metabolite found with APAP for each assay.	57
Table 4: Metabolites found with MDMA for each system.....	60
Table 5: Metabolites found with METH for each assay.....	67
Table 6: Metabolites found with THC for three assays.	74
Table 7: Summary table of the MS/MS data collected for glutathione adducts obtained with the HLM assay.....	83
Table 8: Summary table of the MS/MS data collected for GSH adducts obtained with the EC assay.	84
Table 9: MS/MS results for HLM metabolism of APAP, cocaine, and MDMA.....	89
Table 10: MS/MS data for Hb $\beta^{93}\text{Cys}$ peptide adducts observed with the EC oxidation of APAP, cocaine, and THC.	93
Table 11: MRM data for Hb $\beta^{93}\text{Cys}$ peptide adducts observed with the electrochemical oxidation of APAP, MDMA, and THC.....	99

LIST OF FIGURES

FIGURE	PAGE
Figure 1: Catalytic cycle of dioxygen activation by cytochrome P450.....	10
Figure 2: Synthetic metalloporphyrin derived from cytochrome P450 active site. ³⁷	14
Figure 3: Schematic representation of a three-electrode EC cell for cyclic voltammetry experiments. ⁴⁰	16
Figure 4: Typical window of detection of drugs and their metabolites in blood, urine, and hair.....	19
Figure 5: Chemical structure of the porphyrin ring system of heme b complex of Hb.	23
Figure 6: ESI ionization source, adapted from NHMFL. ⁷⁰	27
Figure 7: Schematic representation of the 6530 Q-TOF mass analyzer from © Agilent Technologies, Inc. ⁷²	29
Figure 8: Peptide fragmentation patterns labeled with the common “a,b,c” and “x,y,z”	31
Figure 9: Structures and exact mass of drugs under study.	34
Figure 10: Schematic representation of the sample preparation via liver microsomes metabolic assay.....	36
Figure 11: Schematic representation of the sample preparation via synthetic metalloporphyrin catalysts.	39
Figure 12: Schematic representation of the bulk electrolysis performed for the generation of metabolites via EC assay.	42
Figure 13: Flowchart of workflow for Hb $\beta^{93}\text{Cys}$ peptide adduct analysis.	44
Figure 14: MetaSite liver metabolism prediction for THC.	46
Figure 15: MetaSite liver metabolism prediction for MDMA.....	46
Figure 16: FIA QTOF-MS full scan spectrum of the BMO screening kit for a) APAP; b) MDMA; c) METH; and d) THC.	48

Figure 17: Proposed chemical structures of the four novel metabolites found with the screening BMO kit with the aid of MetaSite software predictions.	49
Figure 18: Cyclic voltammogram of APAP, using glassy carbon as the WE, calomel standard as the RE, and Pt/Ti rod as the CE.	50
Figure 19: XIC spectra for NAPQI obtained with the three methods.....	52
Figure 20: XIC spectra for HHMA obtained with the three methods.	53
Figure 21: XIC spectra for MDA obtained with the three methods.....	53
Figure 22: XIC spectra for AMP obtained with the three methods.	54
Figure 23: XIC spectra for methcathinone obtained with the HLM assay and synthetic metalloporphyrin catalysts.	55
Figure 24: XIC spectra for 11-COOH-THC obtained with the three methods.	56
Figure 25: XIC spectra for 11-CHO-THC obtained with the three methods.	56
Figure 26: LC-QTOF-MS/MS spectra for the peaks of interest observed for the APAP metabolite NAPQI, obtained with a) HLM assay; b) EC assay; c) synthetic MP catalysts; d) fragmentation pattern for NAPQI.....	58
Figure 27: Reaction scheme of the EC oxidation of APAP to NAPQI.	58
Figure 28: Reaction scheme of the EC redox transformation of MDMA to generate HHMA.....	61
Figure 29: LC-QTOF-MS/MS spectra for the peaks of interest observed for the MDMA metabolite HHMA, obtained with a) HLM assay; b) EC assay; c) synthetic MP catalysts; d) fragmentation pattern for HHMA.	62
Figure 30: Reaction scheme of the EC redox transformation of MDMA to generate MDA.	62
Figure 31: LC-QTOF-MS/MS spectra for the peaks of interest observed for the MDMA metabolite MDA, obtained with a) HLM assay; b) EC assay; c) synthetic MP catalysts; d) fragmentation pattern for MDA.	63
Figure 32: Reaction scheme of the EC redox transformation of MDMA to generate HFA.	64

Figure 33: LC-QTOF-MS/MS spectra for the peaks of interest observed for the MDMA metabolite HFA, obtained with a) HLM assay; b) EC assay; c) synthetic MP catalysts; d) fragmentation pattern for HFA.....	64
Figure 34: LC-QTOF-MS/MS spectra observed for the MDMA metabolites: a) HHA formed with the HLM assay, c) a quinone derivative formed with the EC oxidation, e) HPA formed with the synthetic MP. The proposed fragmentation pattern for each metabolite is also shown, b) HHA, d) quinone derivative, and f) HPA.....	65
Figure 35: Reaction scheme of the EC redox transformation of MDA to generate the quinone derivative.	66
Figure 36: Reaction scheme of the EC redox transformation of METH to generate the AMP.....	68
Figure 37: LC-QTOF-MS/MS spectra for the peaks of interest observed for the METH metabolite AMP, obtained with a) HLM assay; b) EC assay; c) synthetic metalloporphyrin catalysts; d) fragmentation pattern for AMP.	69
Figure 38: LC-QTOF-MS/MS spectra for the peaks of interest observed for the METH metabolite methcathinone, obtained with a) HLM assay; b) synthetic MP catalysts; c) fragmentation pattern for methcathinone.....	70
Figure 39: Reaction scheme of the EC redox transformation of METH to generate the N-OH-METH.....	70
Figure 40: LC-QTOF-MS/MS spectra for the peaks of interest observed for the METH metabolite N-OH-METH, obtained with a) HLM assay; b) EC assay; c) fragmentation pattern for N-OH-METH.....	71
Figure 41:LC-QTOF-MS/MS spectra observed for the METH metabolites: a) N-OH-AMP formed with the HLM assay; c) an imine derivative formed with the electrochemistry oxidation, e) p-OH-METH formed with the synthetic MP. The proposed fragmentation pattern for each metabolite is also shown, b) N-OH-AMP; d) imine derivative, and f) p-OH-METH.....	72
Figure 42: Reaction scheme of the EC redox transformation of METH to generate the imine derivative.....	73
Figure 43: Reaction scheme of the EC redox transformation of THC to generate 11-COOH-THC.....	75

Figure 44: LC-QTOF-MS/MS spectra for the peaks of interest observed for the THC metabolite 11-COOH-THC, obtained with a) HLM assay; b) EC assay; c) synthetic MP catalysts; d) fragmentation pattern for 11-COOH-THC.	76
Figure 45: Reaction scheme of the EC redox transformation of THC to generate 11-CHO-THC.....	77
Figure 46: LC-QTOF-MS/MS spectra for the peaks of interest observed for the THC metabolite 11-CHO-THC, obtained with a) HLM assay; b) EC assay; c) synthetic MP catalysts, d) fragmentation pattern for 11-CHO-THC.	77
Figure 47: Reaction scheme of the EC redox transformation of THC to generate methylidene-THC.	78
Figure 48: LC-QTOF-MS/MS spectra for the peaks of interest observed for the THC metabolite methylidene-THC, obtained with a) HLM assay; b) EC assay; c) synthetic MP catalysts; d) fragmentation pattern for methylidene-THC.	79
Figure 49: LC-QTOF-MS/MS spectra for the peaks of interest observed for the THC metabolite 11-OH-THC, obtained with a) HLM assay, b) EC synthetic MP catalysts, c) fragmentation pattern for 11-OH-THC.	80
Figure 50: Reaction scheme of the EC redox transformation of THC to generate 11-dihydroxy-THC.	80
Figure 51: LC-QTOF-MS/MS spectra for the peaks of interest observed for the THC metabolite 11-dihydroxy-THC, obtained with a) EC assay, b) EC synthetic MP catalysts, c) fragmentation pattern for 11-dihydroxy-THC.	81
Figure 52: MS/MS data for the APAP GSH adducts obtained with the EC assay. The data are shown at 10 eV (top), 20 eV (middle), and 40 eV (bottom). Arrows point to relevant peaks.	85
Figure 53: MS/MS data for the THC GSH adducts obtained with the EC assay. The data are shown at 10 eV (top), 20 eV (middle), and 40 eV (bottom). Arrows point to relevant peaks.	86
Figure 54: MS spectra of A) control and B) IAM adducted Hb $\beta^{93}\text{Cys}$ peptide. ...	88
Figure 55: QTOF MS/MS spectra of Hb $\beta^{93}\text{Cys}$ peptide modified by APAP obtained with the HLM trapping assay, A) Hb peptide + APAP + K, B) Hb peptide + NAPQI + OH + CH ₃ , and C) Hb peptide + 1,4-benzoquinone + OH. ...	90
Figure 56: QTOF MS/MS spectra of Hb $\beta^{93}\text{Cys}$ peptide modified by APAP obtained with the HLM trapping assay, A) Hb peptide + ecgonidine + CH ₃ , B)	

Hb peptide + HHA + H + CH₃, C) Hb peptide + Aminochrome + O + OH, D) Hb peptide + methcathinone. 91

Figure 57: QTOF MS/MS spectra of Hb β⁹³Cys peptide modified by APAP obtained with the EC trapping assay, A) Hb peptide + APAP, B) Hb peptide + APAP + OH, and C) Hb peptide + NAPQI. 94

Figure 58: QTOF MS/MS spectra of Hb β⁹³Cys peptide modified by COC, MDMA, METH and THC obtained with the EC trapping assay, A) Hb peptide + ecgonidine + CH₃, B) Hb peptide + MDMA, C) Hb peptide + benzoic acid + OH + CH₃ and D) Hb peptide + 11-CHO-THC + OH. 95

Figure 59: Licorice representation of Hb β⁹³Cys peptide generated with the Visual Molecular Dynamics (VMD) software..... 97

Figure 60: MRM spectra of Hb β⁹³Cys peptide modified by APAP (A-B), MDMA (B), and THC (D) obtained with the electrochemical trapping assay. 100

ABBREVIATIONS AND ACRONYMS

APAP	Acetaminophen
CE	Counter electrode
COC	Cocaine
CSA	Controlled Substances Act
CV	Cyclic voltammetry
CYP	Cytochrome P450 enzymes
Cys	Cysteine
DEA	Drug Enforcement Administration
EC	Electrochemical
ESI	Electrospray ionization
FIA	Flow injection analysis
G6P	Glucose-6-phosphate
G6PD	Glucose-6-phosphate dehydrogenase
GSH	Glutathione
Hb	Hemoglobin
HLM	Human liver microsomes
HRMS	High resolution mass spectrometry
IAM	Iodoacetamide
LC	Liquid chromatography

<i>m/z</i>	Mass-to-charge ratio
MDMA	Methylenedioxymethamphetamine
METH	Methamphetamine
MP	Metalloporphyrin
MRM	Multiple reaction monitoring
MS	Mass spectrometry
MS/MS	Tandem mass spectrometry
NADPH	β -nicotinamide adenine dinucleotide phosphate
NAPQI	N-acetyl-p-benzoquinone imine
RE	Reference electrode
RM	Reactive metabolites
SCE	Saturated calomel electrode
SM	Stable metabolites
PA	Pyrrolizidine alkaloids
QqQ	Triple quadrupole
QTOF	Quadrupole time-of-flight
THC	Δ^9 -tetrahydrocannabinol
TOF	Time-of-flight
VMD	Visual Molecular Dynamics
WE	Working electrode
XIC	Extracted ion chromatogram

1. INTRODUCTION

1.1. Statement of the Problem

The detection and confirmation of human exposure to drugs typically relies on the measurement of parent compounds or specific metabolites in blood, urine, or an alternative matrix.¹ This “biomonitoring” approach is widely employed for forensic toxicological applications and has been standardized for many xenobiotics.^{2, 3} However, except for highly lipophilic compounds, most drugs and their metabolites are cleared from these matrices within a week. As a result, blood or urine measurements alone generally cannot provide data on past episodic exposure, cumulative exposure, or time-dependent exposure profiles for drugs. Nevertheless, this kind of data may be critically important in forensic toxicology, such as evidence in drug facilitated crimes, measurement of drug compliance or abstinence in pain drug management, addiction rehabilitation programs, and probation/parole criminal justice situations.

Assessment of long term drug use or exposure is limited to analysis of hair nowadays, for which numerous methods and a large literature database exists.⁴⁻⁶ Although widely used for this purpose, hair analysis presents many challenges, such as external contamination, interindividual differences, and difficult processing.⁷ An alternative to hair analysis is the measurement of covalent binding of drugs to proteins and/or peptides, such as hemoglobin (Hb), and glutathione (GSH) to form drug-protein/peptide “adducts.” In the case of proteins, such modifications remain in the body for the lifetime of the molecule and can provide a much longer window of detection of exposure than is generally possible by direct

measurement of parent compound or a metabolite in blood.⁸ While often used in biomonitoring assessment for environmental and occupational chemicals, applications of protein adducts as markers of illicit drug exposure are virtually nonexistent.^{9, 10}

1.2. Significance of Study

The development of a robust protein adduct based biomarker assay for drugs of abuse could allow for exposure assessment of these compounds over a much longer detection window than is currently possible in blood while providing an alternative or complement to hair analysis. A longer window of detection for drugs of abuse is extremely important in forensic toxicology. For instance, analysis of these drugs can be used as evidence in drug facilitated crime cases or to identify individuals suspected of illicit synthesis of drugs. Research into the physiochemical properties, specificity, and mechanisms of drug-protein adduction could lead to the use of such adducts as measures of individual metabolic capacity or even as biomarkers of addiction. Consequently, this novel approach is anticipated to significantly benefit forensic science by providing additional tools for detecting compounds of forensic interest in biological specimens over longer periods of time.

In order to support development of protein adduct based biomarkers for drugs of abuse, preliminary studies are necessary to identify RM of such drugs and determine their ability to covalently modify potential target sites in relevant peptides and proteins. In addition, adducted peptide standards are needed for use in MS-based screening/confirmatory assays using this approach. For these purposes, *in vitro* metabolic trapping assays are ideal.

1.2.1. Task 1 – Generation and identification of SM and RM of selected drugs:

The first part of this study will be the identification and comparison of the stable and reactive metabolites formed by three different *in vitro* assay systems: 1) human liver microsomal (HLM) metabolic assay, 2) synthetic metalloporphyrin catalysts, and 3) electrochemical (EC) oxidation assay. While enzyme-based assays are widely employed for drug metabolite generation in forensic toxicology, alternative *in vitro* systems have not been extensively tested. Furthermore, no such direct comparison of all three approaches for investigating drug (licit or illicit) metabolism has previously been reported. The present study generates such data for acetaminophen, MDMA, methamphetamine and THC.

1.2.2. Task 2 – Assessment of adduction potential of drug RM with model peptides:

The capability of selected drugs of abuse to covalently adduct model peptides will be investigated by trapping the reactive metabolites generated using each method with nucleophilic thiol moieties present in GSH and the β -globin tryptic peptide containing the free thiol at the ^{93}Cys position (i.e., GTFATLSELH ^{93}Cys CDK; “Hb $\beta^{93}\text{Cys}$ peptide”). The instrumentation selected for this task is an LC-quadrupole-time of flight (Q-TOF) mass spectrometer operated in positive ESI targeted MS/MS mode. Mass spectral data will be collected, and MS/MS analysis will allow for the determination of the specific drug-peptide adducts formed.

1.2.3. Task 3 – Development of a predicted MRM assay for routine peptide adduct screening:

In this task, data developed during the *in vitro* trapping experiments and QTOF-MS analysis for each drug/peptide combination will facilitate preliminary studies to adapt an approach developed by Osaki *et al.* for identification of peptide adducts by a QqQ-MS based MRM method.¹¹ This step is critical to the ultimate development of a routine screening method for such adducts that could be implemented by forensic laboratories. The method consists of populating a table of MS $\Delta m/z$ shift values associated with the peptide precursor ion (e.g., [Hb peptide $M+\Delta+nH$]ⁿ⁺ ion) and corresponding product ions (e.g., $b_{n+\Delta}$ and $y_{n+\Delta}$ ions). The precursor/product ion pairs will be selected as multiple reaction monitoring (MRM) transitions based on m/z intensities and reproducibility in repeated experiments, these will include typical b_2 and y_2 type peptide fragment ions.

2. LITERATURE REVIEW

2.1. Drugs of abuse

Humans have been using psychoactive substances since prehistoric times, such as chewing of coca leaves by early Andean people, archaeological evidence has been found in mandibles and hair samples of ancient human populations from the southern coast of Peru.¹² Drug use and abuse have been a constant in human society to this day. According to the most recent World drug report (WDR) in 2020, approximately 284 million people around the world between the ages of 15 and 64 had used an illegal drug, which represents a 26% increase since 2010.¹³ Addiction can be a never-ending battle for the drug user, and suffering is unnecessarily

increased when they are denied access to treatments or face discrimination. Drug use can cause long lasting damage to the user's relationship with family members, friends, and coworkers. Moreover, illicit drug markets are associated with violence and other forms of criminal activity.

The main legislation controlling addictive substances in the U.S. is the Comprehensive Drug Abuse and Prevention and Control Act, also known as the Controlled Substances Act (CSA), that was created in 1970 to combine all existing federal laws into a single new statute. Prior to the CSA's creation, the existing federal drug laws were not adequate to address, for example, the illegal use of legal controlled substances, such as amphetamines and barbiturates. A drug classification and control system was also created, with five schedules based on each substance's medicinal value, risk of harm, and potential for abuse as shown in Table 1. The extent to which a drug is controlled is based on the schedule in which it falls, and criminal penalties are the most severe for offenses involving Schedule I and II drugs. Many U.S. states have modeled their drug laws on the CSA guidelines.

The U.S. Drug Enforcement Administration (DEA) is a federal law enforcement agency established in 1973 by the United States Department of Justice to combat drug trafficking and distribution within the U.S. It is the lead agency for domestic enforcement of the CSA, and it is responsible for assigning drugs to one of the five schedules for regulatory purposes; registering drug manufacturers; registering dispensers and prescribers; investigating and aiding in the prosecution of drug traffickers and violators of drug enforcement policy.

Table 1: Drug schedule and their descriptions.

Drug schedule	Description
Schedule I	Drugs with no currently accepted medical application in the United States. There is a lack of accepted safety for use of the drug under medical supervision
Schedule II	Drugs that have a currently accepted medical application in the United States or a currently accepted medical use with severe restrictions. Abuse of these drugs may lead to severe psychological or physical dependence
Schedule III	Drugs that have a currently accepted medical use application in the United States. Abuse of the drug may lead to moderate or low physical dependence or high psychological dependence
Schedule IV	Drugs that have a currently accepted medical use application in the United States. Abuse of these drugs may lead to limited physical dependence or psychological dependence relative to Schedule III drugs
Schedule V	Drugs that have a currently accepted medical use application in the United States. Abuse of these drugs may lead to limited physical dependence or psychological dependence relative to Schedule IV drugs

Drugs of abuse can also be classified according to their symptoms or side effects; these categories include stimulants, cannabinoids, depressants, opioids, hallucinogens, anesthetics, and analgesics. The drugs of interest in this study are acetaminophen (APAP), cocaine (COC), methylenedioxymethamphetamine (MDMA), methamphetamine (METH), and Δ^9 -tetrahydrocannabinol (THC). Table 2 shows the drugs to be investigated in this research, alongside their abbreviation,

chemical formula, schedule, and drug class. These drugs were selected based on a known potential for addiction and/or dependence and prevalent usage, except for APAP which was selected as a positive control and for which there is a large database on formation of stable and reactive metabolites. All drugs selected are currently among the most used abused substances; cannabis is by far the world's most used drug, and the WDR also shows an overall increase in the use of amphetamines in 2020.¹³ The selected drugs are also commonly identified in authentic specimens from law enforcement cases, rehabilitation centers, correctional facilities, and outpatient therapy.

Table 2: Drugs selected for this study.

Drug	Abbreviation	Formula	Schedule	Class
Acetaminophen	APAP	C ₈ H ₉ NO ₂	N/A	Analgesic
Cocaine	COC	C ₁₇ H ₂₁ NO ₄	II	Stimulant
Methylenedioxymethamphetamine	MDMA	C ₁₁ H ₁₅ NO ₂	I	Stimulant
Methamphetamine	METH	C ₁₀ H ₁₅ N	II	Stimulant
Δ ⁹ -Tetrahydrocannabinol	THC	C ₂₁ H ₃₀ O ₂	I	Cannabinoid

2.2. Drug metabolism

Metabolism is a process by which the body increases the polarity of compounds, thus facilitating excretion. It is a complex process involving transporters and metabolizing enzymes that can impact pharmacological and toxicological effects.¹⁴ Drug metabolism can occur in several biological tissues in the body, including the liver, lungs, kidneys, intestine and skin, however, the liver

is the primary organ of drug metabolism. The liver's contribution to drug metabolism is due to several factors, including its size, being the first organ perfused by chemicals absorbed in the gut, and having very high concentrations of most drug-metabolizing enzyme systems in comparison to other organs.¹⁵

There are two main phases of xenobiotic metabolism. Phase I reactions typically create or expose a functional group on a molecule, generally increasing the hydrophilicity of the molecule in the process.¹⁵ Phase II metabolism involves the conjugation of a large and/or polar moiety, such as glucuronic acid or glutathione, to a molecule in order to facilitate excretion. This conjugate may be covalently linked to the parent compound directly or to a metabolite formed via Phase I metabolism processes.¹⁵

Phase I metabolism is primarily performed by cytochrome P450 enzymes (CYP) located in the liver and other tissues.¹⁶ In terms of catalytic versatility and number of xenobiotics detoxified or activated, the CYP system is unrivaled. The hepatic endoplasmic reticulum contains the highest concentration of CYP enzymes involved in xenobiotic biotransformation, but CYP enzymes are found in almost all tissues. All CYP enzymes are heme-containing proteins that catalyze the monooxygenation of one oxygen atom into a substrate, followed by the reduction of the other oxygen atom to water using reducing equivalents derived from β -nicotinamide adenine dinucleotide phosphate (NADPH).¹⁷ The phase I oxidative reaction can be generalized with the following equation:



CYP catalyzes the following types of reactions: oxidation, reduction, hydrolytic cleavage, N-oxidation, alkylation (methylation), dealkylation, ring cyclization, dimerization, transamidation, isomerization, and decarboxylation. CYP does not directly interact with NADPH or NADH during catalysis.¹⁵ Electrons are relayed from NADPH to cytochrome P450 in the endoplasmic reticulum by a flavoprotein called NADPH-cytochrome P450 reductase. Electrons are transferred from NADPH to CYP in mitochondria by ferredoxin and ferredoxin reductase.¹⁷

The mono-oxygenase mediated catalytic cycle is widely accepted to involve sequential one-electron reductions, with those electrons supplied by the NADPH reductase as shown in Figure 1.¹⁷⁻¹⁹ Following substrate binding to the CYP enzyme (b), the first electron is used to convert the Fe(III) ferric species (b) into the Fe(II) ferrous species (c). The ferric-superoxo intermediate is then formed by transferring an electron from iron(II) to O₂ (d). Following that, a second electron and a proton are transferred to the ferric-superoxo intermediate to produce a ferric-(hydro) peroxy intermediate (e), capable of producing the oxo-iron(IV) porphyrin cation radical intermediate (f). The reduced hydroxy ferric species and substrate radical (g) are then produced after a hydrogen atom is extracted from the substrate in solution. This results in the formation of a coordinated oxidized substrate species (h), which then liberates the oxidized substrate and yields the initial low-spin ferric compound (a). If the catalytic cycle is broken, oxygen is released in the form of superoxide anion (O₂⁻) or hydrogen peroxide (H₂O₂).¹⁷

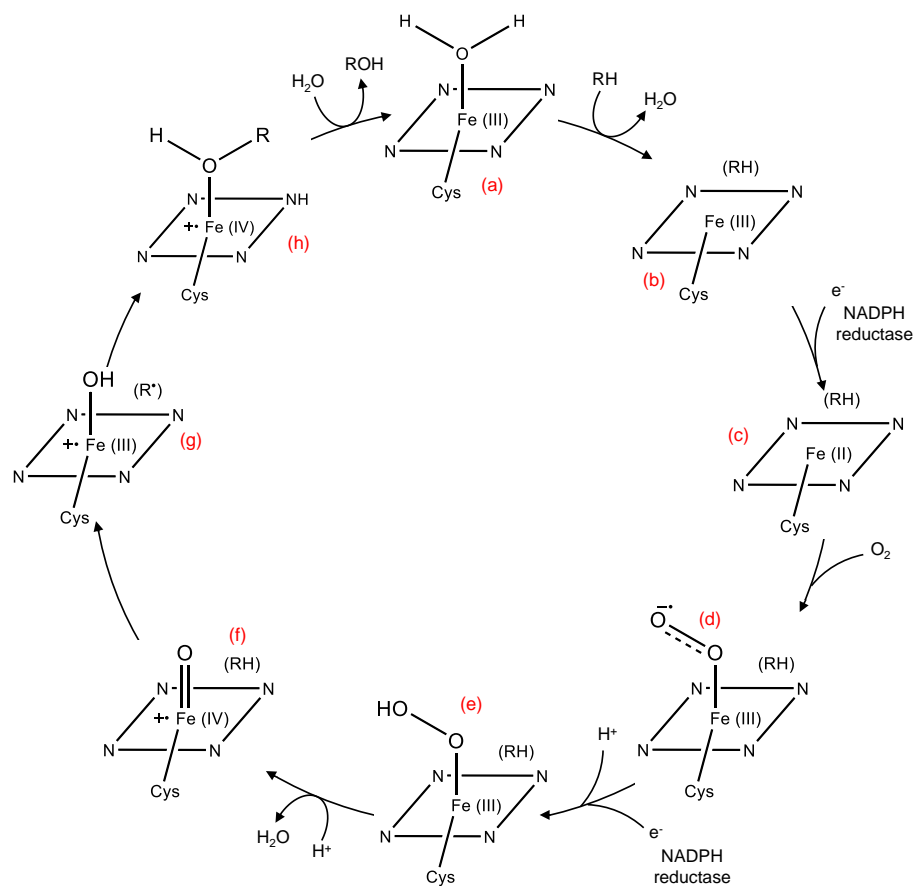


Figure 1: Catalytic cycle of dioxygen activation by cytochrome P450.

2.3. *In vitro* metabolism assays

Various *in vitro* model systems have been used by the pharmaceutical industry, forensic toxicologists, and researchers to assess the extent and rate of xenobiotic metabolism and examine the formation of both stable metabolites (SM) and reactive metabolites (RM) of drugs.^{20, 21} RM can often be identified by the presence of stable hydrolysis products. For drugs of abuse, RM can indicate the formation of toxic biomolecules, since the formation of covalent drug adducts with proteins and peptides can disrupt cellular functions, leading to cell death or even trigger immune responses.²²

To study reactive metabolites, *i.e.*, those which are unstable *in situ* and may react further, a modified *in vitro* system, known as a “trapping” assay, is required. A trapping assay consists of the same components of an *in vitro* metabolic assay with the addition of a trapping agent. The trapping agent is a nucleophilic compound that can covalently bind to the reactive (electrophilic) metabolites, essentially inactivating them and preventing binding to tissue macromolecules or further breakdown to a stable metabolite. These trapping nucleophiles can be small molecules or proteins and peptides that are typically present *in vivo* and that can be used to measure and characterize reactive metabolites *in vitro*.⁸

For example, Ma *et al.*²³ investigated the formation of Hb adducts with pyrrolizidine alkaloids (PA) generated by the metabolic activation of PAs as a primary trigger for hepatotoxicity. The study looked into the potential of pyrrole-Hb adducts as a biomarker of PA exposure in humans. The level and elimination kinetics of pyrrole-Hb adducts were studied in 43 PA-induced liver injury patients' blood samples. The results showed that pyrrole-Hb adducts had notably higher concentrations and a longer persistence than pyrrole-plasma protein adducts, showing they can be used in clinical tests in the future.

The most common *in vitro* model system uses homogenized liver fractions containing various enzymes as the primary contributor of Phase I metabolic activity.^{8, 24-26} The three most commonly used liver fractions obtained by differential centrifugation are the S9 fraction, cytosol, and human liver microsomes (HLM). The S9 fraction is the supernatant obtained by the centrifugation of a liver tissue homogenate at 9,000 x g. When the S9 fraction is centrifuged at 100,000 x g, the

obtained supernatant is the cytosol, while the pellet contains the "microsomes" derived from rough endoplasmic reticulum.²⁷ The assay employed in this study uses HLM as source of the CYP enzymes responsible for Phase I metabolism.

HLM assays are used by pharmaceutical companies to characterize SM and RM formed by natural metabolism processes found in the human body.²⁰ In addition to HLM, several components need to be present in the reaction for the activation of CYP enzymes present in the microsomes. These components include NADPH to catalyze the oxidation reaction; a source for Mg⁺² ions to stimulate CYP activity; glucose-6-phosphate (G-6-P) and D(+)-glucose-6-phosphate dehydrogenase (G-6-P-D) which provide a regeneration system for NADPH.

Schneider and DeCaprio²⁸ looked at how well four popular *in vitro* assay techniques produced metabolic profiles for drugs of abuse that were in line with *in vivo* data. Cocaine was selected as the study's substrate primarily due to the well-researched metabolism it undergoes in both humans and experimental animals. Using LC-QqQ-MS with multiple reaction monitoring, the following samples were examined: HLM, cytosol, human liver S9 fraction, and horseradish peroxidase. There were both qualitative and quantitative variations in analyte generation among the various metabolic systems in Phase I and Phase II activity. Particularly with regard to primary vs secondary metabolite synthesis, assay incubation duration was revealed to be a decisive factor in metabolic profile. In human hepatic metabolic models, the regioselective arene hydroxylation of cocaine was decisively demonstrated, but peroxidase-based test techniques showed less selectivity in oxidative aryl biotransformation.

Gilliland and co-workers²⁴ used a HLM metabolic assay with GSH as a nucleophilic trapping agent to examine formation of RM of a series of drugs. Extracted ion MS spectra for all potentially significant ions were collected using LC-QqQ-MS/MS and examined for fragmentation common to GSH-containing compounds, followed by confirmation of adduction and structural characterization performed by LC-QTOF-MS/MS. In addition to the two positive controls APAP and clozapine, ten of the fourteen drugs, including cocaine, MDMA, METH and THC, showed GSH adduction, with several forming multiple adducts, for a total of 22 individual identified adducted species.

Biomimetic alternatives for the study of SM and RM include synthetic metalloporphyrin catalysts²⁹⁻³¹ and electrochemical (EC) assays.³²⁻³⁴ Certain synthetic metalloporphyrin (MP) catalysts have been shown to mimic P450 mediated metabolism of drugs. Because of their role as biological ligands, porphyrins and related macrocycles have received a lot of attention in this regard. The heme cofactor, which is an iron-containing porphyrin, is found at the active site of many metalloproteins and is involved in a wide range of metabolic reactions.³⁵ In this context, synthetic MPs have been intensively developed as model systems for studies of oxidative metabolism and for the synthesis of potential metabolites; an example of this type of molecule is shown in Figure 2. This lays the foundation of a predictive basis of oxidative reactivity to determine the tendency of drugs to form biologically active metabolites and provides a convenient methodology for their preparation.³⁶

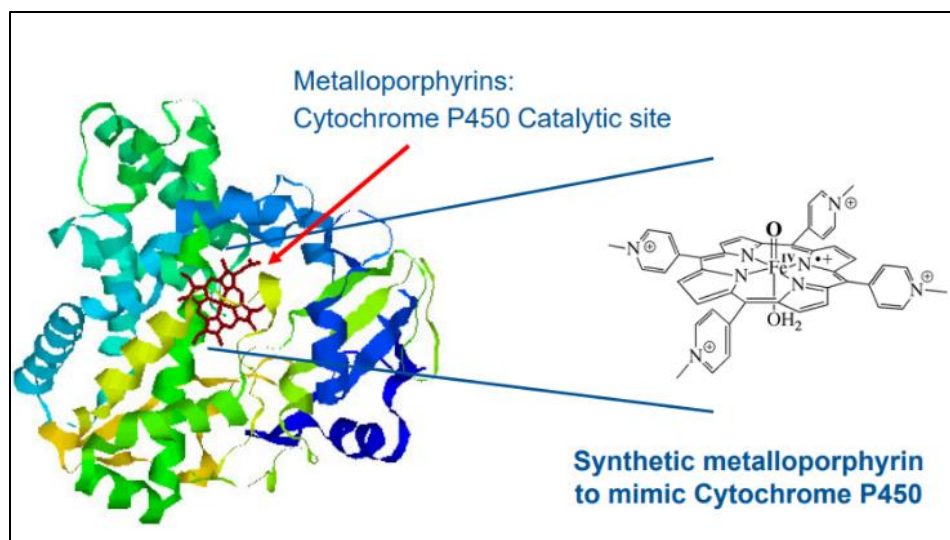


Figure 2: Synthetic metalloporphyrin derived from cytochrome P450 active site.³⁷

The biomimetic oxidation of phenacetin, methacetin, and acetanilide meta-chloroperoxybenzoic, APAP prodrugs, by iron (III) porphyrins chelated by different axial ligands was reported by Chapman and co-workers.³⁸ The study compared the activity of three hindered Fe porphyrin complexes, as variable catalytic efficiency varies from β -pyrrole substituted MPs. To better understand the factors that contribute to function and effect, nine axial ligands with varying pKa (2.8-11.2), size, and heteroatomic identity were studied. In the majority of cases, the thiolate ligands provided the highest APAP yields. It was demonstrated that the optimal FeP/axial ligand combinations differ for each transformation, providing a starting point for potential APAP prodrugs derived from similar starting materials. Furthermore, reactions with S-containing reagents yielded higher APAP yields and produce different products than reactions with N-containing reagents.

Lassila and colleagues³⁰ used a commercial kit containing synthetic metalloporphyrins, called the BMO kit, as a means to metabolize clozapine, ticlopidine, and citalopram. In addition, they used S9 liver fraction incubations to compare the results with the BMO assay. The S9 incubation produced six glutathione conjugates for clozapine, while the BMO assay produced four. The BMO assay detected four of the five phase I metabolites produced by S9 for clozapine. Four glutathione conjugates were detected in the S9 incubation for ticlopidine, but none were detected in the MP assay. Eight of the nine ticlopidine phase I metabolites generated by S9 incubation were detected with the BMO assay. The incubations were analyzed using high-resolution LC/MS/MS.

EC assays are a third alternative for the generation of SM and RM that have been used in mimicking biologic reactions such as oxidative drug metabolism^{32, 34, 39}. For example, EC assays have been used to mimic different phase-I reactions, such as aromatic hydroxylation, dehydrogenation, O- and N-dealkylation, by introducing the compound into an electrochemical cell and applying a constant potential to the solution. A three-electrode setup, consisting of a working electrode (WE), a counter electrode (CE), and a reference electrode (RE), is commonly used in EC cells as shown in Figure 3. The potential applied to the working electrode is either scanned or held constant in order to perform electrochemical transformations in the analyte solution. In cyclic voltammetry (CV) experiments the voltage in the WE is scanned, while in bulk electrolysis experiments the voltage is kept constant. Several materials are used to make the WE, among the most common are glassy carbon, graphite, platinum, and gold.

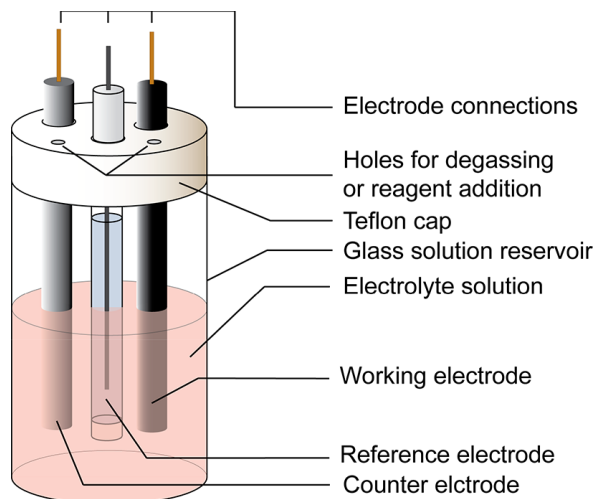


Figure 3: Schematic representation of a three-electrode EC cell for cyclic voltammetry experiments.⁴⁰

The role of the reference electrode is to serve as a reference in measuring and controlling the working electrode potential while no current is passed through it. A RE is one that has a consistent and well-known electrode potential. The most common REs used in aqueous conditions are the saturated calomel electrode (SCE), standard/normal hydrogen electrode, or Ag/AgCl electrodes. The counter electrode performs the reverse electrochemical process to that of the working electrode; oxidation at the WE indicates reduction at the CE and vice versa. The CE thus completes the circuit within the entire electrochemical cell. The CE is almost always a Pt wire or Pt rod in analytical scale applications.⁴⁰

Mielczarek and colleagues⁴¹ demonstrated that an EC system linked in real time with electrospray ionization mass spectrometry successfully mimicked the oxidative metabolism that occurs in liver cells primarily caused by CYP enzymes. Cocaine was chosen as a model drug for these studies and was analyzed with a

boron-doped diamond WE in a 20 mM Tris buffer solution. The results were compared with those produced by a standard procedure using rat liver microsomes. This study showed that cocaine could be converted to norcocaine, a natural metabolite of cocaine in the human body, in a single electrochemical step. This technique could also be used to prepare norcocaine from cocaine, demonstrating that electrochemical reactions can be used in place of laborious and sometimes problematic chemical synthesis.

Trapping molecules can also be added to EC assays to detect reactive metabolites. For example, Madsen *et al.*³³ showed that APAP RMs generated by electrochemical oxidation successfully form adducts with glutathione (GSH). The stability of N-acetyl-p-benzoquinoneimine (NAPQI) electrochemically generated from APAP was investigated, and NAPQI showed the greatest stability at physiological pH. The rate of reaction between NAPQI and GSH was measured using cyclic voltammetry, where NAPQI reacted quantitatively to GSH. NAPQI's reactivity toward other nucleophiles was also investigated, and a time-dependent conjugate formation with N-acetyltyrosine was observed.

2.4. *In silico* prediction of drug metabolism

In silico drug metabolite prediction is widely used as a first step in studying drug biotransformation in pharmaceutical development.⁴² Several commercial software tools for xenobiotic metabolite prediction are available, including MetaSite (Molecular Discovery Ltd, Middlesex, UK), Meteor (Lhasa Limited, Leeds, UK), and MetaDrug (Thomson Reuters, NY, USA). However, in studies of designer drugs or

other toxicologically interesting compounds, prediction using *in silico* methods have not yet become common.⁴³

In the present work, the software MetaSite will be used to predict the metabolism of the drugs of interest. MetaSite predicts reactions and metabolic conversion of phase I metabolism of CYP450 and FMO3 enzymes⁴³. It allows the user to choose the means of the metabolic path, such as liver, skin, brain and specific CYP enzymes⁴⁴. Predictions of metabolites formed with HLM can be accurately made setting up the liver as the metabolic pathway in the software. It is also possible to predict the metabolism of synthetic MPs, by inputting the structure of a specific CYP enzyme that is similar in structure with the MP used.

In one example, Ellefsen *et al.*⁴⁵ investigated the metabolic stability of 4-methoxy- α -PVP using the *in silico* metabolite prediction software MetaSite. Metabolites obtained with HLM and hepatocyte incubations were used to compare with the *in silico* study. To identify potential unexpected metabolites, HRMS was used with full scan data-dependent mass spectrometry, with and without an inclusion list of predicted metabolites. MetaSite predicted eleven phase I metabolites with probability scores greater than 20%, five of which were found in the *in vitro* assays. In addition to the parent compound, the most dominant metabolite in HLM and human hepatocyte samples was 4-hydroxy- α -PVP, which was also predicted as the #1 *in silico* metabolite.

2.5. Retrospective monitoring of drug use or exposure

The analysis of drugs of abuse and their metabolites in biological fluids is an issue of extreme relevance for both clinical and forensic toxicology laboratories. Biological specimens can be obtained from a variety of sources, including blood, urine, hair, oral fluid, and others.⁴⁶ These various tissues and bodily fluids excrete at different rates and durations, resulting in different detection windows for substances, as shown in Figure 4.⁴⁷ Among the conventional matrices, urine has been the most used matrix for the analysis and identification of drugs or toxic substances, due to the high concentration of drugs and their metabolites in this matrix.¹

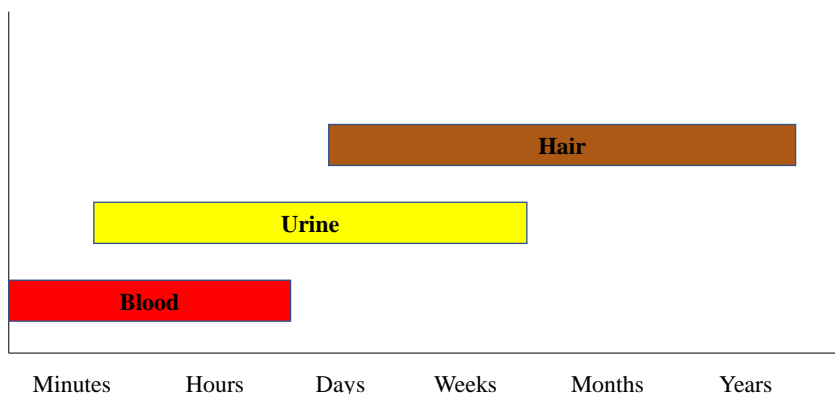


Figure 4: Typical window of detection of drugs and their metabolites in blood, urine, and hair.

The specific site of action of drugs varies from nerve endings to receptors on cells located throughout the body. As sampling from these sites is not normally available, thus, blood is used as a monitoring sample. As most drugs are water soluble, plasma or serum are logical sources to monitor without the interference of

red blood cells. There are, however, occasions when other types of matrices can be tested and, in some cases, may even be necessary to obtain the desired clinical information.^{1, 46}

2.5.1. Hair analysis

Hair analysis is the current primary tool for longer-term or retrospective monitoring of drug use or exposure.^{4, 7, 48} The increased detection window of hair as a biological matrix for drug screening over blood, urine, or oral fluid analysis, as well as the ease of collection, are major advantages. Once a drug (or metabolite) has been incorporated into the hair, the only way to remove it is to cut off the portion of hair in which it is stored, which causes the usable time frame for drug detection using hair analysis to be several months or longer. Typically, analysis is performed by segmenting the sampled hair specimen and analyzing each segment individually. This procedure allows for an estimate of the timing and extent of both past episodic and cumulative drug exposure.

There are other advantages of hair sampling unrelated to the extended window of detection. For example, specimen collection for hair is less invasive than for blood and urine. In contrast to other matrices, hair specimens are generally easy to handle, ship, and store, as collected hair samples only need to be bound, wrapped in aluminum foil, and stored in dry conditions at room temperature. Another advantage is that parent drugs may be found in the hair, allowing for discrimination between exposure sources, such as morphine vs. heroin.

Despite these advantages, forensic hair analysis also presents some challenges with regard to applicability, ease of analysis, and interpretation of

results.⁴⁹ One obvious drawback is that the technique cannot be applied to bald, shaved, or shorthaired individuals. Another complication is that since hair growth may vary from 0.6 cm to 1.4 cm per month among individuals, analysis generally allows for only an approximate timeline of drug exposure.⁴⁸ Another issue is the lack of a general understanding of the mechanisms and compound-specific aspects of drug incorporation into hair. Finally, hair testing results can vary significantly as a function of hair type, making standardized screening problematic. For example, hair specimens generally have different melanin content, which affects the amount of drug that will be incorporated. Bleaching, washing, coloring, and other forms of environmental contamination (including that from the smoking of drugs) may also complicate the reliable detection of drugs in hair samples.

2.5.2. Drug protein/peptide adduction

Protein adducts are formed when electrophilic drug metabolites react covalently with protein nucleophiles.¹⁰ These electrophiles may be endogenous but usually are xenobiotics that can either be reactive themselves or have been generated from metabolic processes.^{50, 51} A "biomarker of exposure" is a biological change that provides physiochemical evidence of xenobiotic exposure. As biomarkers of exposure, protein adducts can not only assess whether individuals have been exposed to certain compounds but may also extend the window of detection for xenobiotics beyond that provided by simple detection of the parent compound or metabolites in the blood and urine.

This is especially true for protein adduction, which results in usually irreversible modifications that last for the life of the molecule or cell because, unlike

DNA, there are no repair mechanisms for exogenous protein modifications⁵⁰. While the length of time that a protein adduct can be detected is strictly dependent on the target protein's *in vivo* lifetime, certain proteins are especially useful as biomarkers of xenobiotic exposure, such as Hb and human serum albumin (HSA). Both proteins are abundant in blood; one milliliter of blood contains about 150 mg of Hb and 30 mg of HSA. In humans, Hb and HSA have a half-life of approximately 126 days and 20 days respectively, allowing them to function as a cumulative dosimeter for xenobiotic exposure.^{52, 53}

The most abundant protein in human plasma is HSA. HSA contains 35 cysteine residues, but 34 of them are bound as intramolecular disulfides. The ³⁴Cys moiety represents the largest fraction of free thiols in serum, approximately 80%.⁵⁴ ³⁴Cys is found close to the surface of HSA, near ³⁸Asp, ³⁹His, and ⁸⁴Tyr. These three residues influence the ³⁴Cys ionization state, thereby modulating its reactivity.⁵⁵ Hb is the most prominent heme protein in blood; it is a heterotetramer composed of two α -subunits and two β -subunits.⁵⁶ The heme is composed of a ferrous ion held in the center of a porphyrin and coordinated by the porphyrin ring's four nitrogen atoms as shown in Figure 5.

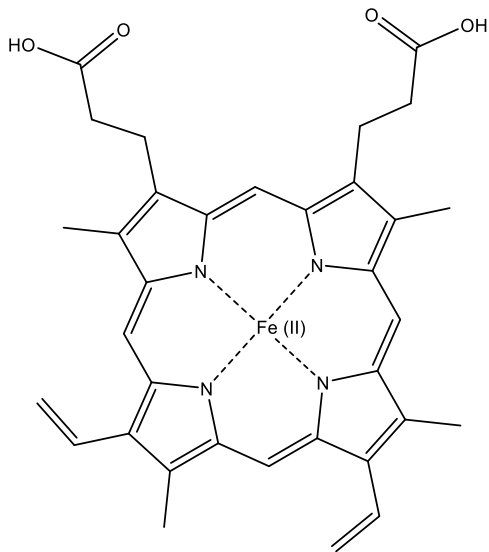


Figure 5: Chemical structure of the porphyrin ring system of heme b complex of Hb.

There are a total of three cysteine residues in the Hb molecule: $\alpha^{104}\text{Cys}$, $\beta^{93}\text{Cys}$ and $\beta^{112}\text{Cys}$. The $\beta^{93}\text{Cys}$ is surface exposed and is the most reactive of all Hb cysteine residues. Thus, the thiol moiety present in $\beta^{93}\text{Cys}$ can act as a nucleophile and covalently bind to drug reactive electrophiles. In contrast, $\alpha^{104}\text{Cys}$ and $\beta^{112}\text{Cys}$ residues are located relatively in the interior portion of Hb and are generally thought to be poorly accessible to chemical reactions.⁵²

A study reported by Möller *et al.*²⁵ investigated the protein adduction of two reactive aniline metabolic products: N-phenylhydroxylamine (PhNHOH) and nitrosobenzene (NOB). Adduction of model peptides with nucleophilic sidechains (Cys, His, and Lys) and selected proteins (β -lactoglobulin-A, bovine and human Hb) were characterized *in vitro*. Peptide data identified the Cys thiol group as the most reactive nucleophile for these metabolites, which was consistent with *in silico* predictions. Sulfinamides were identified as the primary adduction products for PhNHOH, and they remained stable after tryptic digestion. Reactions with NOB,

on the other hand, produced an additional oxidized adduct, the sulfonamide. *In vitro* exposure of human whole blood to PhNHOH and NOB revealed the formation of only sulfinamides. The findings of this study support previous research that sulfinamide and sulfonamide form adducts specifically at ⁹³Cys of human Hb. It was also shown that ¹⁰⁴Cys and ¹¹²Cys of Hb can undergo adduction under certain reaction conditions.

Hundreds of licit drugs, environmental contaminants, and other xenobiotics have been shown to have the potential for covalent protein binding of RM *in vitro* or *in vivo*.^{22, 57} One study found some level of covalent biological thiol binding in 85 of 179 currently marketed drugs.⁵⁸ In contrast to the extensive database available for licit drug and other xenobiotic protein adducts, virtually no work has been reported on the detection and analysis of such modifications as exposure markers for drugs of abuse. The only exception is ethanol, where acetaldehyde-protein adducts have been thoroughly investigated.⁵⁹

Some pertinent data on covalent binding of illicit drugs as related to drug toxicity or addiction mechanisms using *in vitro* metabolism and "trapping" assays or *in vivo* animal models have been reported. *In vitro* and *in vivo* studies of covalent protein binding of morphine and other opiates, for example, revealed the formation of adducts resulting from bioactivation to RM. In non-human species, 8-dihydromorphinonyl adducts were found to form with the biological thiol-containing tripeptide GSH, most likely via the reactive morphine metabolite morphinone.^{60, 61} Todaka and colleagues⁶² investigated the formation of an 8-dihydromorphinonyl adduction product derived from morphinone in human liver-based assays using 2-mercaptoethanol as a trapping agent.

Protein adducts have also been described for several stimulant drugs, again in primarily mechanistic investigations. Cocaine intake is known to result in irreversible protein binding, as demonstrated by histopathological studies, investigations utilizing radiolabeled drug, and analysis of immunogenic antibodies present in the blood of cocaine abusers.⁶³⁻⁶⁵ Various authors have demonstrated that the formation of cocaine-protein adducts parallels the degree of hepatic necrosis, suggesting a direct causal relationship.^{64, 65} Some limited data are also available on covalent protein adduction by cocaine in humans. Schneider *et al.*⁸ studied the incubation of cocaine with thiol-containing peptides in an *in vitro* biotransformation system identified a monooxygenase-mediated event leading to the oxidation of the cocaine aryl moiety and subsequent stable covalent peptide binding. This mechanism provides a novel alternative pathway to protein binding of cocaine and supports the feasibility of employing protein thiol adducts of cocaine as biomarkers of exposure.

Taken together, the findings show that common drugs of abuse (and/or their RM) can adduct protein under physiological conditions, and that this adduction can be detected and quantified. While not a common approach for detecting drug abuse (except in the case of ethanol abuse), the examination of protein adduction products may be an appealing future path for forensic toxicological analysis. The possibility of extending the detection window for commonly abused drugs from days (the current timeline for parent drug and metabolites in the free fraction) to weeks/months (depending on the *in vivo* lifetime of the protein target) may be a

viable option. As a result, protein adducts are attractive as long-term and/or retrospective exposure biomarkers for such drugs.

2.6. Liquid Chromatography - Mass Spectrometry

Liquid chromatography (LC) is an analytical technique that separates the components of a mixture. This separation occurs as a result of the sample's interactions with the mobile and stationary phases. LC employs instruments that can be fully automated, which makes it possible to perform separations and quantitative analysis of a wide range of compounds present in various types of samples in a matter of minutes with high resolution and efficiency.⁶⁶

The coupling of LC and mass spectrometry (MS) became possible after the development of atmospheric pressure ionization sources in the late 1980s. The combination of the two techniques significantly increased laboratories' analytical capacities. Before LC-MS, researchers used conventional optical detectors and now are benefited from MS's analytical potential in terms of sensitivity, selectivity, analytical frequency, and ease of developing analytical methods.⁶⁷

A mass spectrometer measures the mass-to-charge (m/z) ratio of gaseous ions, and consists of an ionization source, one or more mass analyzers, a detection system, and a signal processing system. The analyte must be converted into gas phase ions before mass spectrometry analysis can be performed. There are several ionization sources, including electron ionization, chemical ionization, electrospray ionization, atmospheric pressure ionization, among others, and the choice of which one to use is primarily determined by the type of sample to be studied.⁶⁸

Figure 6 depicts an Electrospray Ionization (ESI) source, which is efficient at ionizing polar molecules with a wide range of masses. ESI ionizes the species while they are still in aqueous solution. Basic compounds are protonated by adding a weak acid, resulting in the formation of the $[M+H]^+$ adduct (positive mode), whereas acidic species are deprotonated by adding a weak base, resulting in the generation of ions. $[M-H]^-$ (negative mode).⁶⁹

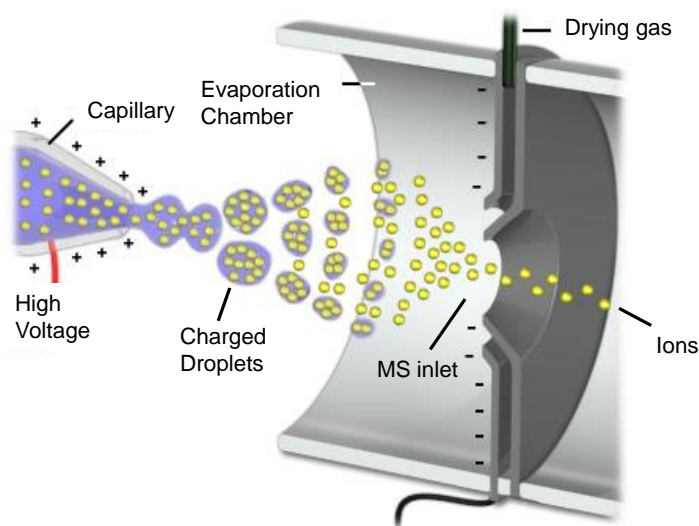


Figure 6: ESI ionization source, adapted from NHMFL.⁷⁰

A high voltage is applied to the capillary containing the ionic solution forming a fine spray with charge accumulation at the capillary outlet. The final production of gas-phase ions can be explained by two major theories. The first theory is the residual charge model, which states that as the solvent evaporates, the volume of each individual droplet is reduced. Then the droplets subdivide, due to the high repulsion between the ions of the same charge, and finally droplets containing only one ion are formed, through successive fissions. The second theory is the ion evaporation model which says that the droplets accumulate charge while the

solvent is evaporated. Then, due to repulsive forces, ions are ejected from the droplets into the gas phase. Thus, the ions present in solution are desorbed to the gas phase and attracted to the MS inlet.⁶⁹

Mass analyzers are used for ion analysis, and the different behavior of the ions is used to separate them according to their m/z in time or space, allowing their individual abundances to be determined. The Time of Flight (TOF) mass analyzer was developed in 1946 by W.E. Stephens,⁷¹ which was first used in the 1950s and has since undergone changes and improvements.⁶⁸ The TOF operating principle is straightforward, it measures the time required for ions to travel through the flight tube and reach the detector. All ions receive the same kinetic energy during instantaneous acceleration, but their velocities are proportional to their m/z , and ions of the same m/z reach the detector at the same time.

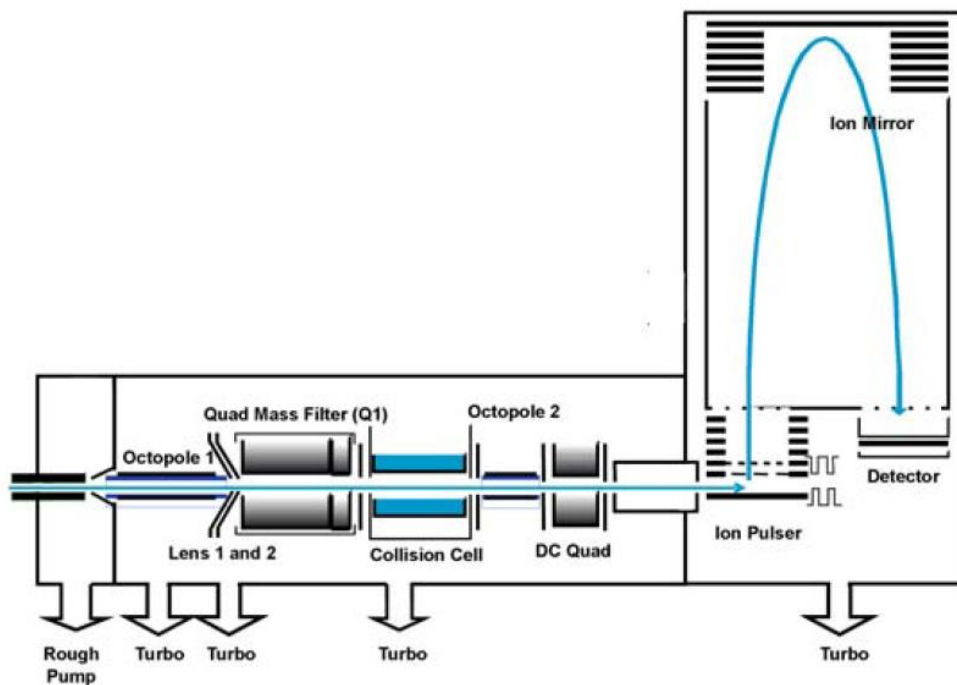


Figure 7: Schematic representation of the 6530 Q-TOF mass analyzer from © Agilent Technologies, Inc.⁷²

A hybrid quadrupole - TOF (Q-TOF) instrument consists of a quadrupole in line with a hexapole collision cell, followed by an orthogonal acceleration TOF detector as shown in Figure 7. The Q-TOF-MS system can collect data in both the MS and tandem mass spectrometry (MS/MS) modes. The quadrupole is used as a mass filter in the MS mode to transmit ions, the collision cell is not pressurized, and all ions are transferred to the TOF-MS for mass determination. In the MS/MS mode, the quadrupole is used as a mass filter to select parent ions for collision-induced dissociation, the product ions are sent to the TOF and then to the detector for further mass analysis.⁷³

A quadrupole mass spectrometer consists of four parallel cylindrical rods that serve as electrodes. A potential difference accelerates ions into the space between the rods. At any given time, all ions except those with a m/z value range strike the rods and are converted to neutral molecules. As a result, only ions with a narrow range of m/z values reach the transducer. A triple quadrupole (QqQ) mass analyzer comprises of three quadrupoles connected in series. The first of these quadrupoles (Q1) is used to control which ions pass through the instrument. The second quadrupole (q or Q2) is used as a collision cell for collision induced dissociation (CID) to generate distinct fragments. The third quadrupole (Q3) is used to select which collision cell fragments will pass through to the detector. Depending on the m/z ratios used, a QqQ can perform a variety of scanning modes

such as product ion scans, precursor ion scans, neutral loss scans, and selected reaction monitoring or multiple reaction monitoring (MRM).⁶⁸

2.7. LC-MS protein and peptide analysis

A major approach to qualitative and quantitative analysis of protein adducts is HRMS-based “bottom-up” proteomics. Bottom-up proteomics utilizes enzymatic cleavage of a protein into peptides prior to their introduction into the MS.⁷⁴ Tandem mass spectrometry (MS/MS) is utilized to fragment enzymatically cleaved peptides, and the resultant ions are analyzed using bioinformatics software to elucidate an amino acid sequence for each peptide. This method is most typically used for the identification of protein modifications, particularly when the modification creates a predictable mass shift that can be observed via MS or MS/MS.⁷⁵

Peptide analysis by mass spectrometric techniques is critical to characterizing protein modifications by reactive drug metabolites. A peptide fragmentation model was created in 1984 by Roepstorff and Fohlman⁷⁶ and will be used in this work. Adducted peptides fragmentation generally happens at the amide bonds, producing a series of “b” and “y” fragment ions without prominent and reliable constant neutral losses. When the charge is retained at the N-terminal fragment of the peptide, the three possible cleavage points are called a, b, c. When the charge is retained by the C-terminal fragment they are called x, y, z as shown in Figure 8. The numbering indicates which peptide bond is cleaved, starting at the N- and C-termini, and thus the number of amino acid residues in the fragment ion. In typical experiments, b and y series ions are most commonly observed.

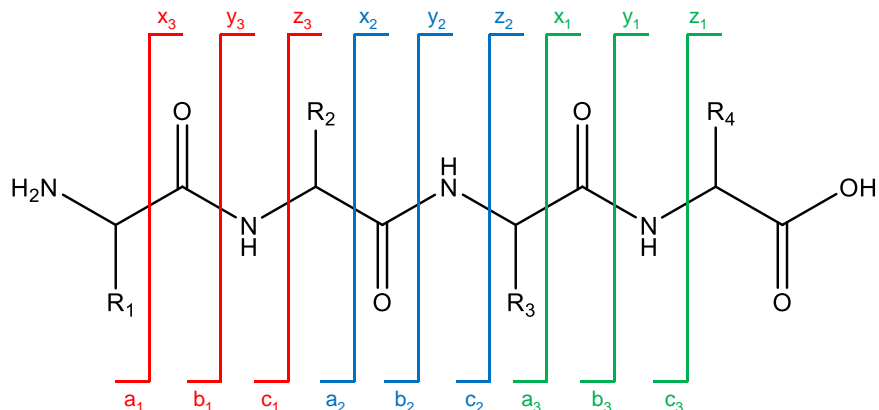


Figure 8: Peptide fragmentation patterns labeled with the common “a,b,c” and “x,y,z”

There are several algorithms that provide a sequence database for the analysis of protein and peptides with MS/MS data, some of the tools available are PeptideSearch, Sequest, Mascot, Sonar MS/MS, and ProteinProspector. ProteinProspector is a free online software developed by the University of California, San Francisco, and will be used in this work to aid in the peptide MS/MS data interpretation. The MS-Product feature of ProteinProspector generates theoretical fragmentation and annotation of MS/MS spectra. The software also offers the inclusion of mass modifications to be inserted in the searching criteria which allows for the discovery of drug-peptide adducts.

Thompson and DeCaprio⁵⁰ used LC-MS/MS to investigate the *in vitro* adduction of the nitrogen mustards mechloroethamine (HN-2) and tris-(2-chlorethyl)amine (HN-3) to nucleophilic amino acid residues. The model peptides used in the study contained cysteine, lysine, and histidine. The study evaluated the composition of the produced adducts, their concentration–response relationships, and their temporal stability. All three model peptides were found to

undergo covalent adduction to nucleophilic residues after first forming a reactive aziridinium intermediate for mechloroethamine and tris-(2-chlorethyl) amine. Adduction was discovered to happen most frequently with cysteine, but it was also noticed at lysine and histidine, showing that mechloroethamine and tris-(2-chlorethyl) amine are capable of adduction at a variety of nucleophilic sites. Adducts produced with mechloroethamine were stable for up to three weeks after solid phase extraction cleanup. Tris-(2-chlorethyl) amine adducts were less stable, although over the course of three weeks, hydrolyzed secondary adducts were still visible.

2.8. Research objectives

The primary goals of this study are to utilize *in vitro* HLM metabolic assays, synthetic MP catalysts, and EC redox assays to characterize SM and RM of drugs of abuse. In addition, this study assesses the capability of reactive species to form adducts with reactive peptide thiols to support ongoing work to develop long-term biomarkers of exposure for drugs of abuse. The present work builds upon previous proof of concept studies performed in the DeCaprio Laboratory at FIU. Analysis of potential drug-thiol adducts will be performed through LC-MS analysis utilizing GSH and a target thiol-containing tryptic peptide derived from Hb (*i.e.*, Hb β^{93} Cys peptide) as biological trapping agents.

3. METHODOLOGY

3.1. Instrumentation

HRMS analysis was performed on an Agilent Technologies (Santa Clara,

CA, USA) 1290/6530 liquid chromatograph/quadrupole time-of-flight mass spectrometer (LC-QTOF-MS), equipped with an Agilent Dual Jet Stream Electrospray Ionization in positive ionization mode. LRMS MRM analysis was performed on an Agilent Technologies (Santa Clara, CA, USA) 1290/6460 liquid chromatograph/triple quadrupole mass spectrometer (LC-QqQ-MS), equipped with an Agilent Jet Stream Electrospray Ionization in positive ionization mode. The QTOF source parameters were as follows: gas temperature, 350°C; gas flow 10 L/min; nebulizer 20 psi; sheath gas temperature 400°C; sheath gas flow 12 L/min; capillary voltage 3,500 V; and nozzle voltage 1000 V. The QqQ source parameters were as follows: gas temperature, 300°C; gas flow 8 L/min; nebulizer 35 psi; sheath gas temperature 350°C; sheath gas flow 11 L/min; capillary voltage 3,500 V; and nozzle voltage 1000 V.

Chromatographic separations were performed using an Agilent Zorbax Rapid Resolution HD Eclipse Plus C18 column (3.0 x 100 mm, particle size 1.8 µm) in both instruments. A biphasic elution system consisting of eluent A: water with 0.1% formic acid, and B: acetonitrile with 0.1% formic acid was utilized for both instruments. The elution gradient varied between different experiments and is discussed below. Elution solvent flow rate was 0.3 mL/min and the injection volume was 10 µL for all runs. Data acquisition for the QqQ and QTOF was performed using Agilent's MassHunter Acquisition software (version B.06.00 for both systems). Data analysis was performed using Agilent's MassHunter

Qualitative software (version B.07.00), with supplementation by Agilent's BioConfirm software (version B.08.00).

3.2. Drug selection

Specific drugs to be investigated were chosen to provide a range of licit and illicit abused compounds with consideration of previous data generated in the DeCaprio Laboratory and other published work. Figure 9 shows the molecular structure and exact mass of the drugs under study. In addition, the well characterized adduct-forming drug acetaminophen was utilized as a positive control to ensure active mechanisms necessary for biotransformation-induced adduct formation.

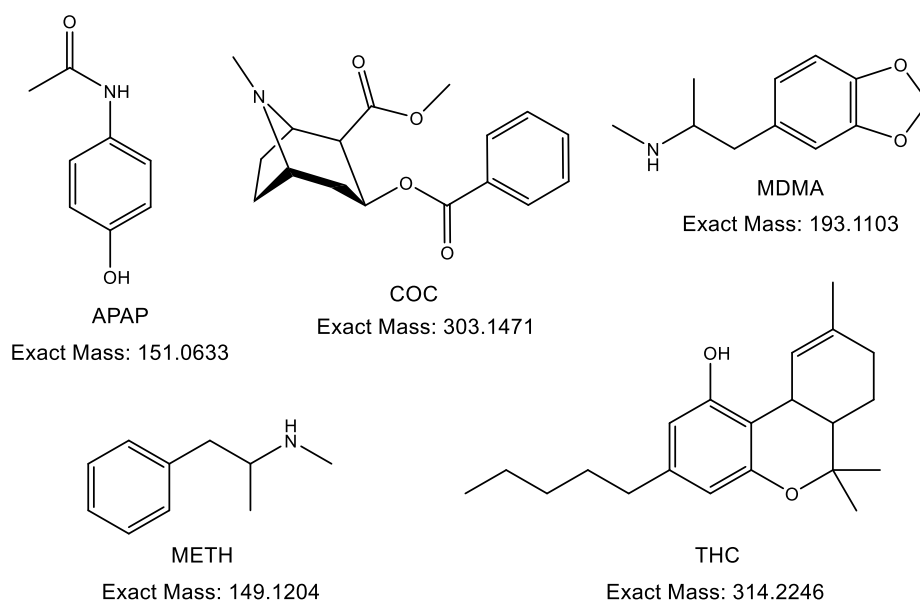


Figure 9: Structures and exact mass of drugs under study.

3.3. Chemicals and reagents

Ammonium bicarbonate, magnesium chloride, glucose-6-phosphate sodium salt, iodoacetamide, and acetaminophen were purchased from Sigma

Aldrich (St. Louis, MO, USA). Drug standards for cocaine, 3,4-methylenedioxy methamphetamine HCl, methamphetamine HCl, and Δ^9 -tetrahydrocannabinol were purchased from Cayman Chemical (Ann Arbor, MI, USA). Formic acid (Optima grade for LC/MS), dimethyl sulfoxide (DMSO), β -nicotinamide adenine dinucleotide phosphate reduced, tetrasodium salt (NADPH), D(+)-glucose-6-phosphate dehydrogenase sodium salt, human liver microsomes, glutathione (reduced), water (Optima LC/MS grade), and acetonitrile (Optima LC/MS grade) were purchased from Thermo Fisher Scientific (Waltham, MA, USA). The Hb $\beta^{93}\text{Cys}$ peptide (GTFATLSELHCDK) was custom synthesized by BioMatik (Kitchener, Ontario, Canada). For the synthetic MP assay, commercial biomimetic oxidation kits (BMO kits) were purchased from HepatoChem, Inc. (Beverly, MA).

3.4. HLM assay

3.4.1. Generation of drug metabolites

The assay used for the HLM assay was adapted from work previously developed in the DeCaprio lab^{8, 24} and was employed for the generation of the metabolites for the drugs of interest as shown in Figure 10. All incubations were performed at 37°C in 25 mM ammonium bicarbonate buffer, pH 7.4 to mimic human physiological conditions. The components of the assay were combined in a total volume of 250 μL with their final concentrations were 4 mM of drug, 0.5 mg/mL of HLM, 1.5 mM of MgCl_2 , 1 mM of NADPH, 1.5 mM of G-6-P and 0.2 U/mL of G-6-P-D.

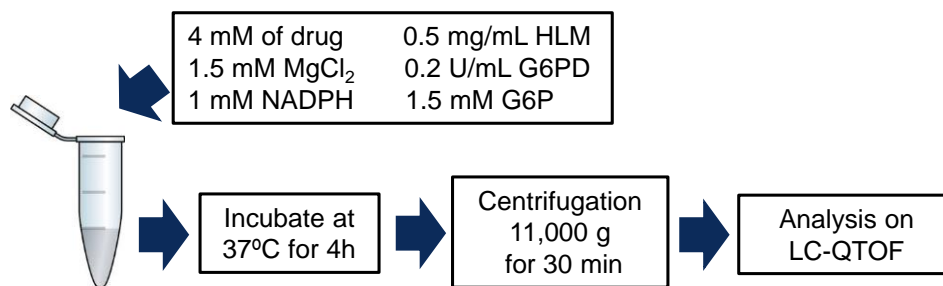


Figure 10: Schematic representation of the sample preparation via liver microsomes metabolic assay.

Following addition of assay components in a microfuge vial and vortexing briefly to ensure uniformity, the incubation was performed for 4 h. Upon completion of the incubation, vials were immediately centrifuged at 11,000 × g for 30 min. After centrifugation, aliquots of 200 µL of supernatant were removed from each vial and placed in separate, clean LC vials for analysis by high resolution mass spectrometry (HRMS). Negative controls, in which NADPH or drug of interest were omitted from the incubation mixture, were also prepared. All controls were run in parallel with positive samples, processed and analyzed in the same manner.

Initial analyses by QTOF-MS were performed in full scan mode. In this mode, the mass range was m/z 50-1000, with fragmentor voltage set to 100 V and no collision induced dissociation. The elution gradient started at 5% of B and ramped to 95% B over 17 min of analysis time, with 2 min of post-run for re-equilibration of the instrument. The analytical column was held at a temperature of 40°C during separation. Once the retention times of the metabolites generated were recorded, targeted MS/MS analysis was performed. MS/MS data were collected with the mass range set to m/z 50–1000 with collision energies of 10, 20, and 40 eV to allow for full visualization of fragments formed.

3.4.2. Adduction to selected peptides

To complement the negative ionization mode data previously performed in the DeCaprio laboratory,²⁴ analysis on the positive ionization mode of the drugs adducted to GSH were performed. The components of the HLM assay were combined in a total assay volume of 125 μ L of 50 mM sodium phosphate buffer, pH 7.4, at the following final concentrations: 1 mM drug of interest, 1 mg/mL HLM, 3 mM MgCl₂, 2 mM NADPH, 3 mM G6P, 0.4 U/mL G6PD, and 2 mM GSH. Assay components without GSH were first combined in a microfuge vial and vortexed briefly to ensure uniformity, followed by a pre-incubation of 15 min at 37°C. GSH was then added to complete the assay and achieve final assay volume, and vials were once again vortexed to ensure proper mixing. Incubation then ensued at 37°C for 3 h. Upon completion of incubation, vials were immediately centrifuged at 15,000 \times g at 4°C for 30 min. Following centrifugation, 100 μ L aliquots of supernatant were removed from each vial and placed in separate, clean LC vials, and analyzed as described in the previous section.

Before performing an incubation with the drugs of interest using the Hb β^{93} Cys peptide, an incubation with iodoacetamide (IAM) was done to provide a positive control with stoichiometric modification of the cysteine thiol. For this synthesis, 0.1 mg/mL of Hb β^{93} Cys peptide and 6 mM of IAM were prepared in 25 mM ammonium bicarbonate buffer, pH 7.4. Incubation then ensued in the dark for 1 h at 37°C. After the incubation, samples were analyzed using the LC-QTOF-MS in flow injection analysis (FIA; without LC column). The FIA experimental parameters consisted of an isocratic elution with 50% A and 50% B, 5 min of

analysis time, mass range was m/z 50-1000, with fragmentor voltage set to 100 V and no collision induced dissociation.

After the confirmation of adduction of IAM with the Hb $\beta^{93}\text{Cys}$ peptide, it was determined that the $\beta^{93}\text{Cys}$ present in the peptide was free to react with reactive electrophiles. The next step was to perform a modified HLM assay to metabolize the drugs of interest and generate RM that can act as nucleophiles. The components of the trapping assay were the same as shown in Figure 10 plus 0.5 mg/mL of the unadducted Hb $\beta^{93}\text{Cys}$ peptide that was then added to the mixture to complete the trapping assay. The samples were then incubated for 4 h at 37°C, followed by centrifugation at 11,000 \times g for 30 min. Then 200 μL of the supernatant was removed and placed in LC vials for analysis on the LC-QTOF-MS as described in the previous section, with the mass range set to m/z 50–2000, in order to collect the peptide data.

3.5. Synthetic metalloporphyrins assay

For the synthetic metalloporphyrin assay, commercial BMO kits were employed. The BMO kit utilizes synthetic metalloporphyrin to mimic the oxidative *in vivo* metabolism mediated by liver enzymes (cytochrome P450). In this task, two stages of the BMO kits were used: the screening kit and the optimization kit. The screening kit was used to perform the primary screen of the metabolites generated by each drug using 50 different reaction conditions. Then, the condition that produced the highest yield of the metabolites of interest was selected in order to identify the appropriate corresponding optimization kit. The optimization kit

consisted of further twelve reaction conditions and was used to identify the best condition to produce the metabolites of interest.

The sample preparation using the screening kit (Figure 11) consists of preparing two 6.25 mM drug solutions with both solvents provided with the kit, then the drug solution and provided reagent solutions are added to a well plate which contains solid reagents inside the wells. After all the components have been added, the plate is incubated at room temperature on an orbital shaker for 2 h. Then 50 μL of DMSO is added to each well to stop any further reaction. Finally, 20 μL aliquots are collected from each well and transferred to LC vials containing 200 μL of acetonitrile. A blank of each reaction condition was also obtained without the addition of any analyte, in order to differentiate drug metabolites from the reaction mix components. The diluted samples are then analyzed in the LC-QTOF-MS. An initial analysis was performed in FIA mode to determine the conditions that generated the metabolites of interest, then chromatographic separation was performed on the samples with the best experimental conditions.

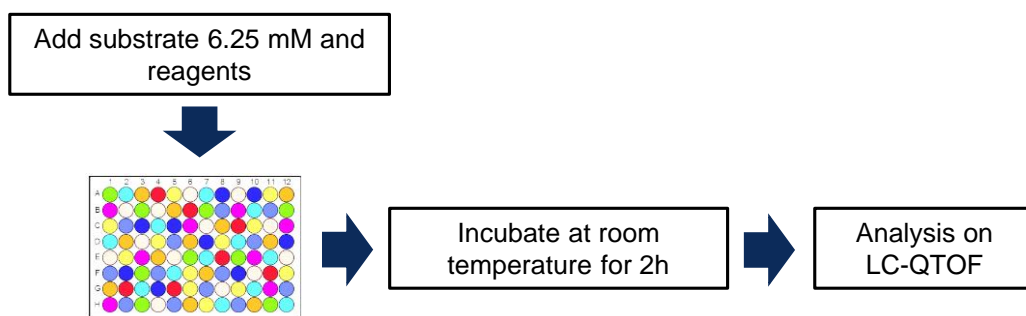


Figure 11: Schematic representation of the sample preparation via synthetic metalloporphyrin catalysts.

For the optimization kit, the sample preparation involved preparing a 6.25 mM solution of the drug of interest with the provided solvent, then adding 50 μL of the drug solution to each of the 12 wells. The next step was to add the provided reagent solutions to each well and incubate for 2 h on an orbital shaker at room temperature. Fifty μL of DMSO was then added to each well and 20 μL aliquots of the resulting solutions were transferred to HPLC vials containing 200 μL of acetonitrile. Then, each condition was tested on the HRMS system to determine the condition that produced the highest yield of the desired metabolites in the same manner as for the screening kit.

3.6. Electrochemical assay

3.6.1. Optimization of EC assay

The EC experiments were performed on an eDAQ ER 466C Integrated Potentiostat System (Colorado Springs, CO, USA). For the optimization of the EC assay the following experimental conditions were tested: WE, bulk electrolysis potential and duration. Two electrodes were tested for the initial studies with the EC assay: a gold electrode and a glassy carbon electrode. For the adduction studies, a Pt mesh electrode with higher surface area was utilized. Two potentials were tested for the bulk electrolysis for each drug, chosen based on the cyclic voltammetry (CV) results for the drug. Lastly, the duration of the bulk electrolysis was also evaluated with aliquots collected at 5, 10, 20, 30, 40, 50 and 60 min.

3.6.2. Generation of drug metabolites

A CV experiment was conducted for each drug of interest to determine the

oxidation voltage to be used during the bulk electrolysis analysis. Additionally, a CV was performed on the buffer solution without any added drug to differentiate redox peaks generated by the buffer and drugs of interest. Two WEs were tested at this phase; a gold electrode and a glassy carbon electrode, both with 3 mm diameter. A saturated calomel electrode (SCE) was used as RE, and a Pt/Ti rod as CE. For both CV and bulk electrolysis experiments, a 4 mM solution of the drug of interest was prepared in 100 mM ammonium bicarbonate buffer with pH of 7.4.

Then, for the bulk electrolysis, the redox potential was fixed at the voltage identified by the CV. A two-compartment cell vial was used with 1 mL of the drug solution in the first compartment (glass cylinder) with the WE; and the buffer solution was placed in the second compartment (beaker) with the CE and RE as shown in Figure 12. The solutions were maintained under magnetic stirring at room temperature for the entire duration of the experiment. Aliquots were collected at 5, 10, 20, 30, 40, 50 and 60 min to determine the ideal bulk electrolysis time. Finally, the aliquots collected were analyzed by HRMS in the same way as described in section 3.4.1.

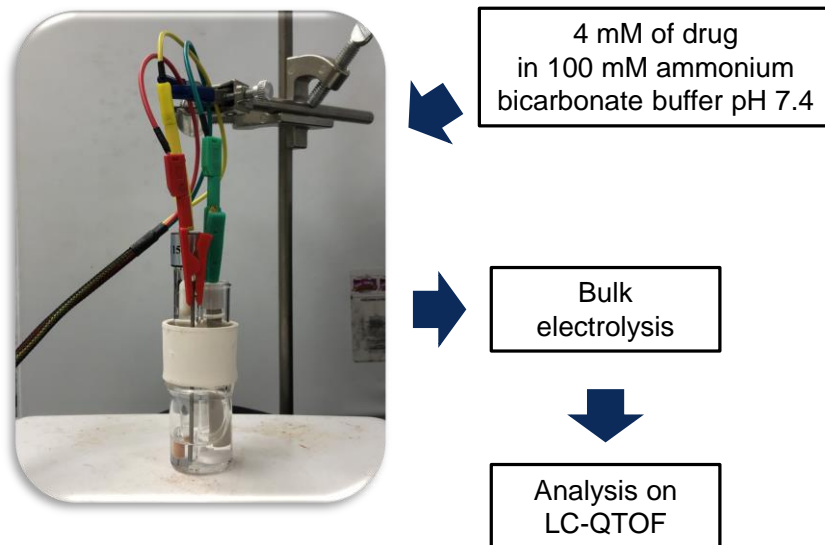


Figure 12: Schematic representation of the bulk electrolysis performed for the generation of metabolites via EC assay.

3.6.3. Adduction to selected peptides

For the EC trapping assay, a Pt gauze, expanded metal mesh, 0.34 mm thick electrode (Alfa Aesar, Ward Hill, MA, U.S.) was used as the WE electrode. The same experimental procedure was performed as described in the previous section with the addition of the trapping agent. Fifty μL of a 2 mg/mL Hb $\beta^{93}\text{Cys}$ peptide solution in ammonium bicarbonate buffer 100 mM, pH 7.4 was pipetted to an LC vial. Then 150 μL of the bulk electrolysis aliquot was added to the vial, followed by a 10 min incubation on an orbital shaker at room temperature. Finally, samples were analyzed by HRMS.

3.7. *In silico* methods

The chemical structure of each drug of interest was drawn in the MetaSite software (v.6.0; Molecular Discovery, Pinner, UK), and a prediction of possible

metabolites and electrophilic hotspots was performed using the liver metabolic pathway. After the predictions were generated, the top 10 metabolites for each drug were selected, based on their likelihood of formation and potential electrophilic reactivity. The predictions made were then compared with the *in vitro* experimental results.

The Visual Molecular Dynamics (VMD) software was used to generate the structure of the Hb $\beta^{93}\text{Cys}$ peptide in solution. The pdb file containing the sequence of the Hb $\beta^{93}\text{Cys}$ peptide was uploaded to the software. The VMD software can display the 3D representation of the molecule using several drawing styles. In this work, the licorice representation was selected in the Drawing Method tab.

3.8. LC-QqQ-MS dMRM analysis

For the development of a dMRM method to analyze drug-peptide adducts, Agilent MassHunter Optimizer software was employed to determine the best data acquisition parameters for dMRM. The Optimizer report includes precursor ion, product ions identified, collision energies, fragmentor voltage, and abundances. Optimizer analysis was performed in FIA mode and the experimental parameters consisted of an isocratic elution with 20% A and 80% B, 1 min of analysis time, mass range of m/z 50-2000, fragmentor voltage set to 100 V, and no collision induced dissociation.

Collected transitions were used to develop the dMRM method. Chromatographic separation was achieved using a gradient consisting of 5% of B

and ramped to 95% B over 17 min of analysis time, with 2 min of post-run for re-equilibration of the instrument. The analytical column was held at a temperature of 40°C during separation. A dMRM method was chosen to increase selectivity, using analyte retention times, detection windows of 0.5 min, and scan cycle time of 500 ms to allow for the detection of multiple analytes in a small window.

3.9. Peptide adducts analysis

Agilent's MassHunter BioConfirm software (version B.08.00) was used to analyze the data collected for the peptide adducts. The "peptide digest" method was used, the condition was "reduced," the Hb $\beta^{93}\text{Cys}$ peptide sequence was added, trypsin was used as the enzyme, and the modifications were methylation, hydroxylation, and any appropriate custom modifications. The custom modifications were created individually for each drug of interest based on both metabolites reported in the literature and those generated *in silico* by MetaSite. Once the workflow was completed for the MS studies, the predicted modifications were targeted and analyzed via BioConfirm software, where any potential drug adducts were recorded. A flow chart with the work flow for the Hb $\beta^{93}\text{Cys}$ adducts is shown in Figure 13.

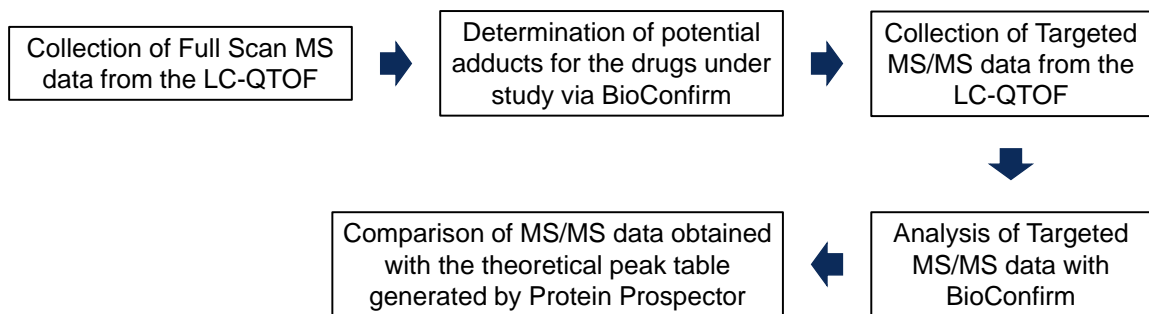


Figure 13: Flowchart of workflow for Hb $\beta^{93}\text{Cys}$ peptide adduct analysis.

The spectra were collected for the Targeted MS/MS studies, compared to the theoretical peak list supplied by Protein Prospector, and confirmed peaks were recorded. Peaks were considered identified if the observed mass was within 0.1 Da of the mass reported in the theoretical peak table. If the mass differential was less than 0.5 Da, the peak was considered a possible match. All peaks with a mass differential of >0.5 Da were eliminated.

4. RESULTS AND DISCUSSION

4.1. Task 1 – Generation of drug metabolites

The first part of this study was the identification and comparison of the SM and RM formed by the three different approaches: 1) HLM assay, 2) EC assay and 3) synthetic MP catalysts. No such direct comparison of all three approaches to drug (licit or illicit) metabolism has previously been reported. Ultimately, these methods were evaluated for production of specific adducted GHS and Hb peptides for use as standards in the LC-QqQ-MS based assay.

4.1.1. *In silico* generation of drug metabolites:

MetaSite generated several possible metabolites for each drug of interest, most of them were well known metabolites, and some were not generated by any *in vitro* system evaluated in this work. However, novel metabolites of THC and MDMA were correctly predicted by MetaSite and later seen with the *in vitro* metabolism. In Figure 14, there is a screenshot of THC as the prediction substrate and the top three metabolites predicted. The first one is the well-known THC

metabolite 11-OH-THC, the other two were not previously reported in the literature and were named as nor-9-methylidene- Δ^9 -tetrahydrocannabinol (methylidene-THC), and 9-carbaldehyde- Δ^9 -tetrahydrocannabinol (11-CHO-THC).

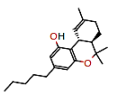
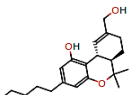
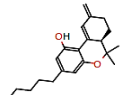
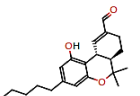
Substrate	MiM	LogP	LogD4	LogD7	LogD9	
 THC	314.224580	7.07	7.07	7.07	7.04	
Metabolite	MiM	LogP	LogD4	LogD7	LogD9	Mechanism
 11-OH-THC	330.219495	5.59	5.59	5.59	5.56	Aliphatic Hydroxylation
 methylidene-THC	312.208930	6.64	6.64	6.62	5.82	Vinylic Dehydrogenation
 11-CHO-THC	328.203845	5.70	5.70	5.69	5.67	Aliphatic Carbonylation

Figure 14: MetaSite liver metabolism prediction for THC.

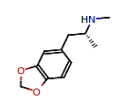
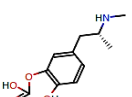
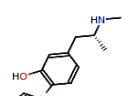
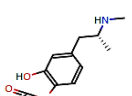
Substrate	MiM	LogP	LogD4	LogD7	LogD9	
 MDMA	193.110279	1.99	-1.49	-0.44	1.40	
Metabolite	MiM	LogP	LogD4	LogD7	LogD9	Mechanism
 3,4-dihydroxy-N,N-dimethylamphetamine	225.100108	1.41	-2.08	-1.03	0.81	O-Dealkylation
 3,4-dihydroxy-N,N-dimethylamphetamine	209.105193	1.23	-2.25	-0.95	0.80	O-Dealkylation
 3,4-dihydroxy-N,N-dimethylamphetamine	225.100108	1.41	-2.07	-0.88	0.92	O-Dealkylation

Figure 15: MetaSite liver metabolism prediction for MDMA.

In Figure 15, there is a screenshot of MDMA as the prediction substrate and the three of the metabolites predicted. Two predicted metabolites shown in the screenshot were not previously reported in the literature but were found with the *in vitro* systems investigated in this study, they were named as 3-hydroxy-4-phenylformylate amphetamine (HFA), and 3-hydroxy-propylphenoxyformylic acid amphetamine (HPA).

4.1.2. Optimization of the synthetic MP assay:

To find the best reaction conditions for the synthetic MP assay, the first step was to use the BMO screening kit. A set of 50 conditions with two solvents was tested and analyzed using flow injection analysis (FIA) on the LC-QTOF-MS. A summary of the positive mode ions found for each condition is shown in Appendix 1 a-d. The set of conditions that best produced metabolites for APAP was A6 with solvent 1; for MDMA was A5 with solvent 1; for METH was A2 with solvent 2; and for THC was D4 solvent 1. The FIA full scan QTOF mass spectra for these products are shown in Figure 16. The choice of the best conditions was based on the number of metabolites found and their ion intensity.

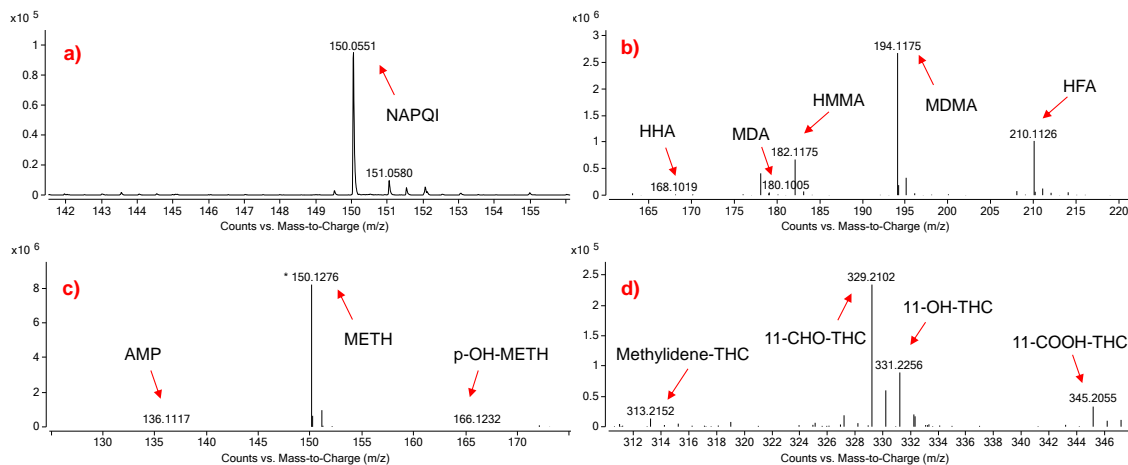


Figure 16: FIA QTOF-MS full scan spectrum of the BMO screening kit for a) APAP; b) MDMA; c) METH; and d) THC.

The only metabolite of APAP found was NAPQI, with mass error of 0.7 ppm, shown in Figure 16a. Three metabolites of MDMA were identified as can be seen in Figure 16b; 3,4-dihydroxyamphetamine (HHA), 3,4-methylenedioxyamphetamine (MDA), 3,4-dihydroxymethamphetamine (HHMA), HFA, with mass errors of -3.6, -11.1, -0.6, and 0.5 ppm, respectively. Two metabolites of METH were identified, as can be seen in Figure 16c; amphetamine (AMP) and p-hydroxymethamphetamine (p-OH-METH), with mass errors of -6.6 and 3.6 ppm, respectively. Four metabolites of THC were identified, as seen in Figure 16d; 11-hydroxy- Δ^9 -tetrahydrocannabinol (11-OH-THC), 11-nor-9-carboxy- Δ^9 -tetrahydrocannabinol (11-COOH-THC), methylidene-THC and 11-CHO-THC with mass errors of, -5.1, -3.2, -2.7, and -3.2 ppm respectively. Three novel metabolites were found with the BMO screening kits and with the aid of MetaSite software prediction. The proposed structures for these metabolites are shown in Figure 17.

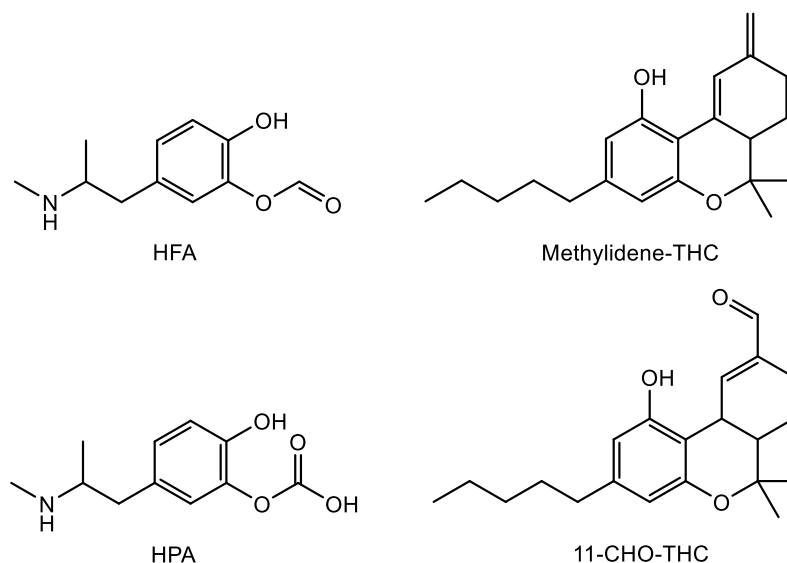


Figure 17: Proposed chemical structures of the four novel metabolites found with the screening BMO kit with the aid of MetaSite software predictions.

The next step was to use the BMO optimization kit to ramp up the reaction to semi-preparative levels. The optimization kits used for each drug were unique, since the best conditions selected with the screening kit were different for each drug of interest. The optimization kit contained 12 reaction conditions to be tested. The condition that best produced metabolites for APAP was A2; for MDMA was A5; for METH was A11; and for THC was A10. A summary of the positive mode ions found for each condition is shown in Appendix 1 e-h. The full scan QTOF mass spectra for these products are shown in section 4.1.4 and the MS/MS spectra will be discussed in section 4.1.5. Only the NAPQI metabolite was identified for APAP. Three metabolites of METH were identified; AMP, p-OH-METH, and methcathinone. Four metabolites of MDMA were identified; HHA, HMMA, HFA and HPA. Five metabolites of THC were identified; 11-OH-THC, 11-COOH-THC, methylidene-THC, 11-CHO-THC, and 8 α ,11-dihydroxy- Δ^9 -tetrahydrocannabinol

(dihydroxy-THC). Another novel metabolite was found with the optimization kit for MDMA; HPA, and its postulated structure is shown in Figure 17.

4.1.3. Optimization of EC assay:

During the EC optimization process, two WEs were tested, gold and glassy carbon, and it was determined that glassy carbon generated a greater number of metabolites. The cyclic voltammograms obtained with the drugs of interest using glassy carbon as the WE, calomel standard as the RE, and Pt/Ti rod as the CE can be seen in Figure 18.

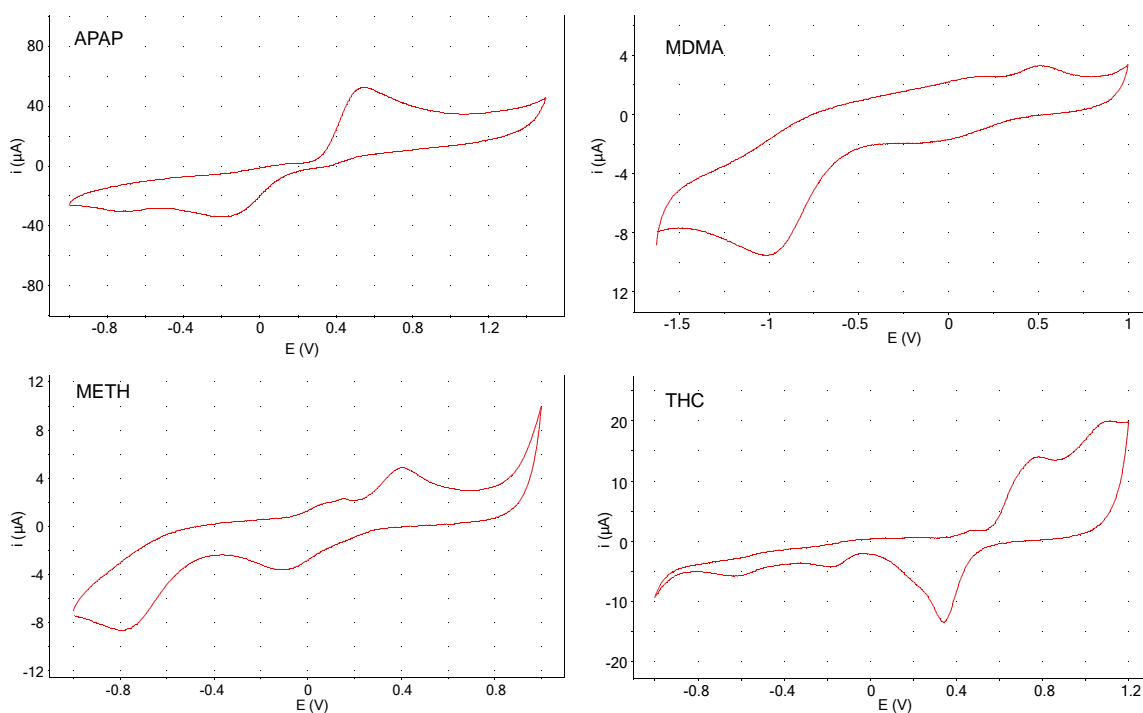


Figure 18: Cyclic voltammogram of APAP, using glassy carbon as the WE, calomel standard as the RE, and Pt/Ti rod as the CE.

For APAP, the scan speed was of 200 mV/s at pH 7.4, and an oxidation peak at +600 mV and a reduction peak at -200 mV were observed. For MDMA, the

scan speed was of 250 mV/s at pH 7.4, and an oxidation peak at +500 mV and a reduction peak at -1 V were observed. For METH, the scan speed was of 100 mV/s at pH 7.4, and an oxidation peak at +480 mV and two reduction peaks at -100 mV and -750 mV were observed. For THC, the scan speed was of 50 mV/s at pH 7.4, and an oxidation peak at +700 mV and a reduction peak at +.340 mV were observed.

The ideal oxidation voltages determined by CV for each of the drugs under study were determined to be +600 mV for APAP, -1.045 V for MDMA, +480 mV for METH, and +700 mV for THC. When analyzing the different aliquots collected at 5, 10, 20, 30, 40, 50, and 60 min for the bulk electrolysis, it was shown that the abundance on the MS spectra did not change significantly over time for each metabolite generated. For some cases, such as NAPQI, the abundance decreased over time, showing potentially that the metabolites generated were being subjected to redox reactions themselves. Based on these results, the duration of the bulk electrolysis was chosen to be 5 min for all drugs of interest.

4.1.4. Full Scan MS analysis of the obtained metabolites:

Optimization of the LC-QTOF acquisition method used for the analysis of the metabolites found in the assay systems ensured that a single method could be used to analyze all drugs of interest. Full scan data was collected for each drug after the metabolism with each *in vitro* approach. Agilent's Qualitative Analysis B.07.00 software was used to analyze the obtained data, where the chromatograms were extracted using the extracted ion chromatogram (XIC) feature. On XIC, the *m/z* of potential metabolites are put on a list of *m/z* values of

interest, then the chromatogram is extracted, and the retention times for each compound are recorded for further analysis using targeted MS/MS.

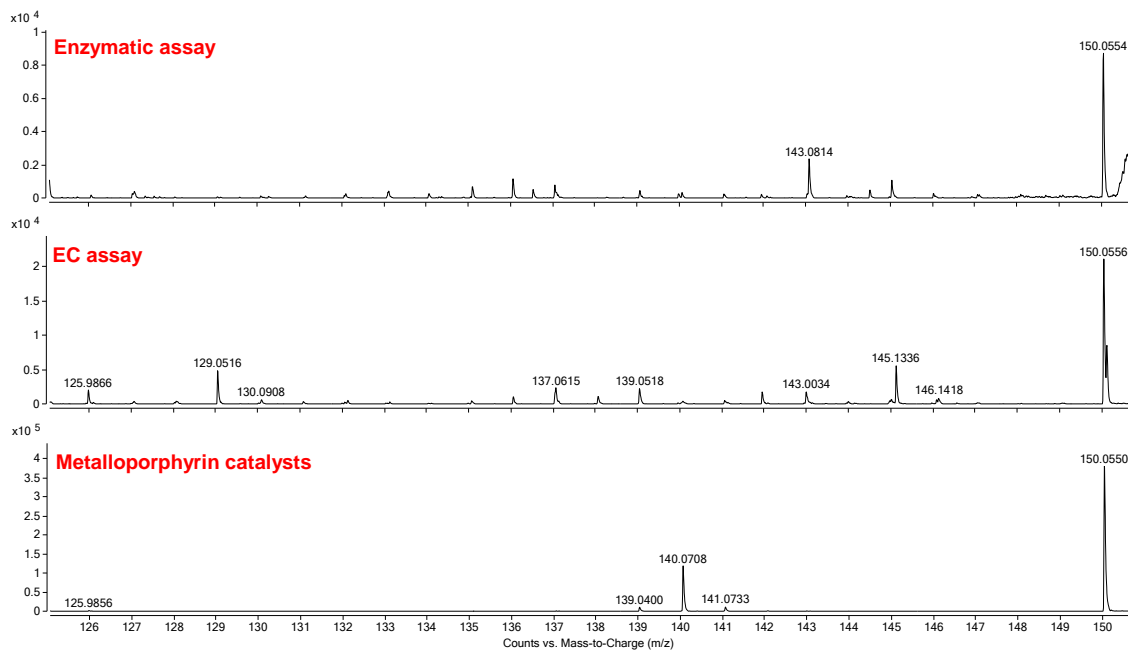


Figure 19: XIC spectra for NAPQI obtained with the three methods.

For APAP, the well-known metabolite N-acetyl-p-benzoquinone imine (NAPQI) with m/z of 150.0550 was found to be formed with all three methods as shown in Figure 19. Two major metabolites were found for MDMA; 3,4-dihydroxymeth-amphetamine (HHMA) and 3,4-methylenedioxyamphetamine (MDA), with m/z of 182.1176 and 180.1025, respectively. These two major metabolites were found with all three *in vitro* methods and XIC data for them is shown in Figures 20 and 21.

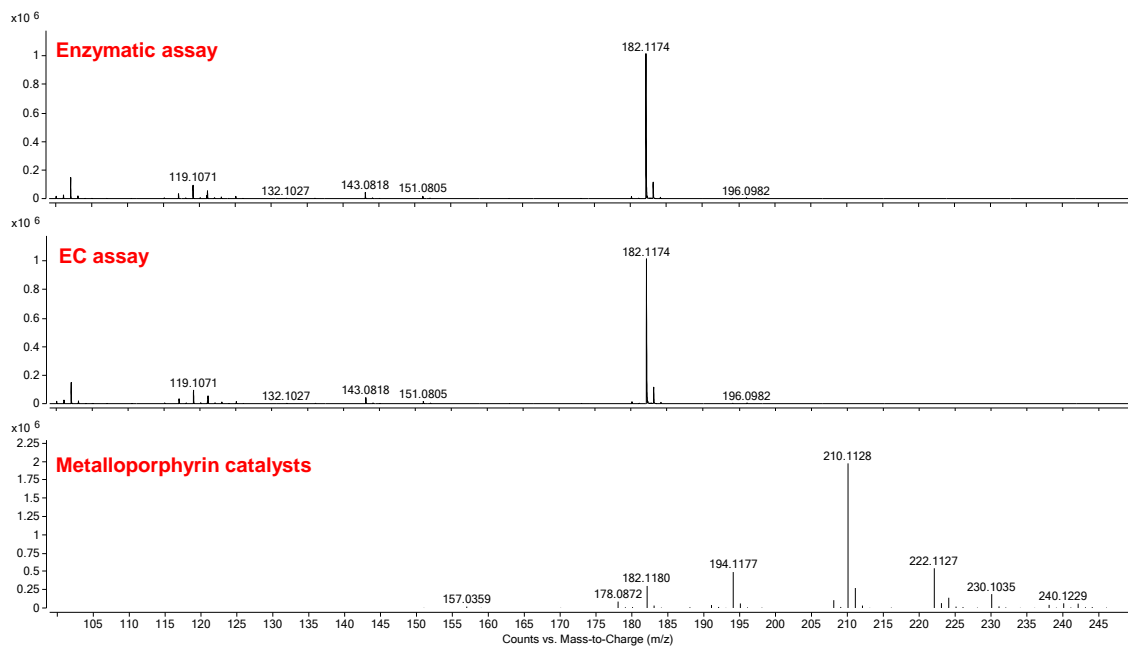


Figure 20: XIC spectra for HHMA obtained with the three methods.

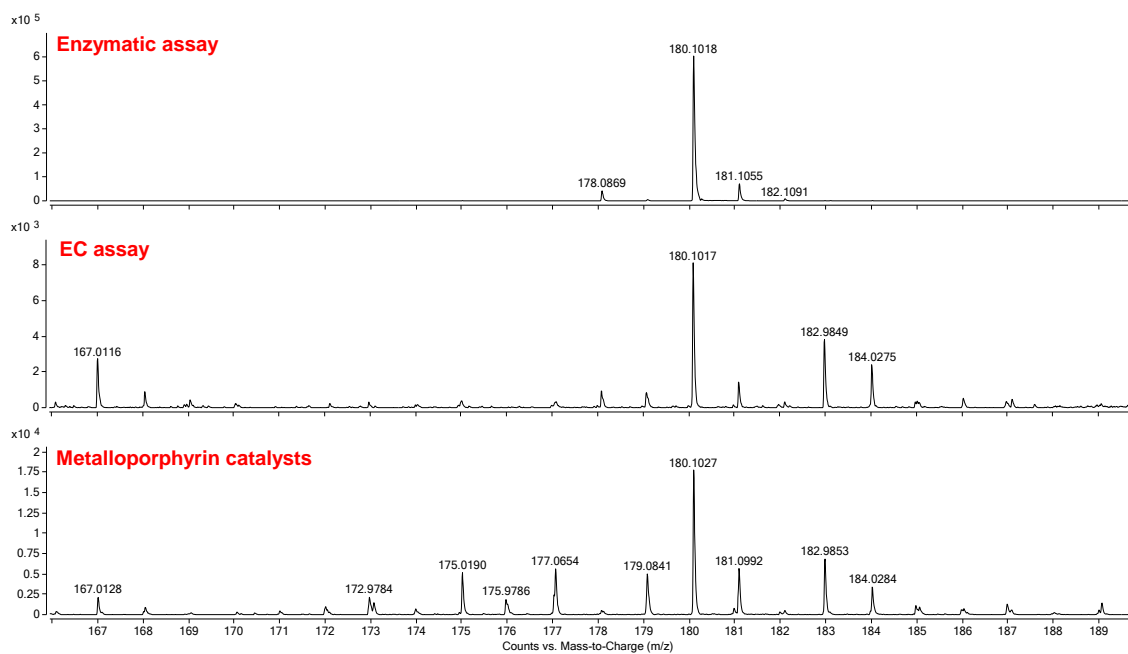


Figure 21: XIC spectra for MDA obtained with the three methods.

Four minor metabolites were also found with MDMA; 3-hydroxy-4-phenylformylateamphetamine (HFA), with m/z of 210.1125 obtained with the three

methods; dihydroxyamphetamine (HHA) with m/z of 168.1025 obtained with the HLM assay only; 4-(2-aminopropyl)-1,2-benzoquinone (quinone derivative) with m/z of 166.0868 obtained with the EC assay only; and 3-hydroxy-propylphenoxyformylic acid amphetamine (HPA) with m/z of 226.1079 obtained with the synthetic MP catalysts only. The XIC data for the minor metabolites found for MDMA can be seen in Appendix 2 a-d.

For the metabolism of METH, a major product was found; amphetamine (AMP) with m/z of 136.1126. AMP was found with the three *in vitro* methods and XIC data for them can be seen in Figure 22. Five other metabolites were also found with the METH metabolism, including a novel metabolite, methcathinone, with m/z of 164.1075 obtained with the HLM assay and synthetic MP catalysts. XIC data for this product can be seen in Figure 23.

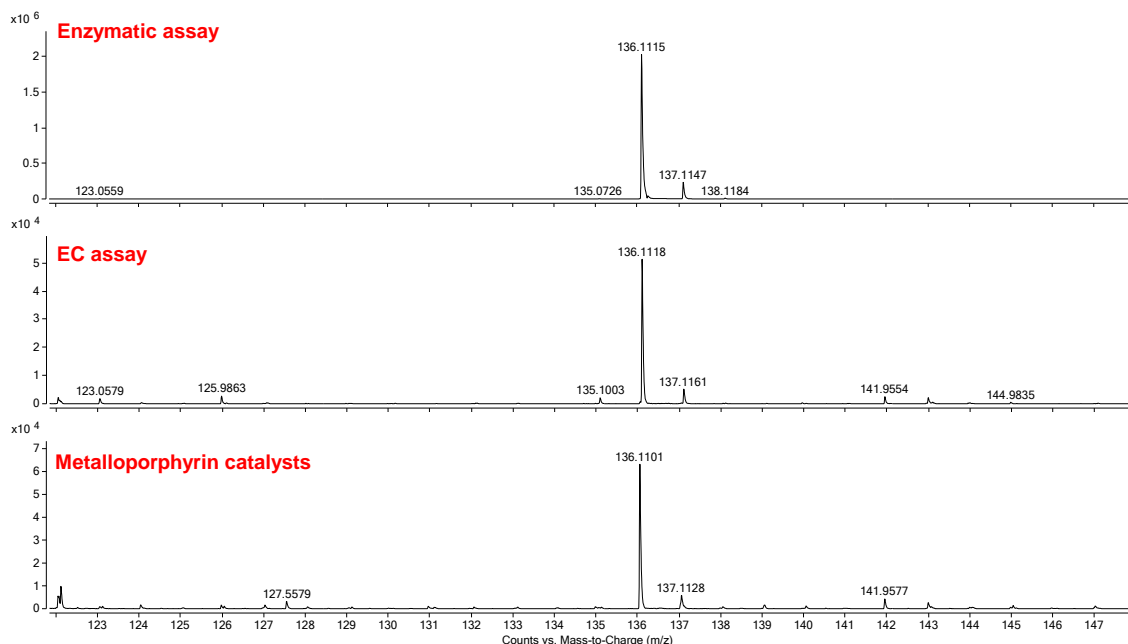


Figure 22: XIC spectra for AMP obtained with the three methods.

Other metabolites included N-hydroxy-methamphetamine (N-OH-METH), with m/z of 166.1226, obtained with HLM assay and EC assay; N-hydroxy-amphetamine (N-OH-AMP) with m/z of 152.1075 obtained with the HLM assay; N-1-Phenylpropan-2-yl (imine intermediate) with m/z of 148.1126 obtained with the EC assay; and p-hydroxy-methamphetamine (p-OH-METH) with m/z of 166.1226 obtained with the synthetic MP catalysts. The XIC data for the minor metabolites found for METH can be seen in Appendix 2 e-h.

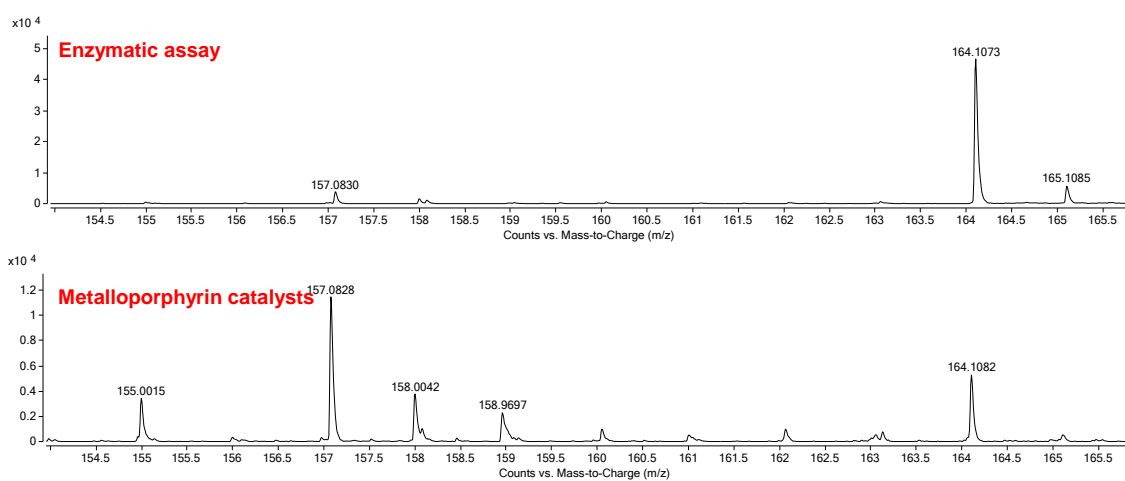


Figure 23: XIC spectra for methcathinone obtained with the HLM assay and synthetic metalloporphyrin catalysts.

Two major metabolites were found for THC; 11-nor-9-carboxy- Δ^9 -tetrahydrocannabinol (11-COOH-THC), and 11-nor-9-carbaldehyde- Δ^9 -tetrahydrocannabinol (11-CHO-THC), with m/z of 345.2066 and 329.2111, respectively. These two major metabolites were found with all three *in vitro* methods; XIC data can be seen in Figures 24 and 25.

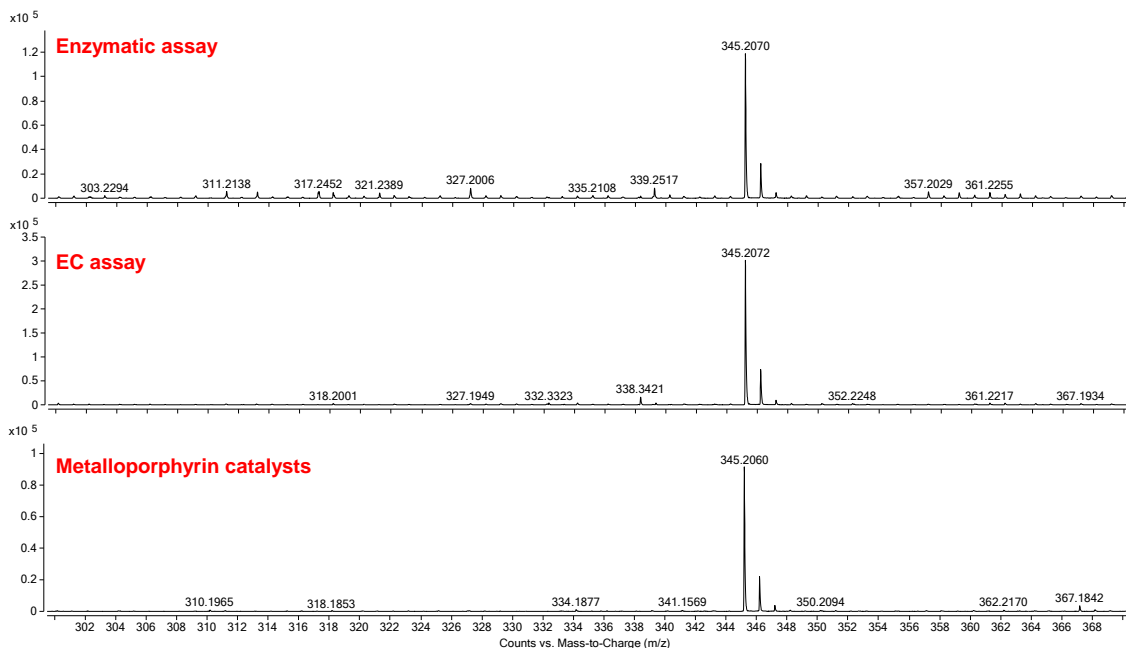


Figure 24: XIC spectra for 11-COOH-THC obtained with the three methods.

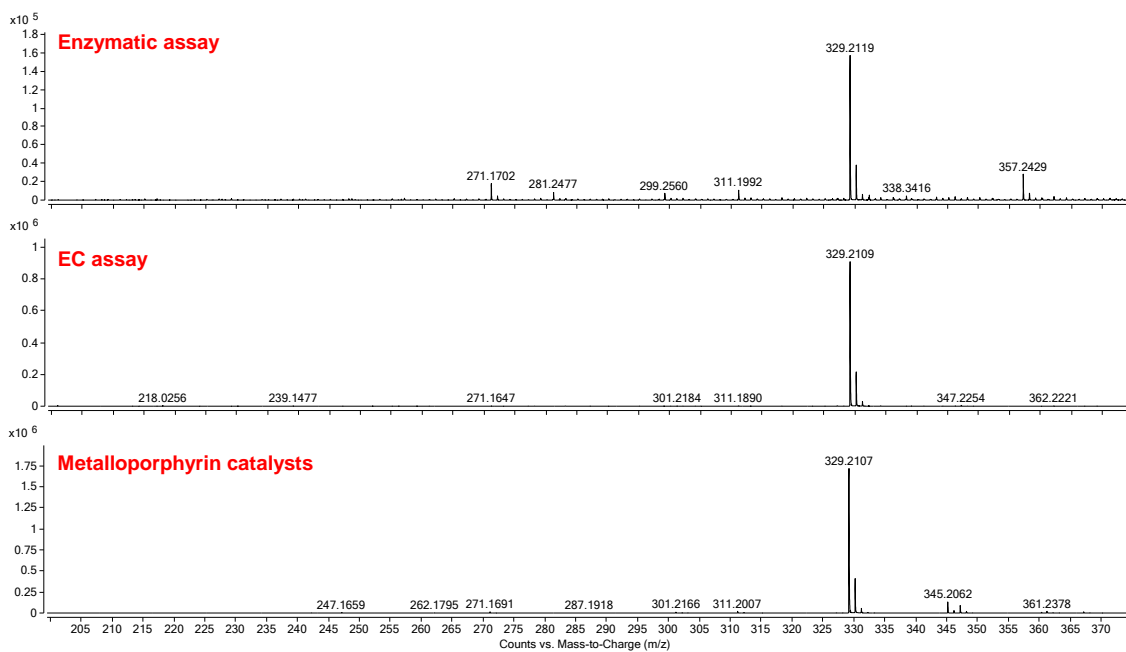


Figure 25: XIC spectra for 11-CHO-THC obtained with the three methods.

Three minor metabolites were also found with for THC; 11-hydroxy- Δ^9 -tetrahydrocannabinol (11-OH-THC) with m/z of 331.2273 obtained with the HLM

assay and synthetic MP catalysts; nor-9-methylidene- Δ^9 -tetrahydrocannabinol (methylidene-THC) with m/z of 313.2162 obtained with all three methods; and 8 α ,11-dihydroxy- Δ^9 -tetrahydrocannabinol (dihydroxy-THC) with m/z of 347.2217 obtained with the EC assay and synthetic MP catalysts. The XIC data for the minor metabolites found for METH can be seen in Appendix 2 i-k.

4.1.5. Targeted MS/MS analysis of the obtained metabolites

4.1.5.1. APAP

The results for the biotransformation of APAP for each of the *in vitro* assays are summarized in Table 3. It was found that NAPQI, the well-known reactive metabolite of APAP was the major and only metabolite found for all three methods.

Table 3: Metabolite found with APAP for each assay.

Metabolite	Formula	<i>In vitro</i> model	Observed m/z	Fragments
NAPQI	C ₈ H ₈ NO ₂ ⁺	HLM assay	150.0546	108.0449, 80.0502
		EC assay	150.0549	108.0413, 80.0493
		Synthetic MP	150.0550	108.0449, 80.0500

The MS/MS spectrum for NAPQI generated with the HLM assay is shown in Figure 26a. Two characteristic transition ions were present at m/z 80.0502 (C₅H₆N⁺) and m/z 108.0449 (C₆H₆NO⁺). NAPQI was expected to be found with the HLM assay, since it is a well-known metabolite of APAP and its oxidation is mediated by CYP2E1, CYP1A2, CYP3A4, and CYP2A6 subfamilies of the P450 oxidase system.⁷⁷

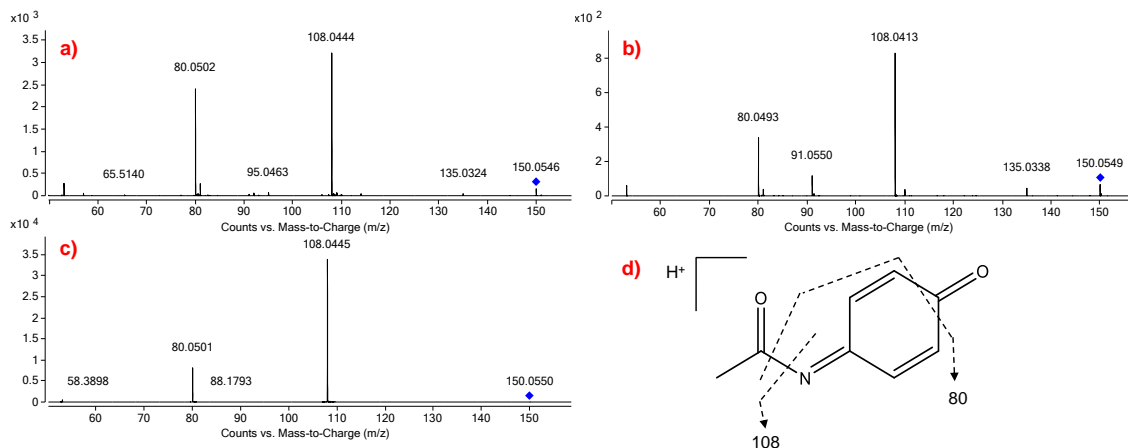


Figure 26: LC-QTOF-MS/MS spectra for the peaks of interest observed for the APAP metabolite NAPQI, obtained with a) HLM assay; b) EC assay; c) synthetic MP catalysts; d) fragmentation pattern for NAPQI.

For the EC assay, the potential for the bulk electrolysis was fixed at +600 mV, as determined by the CV. The MS/MS spectrum for NAPQI generated by EC oxidation is shown in Figure 26b, where APAP is oxidized by losing $2e^-$ and $2H^+$ leading to the formation of NAPQI, as shown in Figure 27. A similar approach was used by Madsen *et al.*³³ to oxidize paracetamol (APAP) into its reactive metabolites, focusing on the electrochemical generation of NAPQI and posterior trapping with GSH.

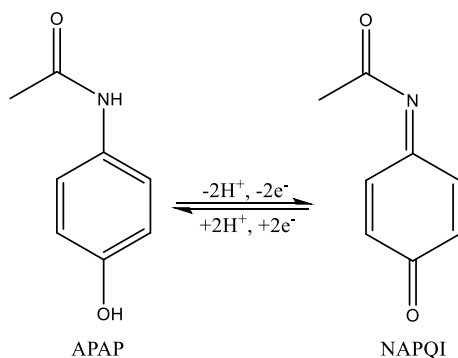


Figure 27: Reaction scheme of the EC oxidation of APAP to NAPQI.

In the present study, the synthetic MP catalysts were able to successfully mimic the peroxidase oxidation of APAP; the MS/MS spectrum for NAPQI produced in this assay is shown in Figure 26c. The formation of NAPQI via the biomimetic system has been well studied. Bearnadou *et al.*⁷⁸ demonstrated the formation of NAPQI with four different water soluble metalloporphyrins containing either Mn or Fe. The best catalyst for the oxidation of APAP was found to be an Fe(III) derivative of tetrasodium meso-tetrakis(p-sulfonatophenyl)porphyrin. Chapman *et al.*³⁸ also showed that an iron(III) porphyrin (FeP) was responsible for the generation of NAQPI from APAP.

4.1.5.2. MDMA

Cytochrome P450 enzymes have been extensively reported to mediate the metabolism of MDMA.^{79, 80} However, the metabolism of MDMA via synthetic metalloporphyrins has not been reported in the literature. Since a commercial kit was used in this study and as the composition of the MP is proprietary, it is speculated that an Fe(III) porphyrin was responsible for the generation of the MDMA metabolites identified.

The voltametric behavior of various amphetamine-like drugs, including AMP, METH, MDA, and MDMA with a glassy carbon electrode was investigated by Garrido *et al.*⁸¹ With the exception of AMP, the authors found that all of the amphetamines studied are electroactive, and their oxidation mechanism is related to an oxidation process occurring on the aromatic nucleus and/or the secondary amine group present in the molecules. It was also found that the redox

biotransformation of MDMA in aqueous media uses the same number of electrons and protons.⁸¹

The results for the metabolism of MDMA with the three approaches are summarized in Table 4. There were two major metabolites that were found in common with the three methods; HHMA and MDA. Additionally, four minor metabolites were also found; HFA, HHA, HPA and a quinone derivative.

Table 4: Metabolites found with MDMA for each system.

Metabolite	Formula	<i>In vitro</i> model	Observed <i>m/z</i>	Fragments
HHMA	C ₁₀ H ₁₆ NO ₂ ⁺	HLM assay	182.1168	151.0754, 133.0652, 123.0446
		EC oxidation	182.1160	151.0755, 133.0646, 123.0434
		Synthetic MP	182.1174	151.0753, 133.0649, 123.0442
MDA	C ₁₀ H ₁₄ NO ₂ ⁺	HLM assay	180.1028	163.0759, 135.0444, 105.0702
		EC oxidation	180.1017	163.0767, 135.0380
		Synthetic MP	180.1051	163.0717, 135.0433, 105.0697
HFA	C ₁₁ H ₁₆ NO ₃ ⁺	HLM assay	210.1121	192.1061, 123.0456, 105.0728
		EC oxidation	210.1123	192.1027, 179.0700, 123.0440
		Synthetic MP	210.1117	179.0702, 151.0749, 123.0441
HHA	C ₉ H ₁₄ NO ₂ ⁺	HLM assay	168.1029	152.0712, 89.0591, 45.0331
Quinone derivative	C ₉ H ₁₂ NO ₂ ⁺	EC oxidation	166.0868	135.0437, 77.0383
HPA	C ₁₁ H ₁₆ NO ₄ ⁺	Synthetic MP	226.1076	195.0876, 166.0865, 136.0726

The formation of HHMA is catalyzed by CYP2D6, CYP1A2, CYP2B6 and CYP3A4 enzymes via O-demethylation, and it is the main metabolite found in humans.^{79, 80, 82} For the EC assay, the potential set for the bulk electrolysis was fixed at -1.045 V, as determined by the CV. The proposed reaction mechanism involves a water molecule cleaving the methylenedioxy ring, forming methanol and a quinone intermediate. The quinone is then reduced to form HHMA as shown in Figure 28.

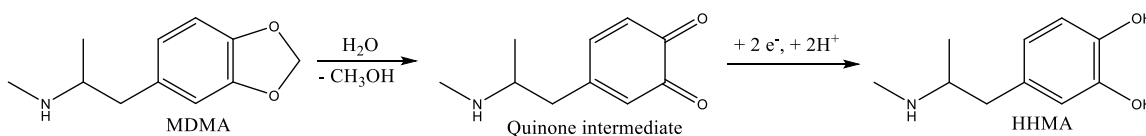


Figure 28: Reaction scheme of the EC redox transformation of MDMA to generate HHMA.

To aid in the interpretation of the QTOF-MS/MS spectra, fragmentation patterns were compiled using published data and, where not available, fragmentation was predicted using ChemDraw Prime software (PerkinElmer, version 21.0.0) to produce plausible fragments. The QTOF-MS/MS spectra obtained for the major metabolite HHMA for each of the *in vitro* methods is shown in Figure 29. The spectrum of HHMA ([M+H]⁺ with *m/z* 182) shows a loss of methylamine forming the fragment ion with *m/z* 151; the fragment ion with *m/z* 133 can be considered as a secondary fragment of the ion with *m/z* 151 and corresponds to a loss of a hydroxyl group. The β-C-C cleavage leads to the fragment *m/z* 123 due to the loss of ethylmethylamine.

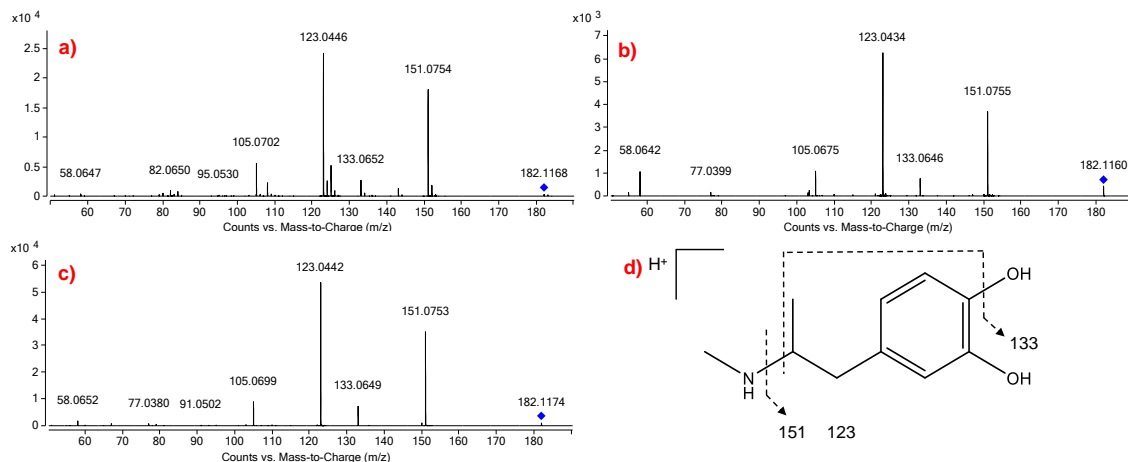


Figure 29: LC-QTOF-MS/MS spectra for the peaks of interest observed for the MDMA metabolite HHMA, obtained with a) HLM assay; b) EC assay; c) synthetic MP catalysts; d) fragmentation pattern for HHMA.

The second major metabolite found was MDA, produced via an N-demethylation reaction catalyzed by CYP2D6, CYP1A2, and CYP2B6 enzymes.⁸² For the EC assay, the proposed reaction mechanism involves a water molecule attacking the methyl group and forming methanol, then a hydrogen shift from the water molecule to the amine group, as seen in Figure 30.

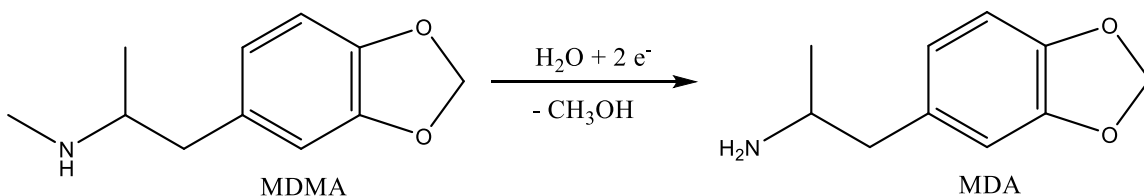


Figure 30: Reaction scheme of the EC redox transformation of MDMA to generate MDA.

The transitions found with the MS/MS spectra of the major metabolite MDA ($[M+H]^+$ with m/z 180) show a loss of NH_3 to a fragment ion with m/z 163 and a β -C-C cleavage leading to a 1,3-benzodioxol-5-ylmethyl cation with m/z 135 due to

the loss of ethylamine (Figure 31). The fragment ion with m/z 105 can be considered as a secondary fragment of the ion with m/z 135 and corresponds to the cleavage of the methylenedioxy ring.

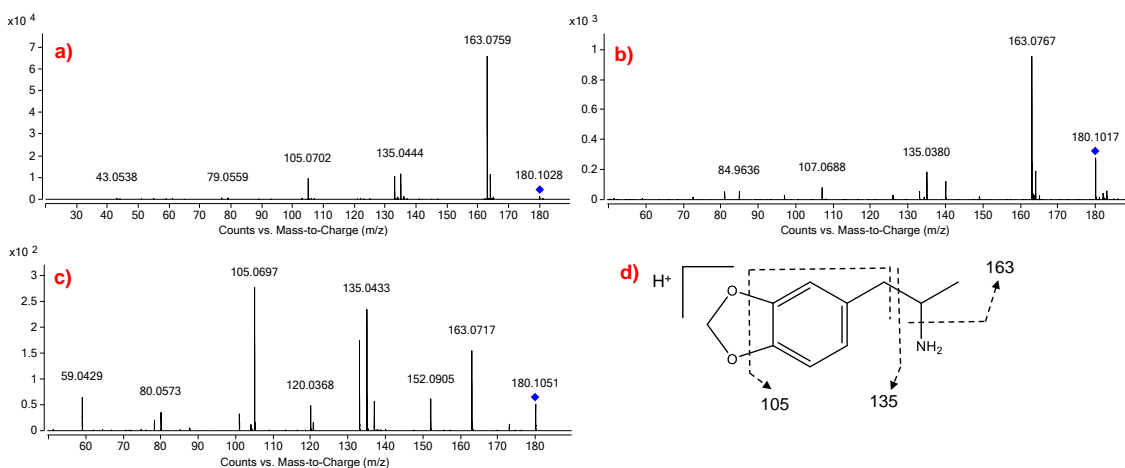


Figure 31: LC-QTOF-MS/MS spectra for the peaks of interest observed for the MDMA metabolite MDA, obtained with a) HLM assay; b) EC assay; c) synthetic MP catalysts; d) fragmentation pattern for MDA.

The minor metabolite HFA ($[M+H]^+$ with m/z 210) was found with all three methods to generate drug metabolites. It is a novel metabolite of MDMA that has not been reported in the literature before. It is proposed that this new metabolite is formed by the oxidation of the dioxolane ring of MDMA, forming a formylate group, mediated by CYP enzymes in the HLM assay. For the EC assay, the proposed reaction mechanism involves the breakage of the methylenedioxy ring and formation of a carbocation that is attacked by a water molecule. Then the formylate group is formed, and two e^- and two H^+ are released, and a hydrogen shift forms the hydroxyl group as shown in Figure 32.

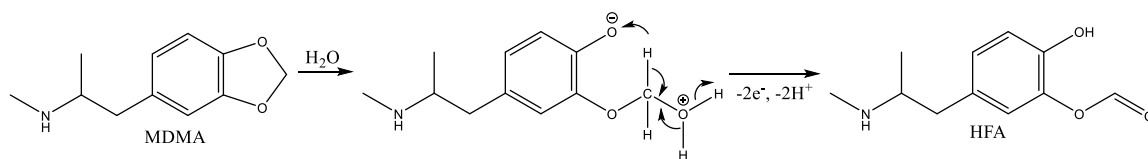


Figure 32: Reaction scheme of the EC redox transformation of MDMA to generate HFA.

The MS/MS spectrum of HFA ($[M+H]^+$ with m/z 210) shows a fragment ion at m/z 192 formed by dihydroxylation and a β -C-C cleavage leading to a fragment with m/z 179 due to the loss of ethylamine (Figure 33). The fragment ion with m/z 151 can be considered as a secondary fragment of the ion with m/z 179 and corresponds to a loss of HC=O due to a C-C cleavage. The fragment ion with m/z 123 can be considered as a secondary fragment of the ion with m/z 151 and corresponds due to a β -C-C cleavage leading to a loss of CH₃CH₂.

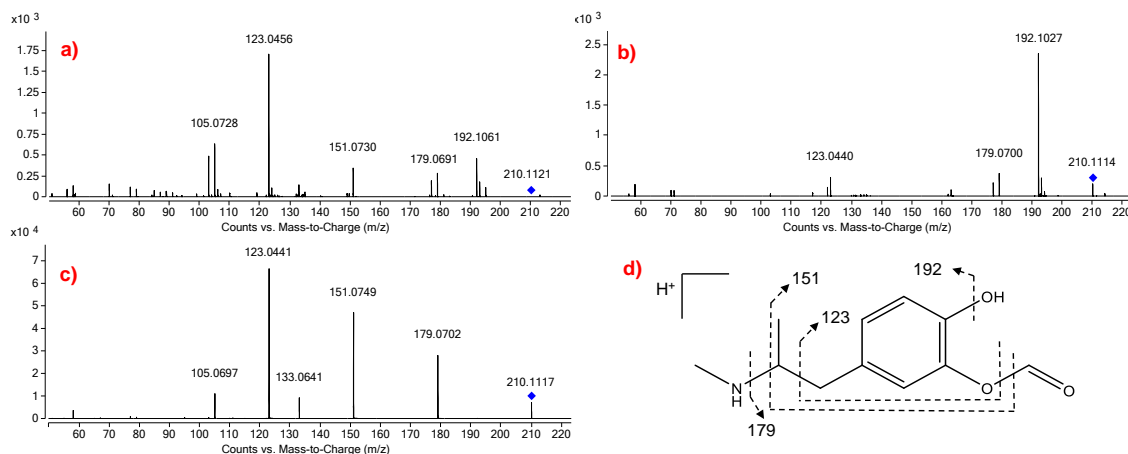


Figure 33: LC-QTOF-MS/MS spectra for the peaks of interest observed for the MDMA metabolite HFA, obtained with a) HLM assay; b) EC assay; c) synthetic MP catalysts; d) fragmentation pattern for HFA.

The minor metabolite HHA ($[M+H]^+$ with m/z 168) was only seen with the HLM assay, produced by the O-demethylation of MDA to generate HHA and

catalyzed by CYP2D6, CYP1A2, CYP2B6 and CYP3A4 enzymes.⁷⁹ The MS/MS spectrum for HHA (Figure 34a) shows a fragment ion with m/z 152 formed by a demethylation and cleavage of the benzyl ring, leading to a fragment with m/z 89 as seen in Figure 34b.

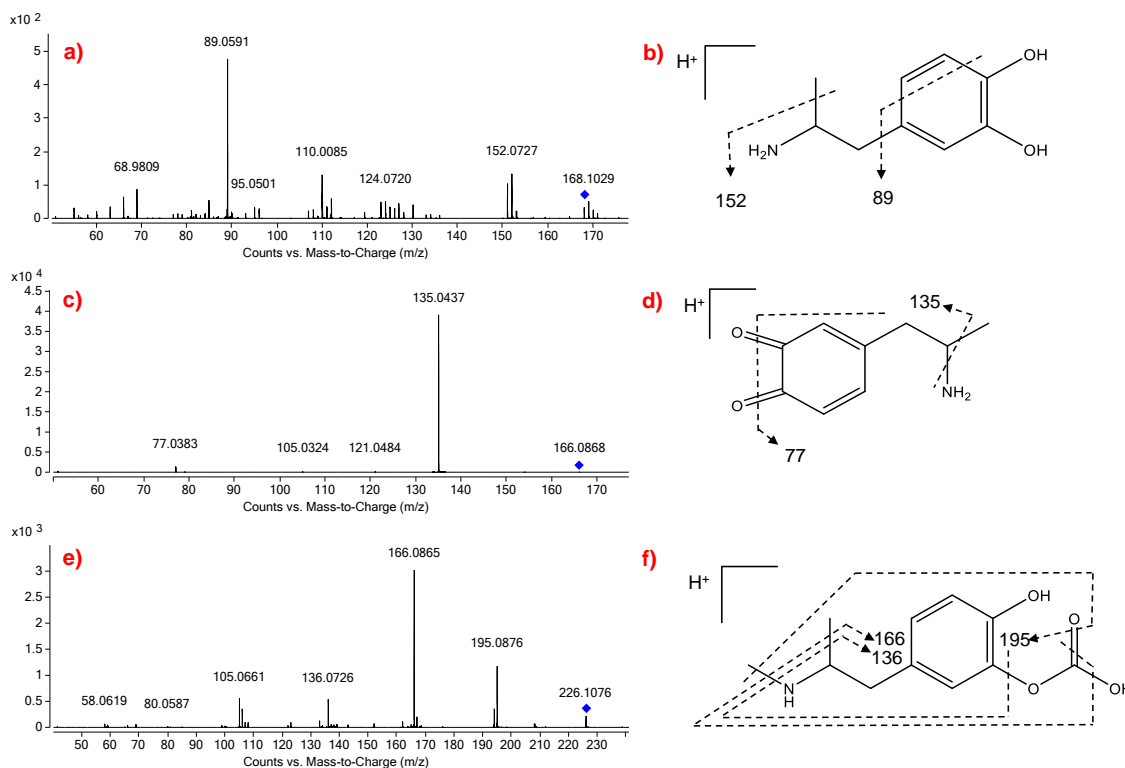


Figure 34: LC-QTOF-MS/MS spectra observed for the MDMA metabolites: a) HHA formed with the HLM assay, c) a quinone derivative formed with the EC oxidation, e) HPA formed with the synthetic MP. The proposed fragmentation pattern for each metabolite is also shown, b) HHA, d) quinone derivative, and f) HPA.

A quinone derivative ($[M+H]^+$ with m/z 166), was found only with the EC assay. This was not anticipated, as it is a reactive species. However, it was detected with HRMS, suggesting it may be fairly stable. The proposed reaction

mechanism involves a water molecule attacking the methylenedioxy ring, breaking the ring, forming methanol and the derivative as seen in Figure 35. The MS/MS spectrum for the quinone derivative (Figure 34c) shows the formation of the fragment with m/z of 77 corresponding to the loss of two oxygen, and a fragment ion with m/z 135 formed by the loss of a methyl group and ammonia (Figure 34d).

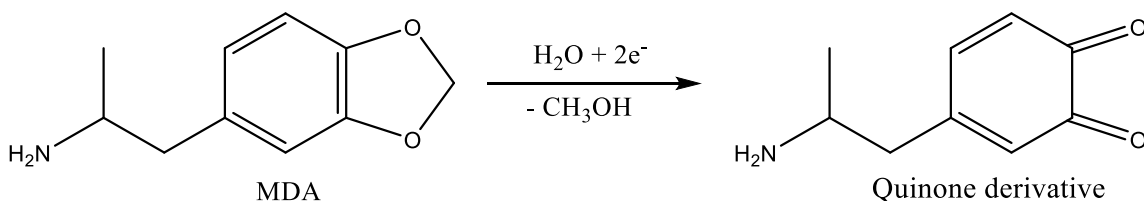


Figure 35: Reaction scheme of the EC redox transformation of MDA to generate the quinone derivative.

The last metabolite found for MDMA was 3-hydroxy-propylphenoxy-formylic acid amphetamine (HPA) ($[M+H]^+$ with m/z 182) via the synthetic MP catalysts. This is also a novel metabolite that has not been reported in the literature. It is hypothesized that it was formed via the metabolic reaction with an iron(III) porphyrin (FeP). The fragmentation profile for HPA shows the formation of a fragment with m/z of 195, corresponding to the demethylation of the amine and loss of an oxygen in the formic group. Fragment with m/z 166 is consistent with the loss of the formyl group and two demethylations. Lastly, the fragment with m/z 136 is consistent with loss of the oxygen in the formyl group and two demethylations.

4.1.5.3. METH

METH is metabolized in humans mainly through CYP2D6 by aromatic hydroxylation and N-demethylation. A summary of the results of the metabolism of METH with the three different assays is shown in Table 5.

Table 5: Metabolites found with METH for each assay.

Metabolite	Formula	<i>In vitro</i> model	Observed <i>m/z</i>	Fragments
AMP	C ₉ H ₁₄ N ⁺	HLM assay	136.1126	119.0861, 91.0549
		EC oxidation	136.1121	119.0864, 105.0664, 91.0539
		Synthetic MP	136.1114	119.0787, 91.0547
Methcathinone	C ₁₀ H ₁₄ NO ⁺	HLM assay	164.1074	148.1119, 135.0803, 107.0490
		Synthetic MP	164.1076	148.1102, 135.0805, 107.0491
N-OH-METH	C ₁₀ H ₁₆ NO ⁺	HLM assay	166.1226	148.1117, 119.0857, 91.0541
		EC oxidation	166.1223	148.1120, 133.0893, 107.0484
		Synthetic MP	166.1214	148.1115, 135.0800, 107.0490
N-OH-AMP	C ₉ H ₁₄ NO ⁺	HLM assay	152.1075	119.0859, 91.0552
p-OH-METH	C ₁₀ H ₁₄ NO ⁺	EC oxidation	166.1214	135.0800; 107.0490
Imine derivative	C ₁₀ H ₁₄ N ⁺	EC oxidation	148.1134	133.0846, 119.0791, 91.0530

Amphetamine was the one major metabolite that was found in common with the three methods. Additionally, five other metabolites were found: methcathinone, N-OH-METH, N-OH-AMP, p-OH-METH, and an imine derivative. The main metabolite found for METH was AMP and it is reported in the literature to be formed by the N-demethylation of METH mediated by CYP2D6 enzyme,^{79, 83} which was the pathway of metabolism for the HLM assay. There are no literature reports of *in vitro* metabolism of METH using EC or synthetic MP biomimetic systems. For the EC assay, the potential set for the bulk electrolysis was fixed at +480 mV, as determined by the CV results. The proposed reaction mechanism involves a water molecule attacking the methyl group bonded to the amine and forming methanol as shown in Figure 36. For the synthetic MP catalysts, it is speculated that the metabolites were generated by an iron (III) porphyrin (FeP) catalyst.

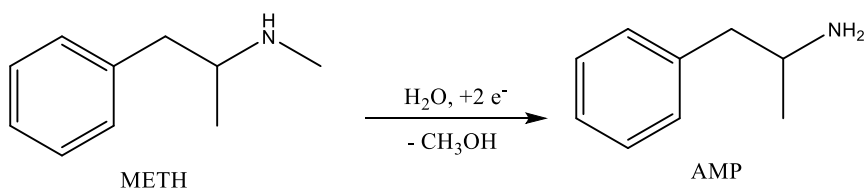


Figure 36: Reaction scheme of the EC redox transformation of METH to generate the AMP.

The QTOF-MS/MS spectra obtained for the major metabolite AMP for each of the *in vitro* methods is shown in Figure 37. The spectra of AMP ([M+H]⁺ with *m/z* 136) show the fragment ion *m/z* 119, resulting from the loss of methylamine; the tropylium ion with *m/z* 91 is formed due to a β-C-C cleavage; and the secondary fragment with *m/z* 105 is due to the loss of a methyl group from the ion *m/z* 119.

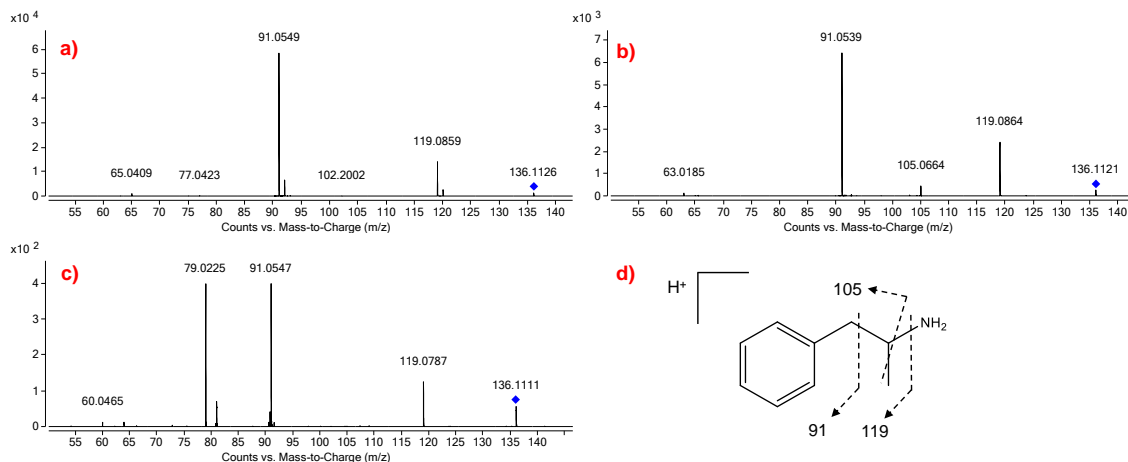


Figure 37: LC-QTOF-MS/MS spectra for the peaks of interest observed for the METH metabolite AMP, obtained with a) HLM assay; b) EC assay; c) synthetic metalloporphyrin catalysts; d) fragmentation pattern for AMP.

Another novel METH metabolite found with the HLM assay and the synthetic MP catalysts was methcathinone. This metabolic pathway has not previously been reported in the literature. It is proposed that methcathinone is formed by the oxidation of METH to form a β -keto substituent, possibly via a hydroxylated intermediate, but further work is needed to confirm this mechanism.

The QTOF-MS/MS spectra obtained for the methcathinone is shown in Figure 38. The spectra of methcathinone ($[M+H]^+$ with m/z 164) shows the fragment with m/z 148 formed due to the loss of oxygen from the ketone group; the fragment ion m/z 135, resulting from the loss of methylamine; and the fragment ion with m/z 107 is formed due to a β -C-C cleavage.

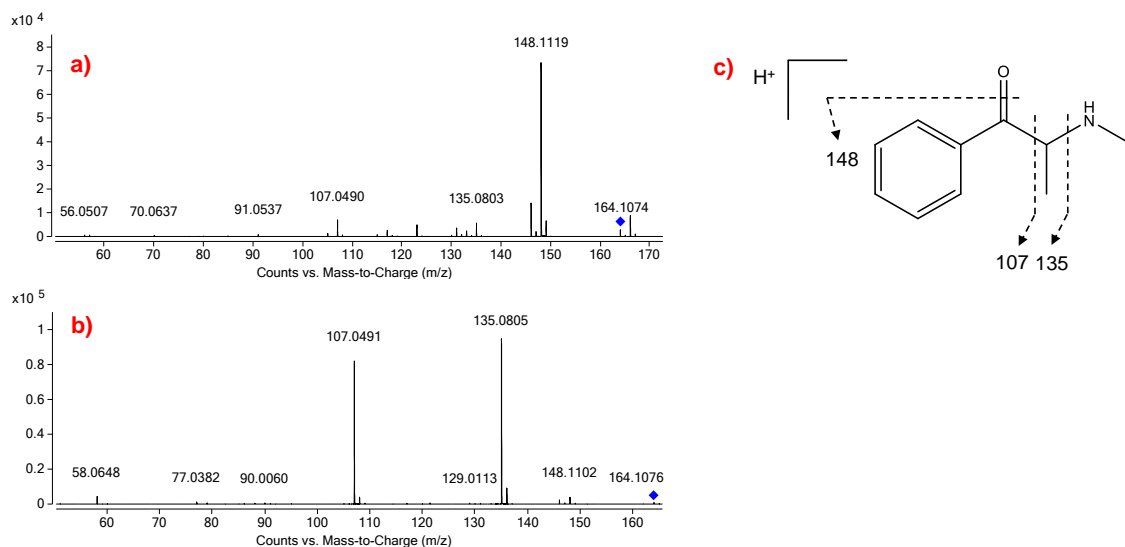


Figure 38: LC-QTOF-MS/MS spectra for the peaks of interest observed for the METH metabolite methcathinone, obtained with a) HLM assay; b) synthetic MP catalysts; c) fragmentation pattern for methcathinone.

The metabolite N-Hydroxy-N-methyl-1-phenyl-2-propanamine (N-OH-METH) was observed with the HLM assay and the EC assay. N-OH-METH is produced by the hydroxylation of the amine of METH.⁷⁹ For the EC assay, the proposed reaction mechanism involves a water molecule attacking the amine group, and forming a hydroxyl group and releasing two e⁻ and two H⁺ are released as shown in Figure 39.

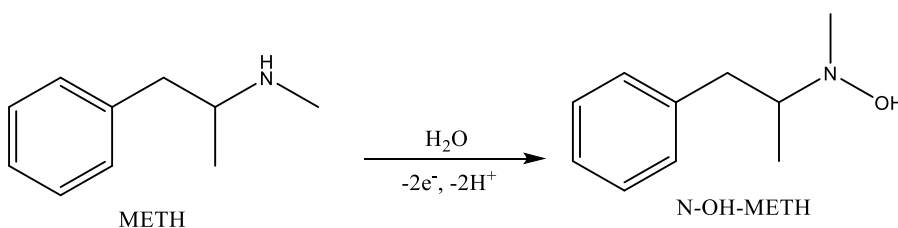


Figure 39: Reaction scheme of the EC redox transformation of METH to generate the N-OH-METH.

The MS/MS spectra for N-OH-METH ($[M+H]^+$ with m/z 166) is shown in Figure 40, the fragment ion with m/z 148 is formed by dihydroxylation of the amine, the fragment ion with m/z 133 is formed by dihydroxylation and demethylation of the amine, the fragment ion with m/z 133 is formed by the loss of the N-methylhydroxylamine group, and the tropylium ion with m/z 91 is formed due to a β -C-C cleavage.

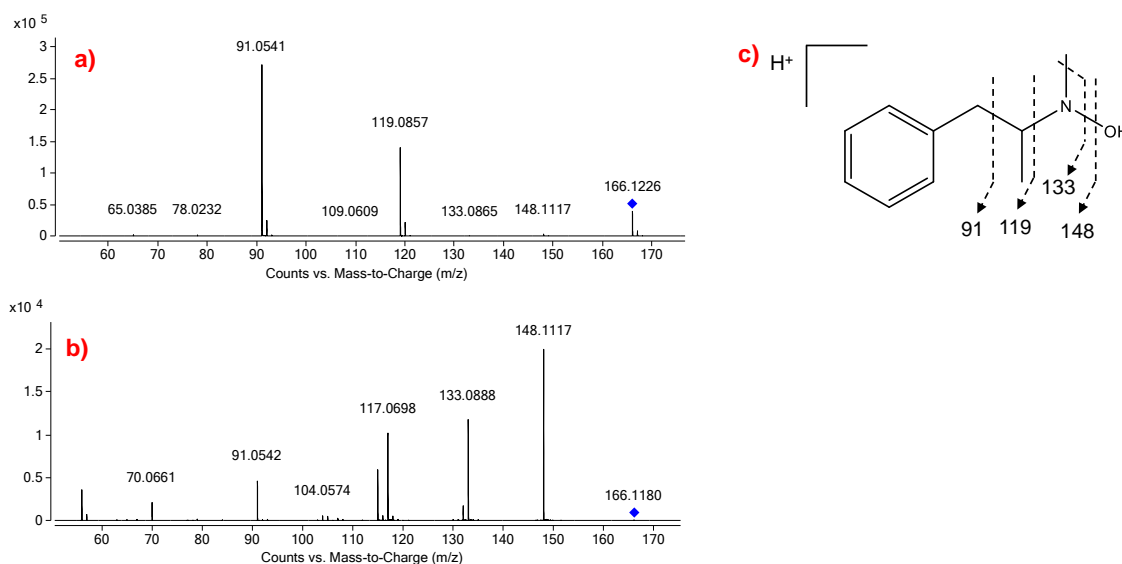


Figure 40: LC-QTOF-MS/MS spectra for the peaks of interest observed for the METH metabolite N-OH-METH, obtained with a) HLM assay; b) EC assay; c) fragmentation pattern for N-OH-METH.

The metabolite N-OH-AMP was seen with the HLM assay only. N-OH-AMP is formed by the hydroxylation of the amine group of the metabolite AMP.⁷⁹ The MS/MS spectra for N-OH-AMP ($[M+H]^+$ with m/z 152) is shown in Figure 41a, the fragment ion with m/z 119 is formed by the loss of hydroxylamine; and the tropylium ion with m/z 91 is formed due to a β -C-C cleavage as seen in Figure 41b.

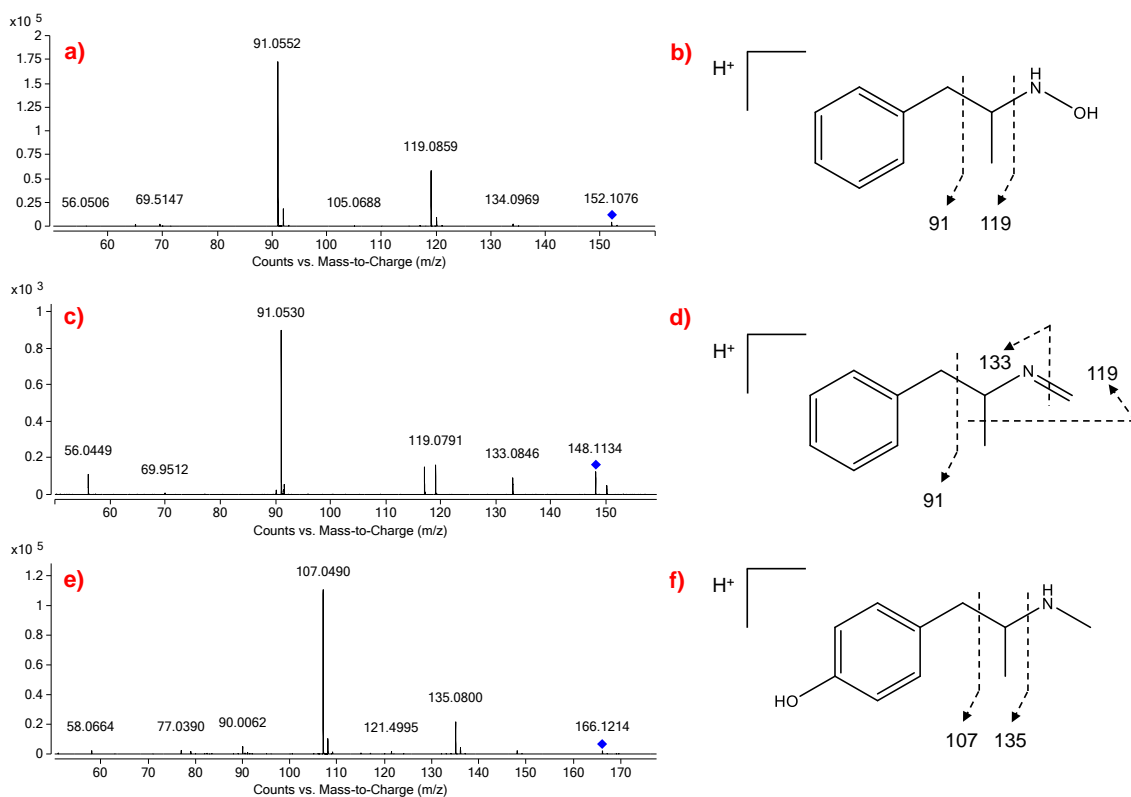


Figure 41: LC-QTOF-MS/MS spectra observed for the METH metabolites: a) N-OH-AMP formed with the HLM assay; c) an imine derivative formed with the electrochemistry oxidation, e) p-OH-METH formed with the synthetic MP. The proposed fragmentation pattern for each metabolite is also shown, b) N-OH-AMP; d) imine derivative, and f) p-OH-METH.

The imine derivative was seen with EC assay only. The proposed reaction mechanism involves the reduction of the methylamine group to form an imine group as shown in Figure 42. The MS/MS spectra for the imine derivative ($[M+H]^+$ with m/z 148) is shown in Figure 41c, the fragment ion with m/z 133 is formed by the demethylation of the amine and double bond formation of $C=N$; the fragment ion with m/z 119 is formed by a demethylation due to a β -C-C cleavage, and the tropylium ion with m/z 91 is formed due to a β -C-C cleavage as seen in Figure 41d.

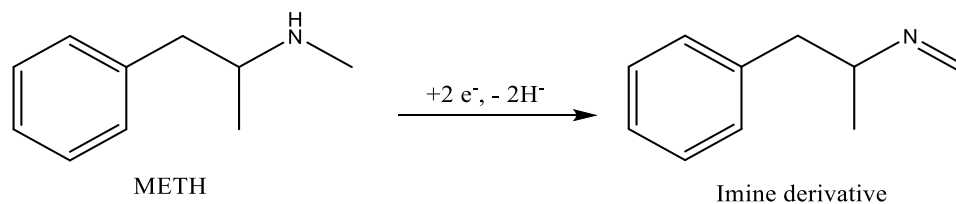


Figure 42: Reaction scheme of the EC redox transformation of METH to generate the imine derivative.

The metabolite p-OH-METH was seen with synthetic MP catalysts only. p-OH-METH is formed by the hydroxylation of the benzene ring of METH. The MS/MS spectrum for p-OH-METH ($[M+H]^+$ with m/z 166) is shown in Figure 41e. The fragment ion with m/z 135 is formed by the loss of hydroxylamine, and the fragment ion with m/z 107 is formed due to a β -C-C cleavage as seen in Figure 41f.

4.1.5.4. THC

The summary of the results obtained with THC with the 3 *in vitro* approaches are shown in Table 6. There were two major metabolites that were found in common with the three methods, 11-COOH-THC, and 11-CHO-THC. Three minor metabolites were also found: 11-OH-THC, 11-dihydroxy-THC, and a methylidene-THC derivative.

Table 6: Metabolites found with THC for three assays.

Metabolite	Formula	<i>In vitro</i> model	Observed <i>m/z</i>	Fragments
11-COOH- THC	C ₂₁ H ₂₉ O ₄ ⁺	HLM assay	345.2074	327.1938, 285.1842, 229.1256
		EC oxidation	345.2062	299.2066, 287.1612, 259.1637
		Synthetic MP	345.2062	327.1956, 303.1613, 285.1544
11-CHO- THC	C ₂₁ H ₂₉ O ₃ ⁺	HLM assay	329.2095	311.2009, 269.1535, 245.1531
		EC oxidation	329.2116	311.2001, 271.1694, 231.1380
		Synthetic MP	329.2109	311.1997, 271.1698, 231.1373
11-OH-THC	C ₂₁ H ₃₁ O ₃ ⁺	HLM assay	331.2281	313.2172, 271.1688
		Synthetic MP	331.2236	313.2129, 271.1691, 193.1232
11- dihydroxy- THC	C ₂₁ H ₃₁ O ₄ ⁺	EC oxidation	347.2202	329.2096, 311.2005, 271.1690
		Synthetic MP	347.2217	329.2101, 311.2001, 271.1673
Methylidene -THC	C ₂₁ H ₂₉ O ₂ ⁺	HLM assay	313.2172	257.1538, 217.1243, 193.2130
		EC oxidation	313.2160	217.1214, 201.0916, 193.1243
		Synthetic MP	313.2137	271.1710, 231.1358, 217.1231

The main metabolite found for THC was 11-COOH-THC, which is a major urinary metabolite *in vivo* reported to be formed by the oxidation of 11-OH-THC by CYP2C9 and CYP2C19 isozymes.^{84, 85} There are no literature reports on the metabolism of THC using either EC or synthetic MP biomimetic systems. For the

EC assay, the potential set for the bulk electrolysis was fixed at +700 mV, as determined by the CV. The proposed reaction mechanism involves oxidation of the methyl group of the cyclohexene ring, forming a carboxylic acid group as shown in Figure 43. For the synthetic MP catalysts, it is speculated that the metabolites were generated by an iron (III) porphyrin (FeP) catalyst.

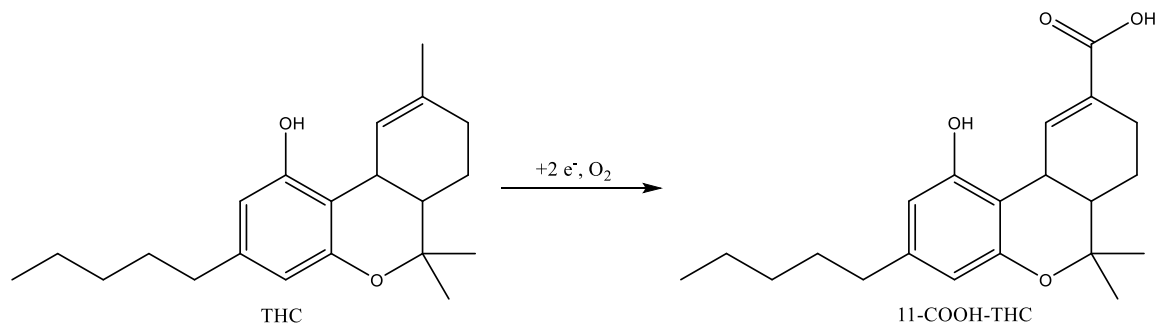


Figure 43: Reaction scheme of the EC redox transformation of THC to generate 11-COOH-THC.

The MS/MS spectrum for 11-COOH-THC ($[M+H]^+$ with m/z 345) is shown in Figure 44, the fragment ion with m/z 299 is formed due to a β -C-C cleavage and loss of the carboxylic group; the fragment ion with m/z 285 can be considered as a secondary fragment of the ion with m/z 299 and corresponds to a loss of methyl group. The fragment ion with m/z 327 is formed by the dihydroxylation of the benzene ring; and the fragment ion with m/z 327 is formed by the C-C cleavage at the pentyl chain.

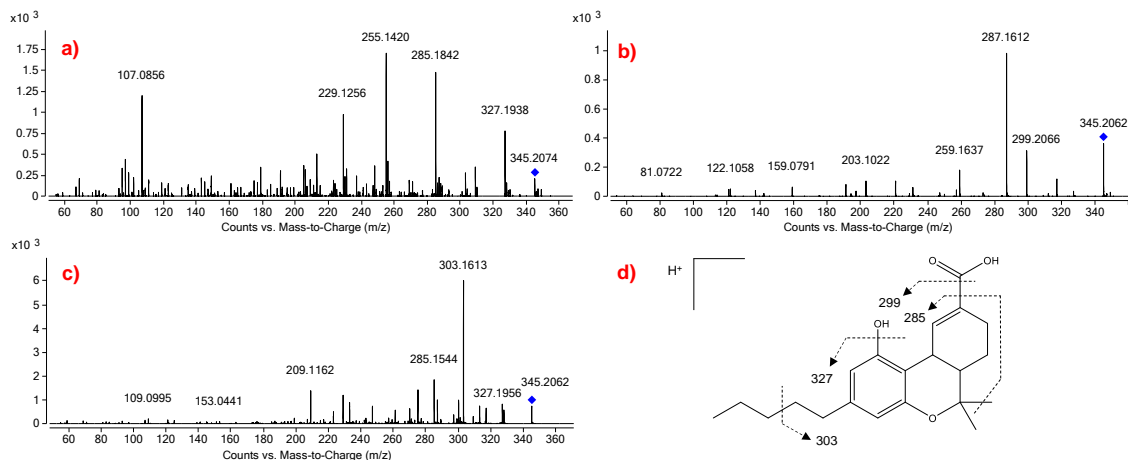


Figure 44: LC-QTOF-MS/MS spectra for the peaks of interest observed for the THC metabolite 11-COOH-THC, obtained with a) HLM assay; b) EC assay; c) synthetic MP catalysts; d) fragmentation pattern for 11-COOH-THC.

Darzi *et al.*⁸⁶ proposed a gentle electrochemical method for converting THC to its corresponding p-quinone isomer. In comparison to THC, the photophysical and electrochemical properties of the resulting quinone showed a significant shift. This straightforward protocol lays the groundwork for the creation of an electrochemical marijuana breathalyzer. In this work we found a metabolite with the same m/z of 329 as the proposed quinone however, the MS/MS spectra did not match that of the quinone. We propose a different structure for 11-CHO-THC, with it being a novel metabolite not reported in the literature. This product was obtained with the three *in vitro* systems. It is proposed that 11-CHO-THC is formed by the oxidation of the methyl group on the cyclohexene ring of the THC molecule. For the EC assay, the proposed reaction mechanism involves the oxidation of THC and the release of a water molecule, as shown in Figure 45.

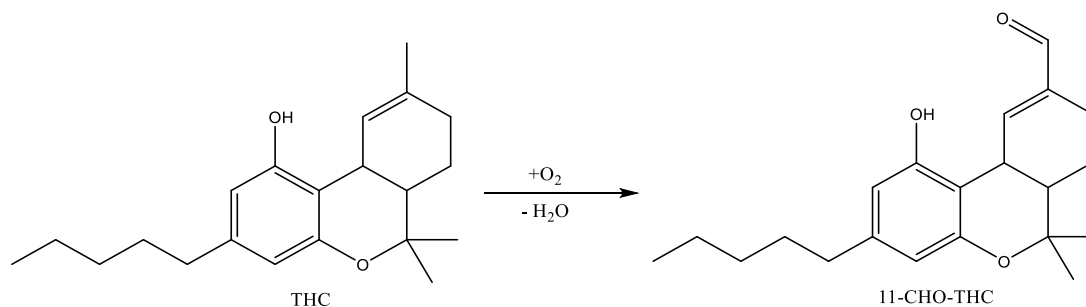


Figure 45: Reaction scheme of the EC redox transformation of THC to generate 11-CHO-THC.

The MS/MS spectra for 11-CHO-THC ($[M+H]^+$ with m/z 329) is shown in Figure 46. The fragment ion with m/z 311 is formed by the dihydroxylation of the benzene ring, while the fragment ion with m/z 271 corresponds to the loss of the two methyl groups and the carbaldehyde group. The fragment ion with m/z 245 is formed by the C-C cleavage at the pentyl chain and the carbaldehyde group.

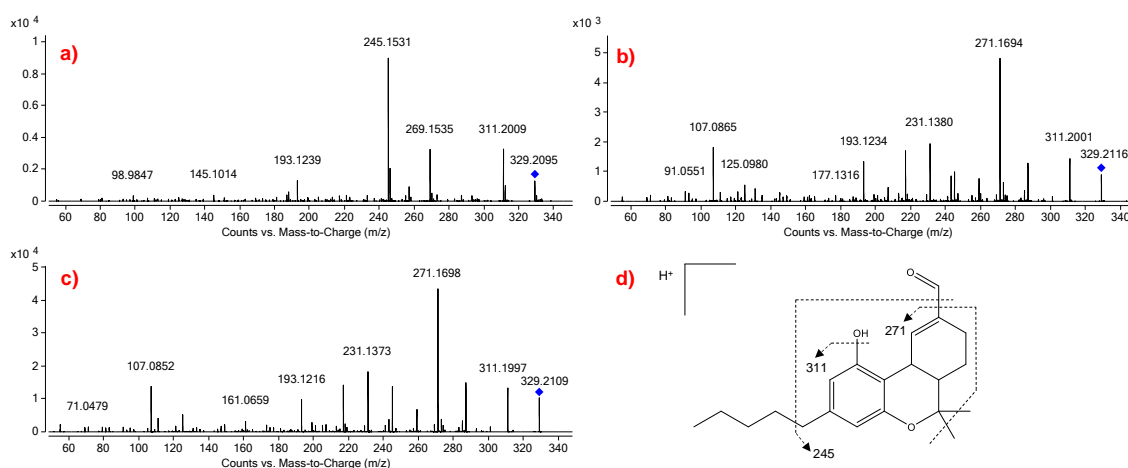


Figure 46: LC-QTOF-MS/MS spectra for the peaks of interest observed for the THC metabolite 11-CHO-THC, obtained with a) HLM assay; b) EC assay; c) synthetic MP catalysts, d) fragmentation pattern for 11-CHO-THC.

Another novel product not previously reported in the literature, a methylidene-THC derivative, was obtained with all three *in vitro* systems. It is proposed that this derivative is formed by the reduction of the methyl group on position 9. For the EC assay, the proposed reaction mechanism involves the reduction of the methyl group of the cyclohexene ring, as shown in Figure 47.

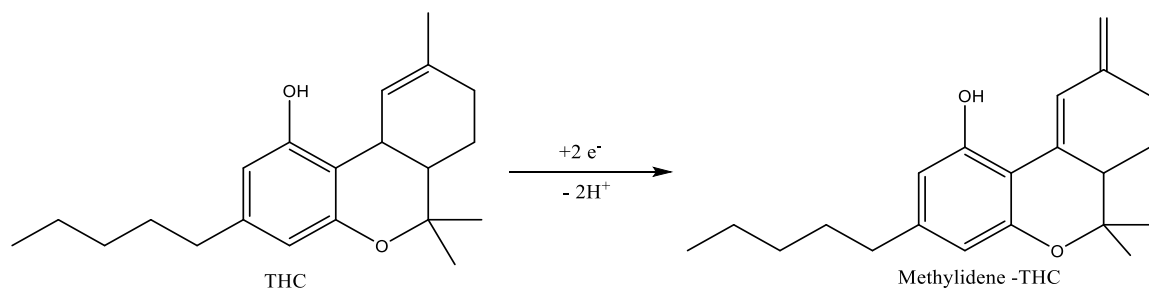


Figure 47: Reaction scheme of the EC redox transformation of THC to generate methylidene-THC.

The MS/MS spectra for the methylidene-THC derivative ($[M+H]^+$ with m/z 313) is shown in Figure 48. The fragment ion with m/z 217 is formed by the loss of the two methyl groups and the pentyl chain, while the fragment ion with m/z 271 corresponds to the loss of the two methyl groups and the methylidene group. The fragment ion with m/z 193 is formed by the loss of the pentyl chain and cleavage of the cyclohexene ring.

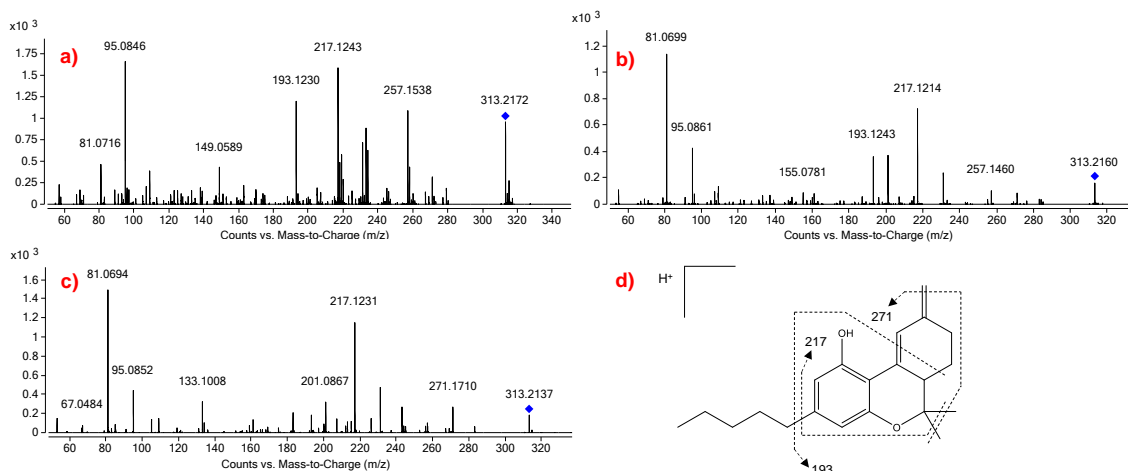


Figure 48: LC-QTOF-MS/MS spectra for the peaks of interest observed for the THC metabolite methylidene-THC, obtained with a) HLM assay; b) EC assay; c) synthetic MP catalysts; d) fragmentation pattern for methylidene-THC.

11-OH-THC was found for the HLM assay and for the synthetic MP catalysts. This metabolite was expected to be found, since it is a well-studied metabolite of THC and it is obtained via the oxidation of the methyl group present on the cyclohexene ring catalyzed via cytochromes CYP2C9 and CYP2C19 isozymes.⁸⁴ The MS/MS spectra for 11-OH-THC ($[M+H]^+$ with m/z 331) is shown in Figure 49. The fragment ion with m/z 313 is formed by the loss of the hydroxyl group on the benzene ring, while the fragment ion with m/z 271 corresponds to the loss of the two methyl groups and the hydroxymethyl group. The fragment ion with m/z 193 is formed by cleavage of the benzene ring.

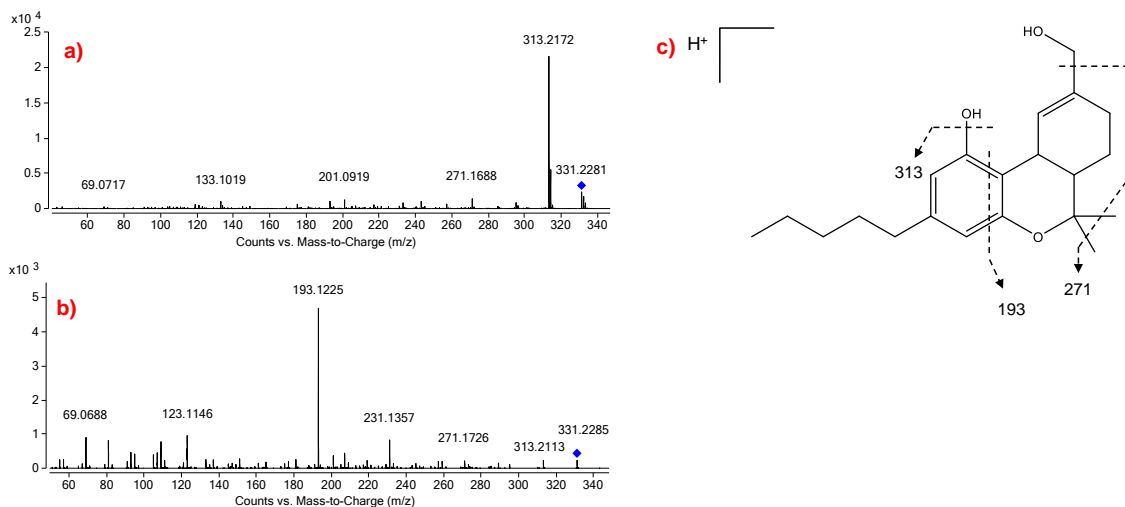


Figure 49: LC-QTOF-MS/MS spectra for the peaks of interest observed for the THC metabolite 11-OH-THC, obtained with a) HLM assay, b) EC synthetic MP catalysts, c) fragmentation pattern for 11-OH-THC.

Another hydroxylated product, 11-dihydroxy-THC, was found for the EC assay and for the synthetic MP catalysts. This metabolite has been reported before in the early 70s by Wall⁸⁷ using an HLM assay, there has been no other report of finding it for the THC metabolism. For the EC assay, the proposed reaction mechanism involves oxidation of the methyl group at the position 9 and the oxidation of the cyclohexene ring, as shown in Figure 50.

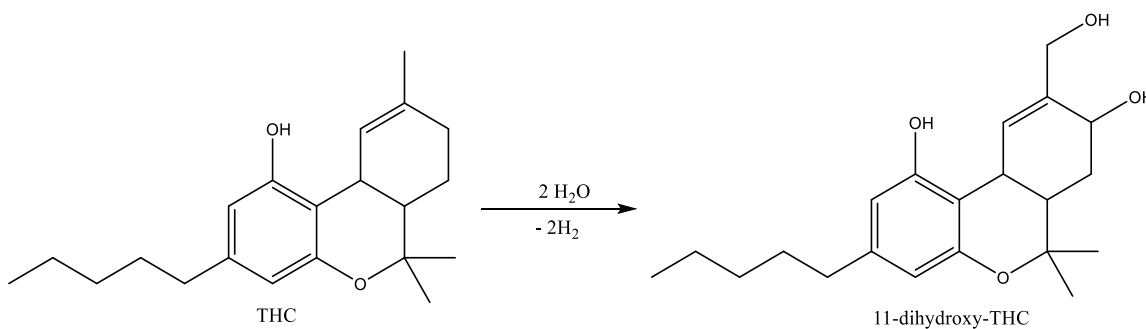


Figure 50: Reaction scheme of the EC redox transformation of THC to generate 11-dihydroxy-THC.

The MS/MS spectra for 11-dihydroxy-THC ($[M+H]^+$ with m/z 347) is shown in Figure 51. The fragment ion m/z 329 is formed by the loss of the hydroxyl group on the cyclohexene ring; the fragment ion m/z 271 corresponds to the loss of the two methyl groups, the hydroxyl group on the benzene ring and the hydroxymethyl group. The fragment ion with m/z 311 is formed by the loss of the hydroxyl group on the benzene ring, and the hydroxyl group on the cyclohexene ring.

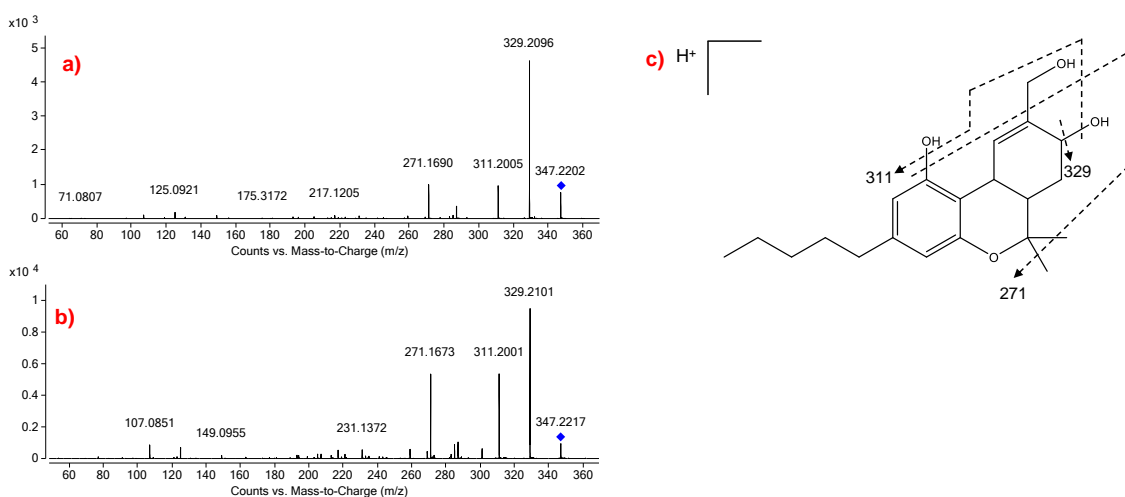


Figure 51: LC-QTOF-MS/MS spectra for the peaks of interest observed for the THC metabolite 11-dihydroxy-THC, obtained with a) EC assay, b) EC synthetic MP catalysts, c) fragmentation pattern for 11-dihydroxy-THC.

In summary, results of the *in vitro* SM and RM assay studies revealed that the metabolites obtained with the three different *in vitro* systems exhibited a few common derivatives but also compounds unique to each system. In addition, major metabolites reported *in vivo* for each drug were also found with all three *in vitro* systems, i.e., NAPQI, HHMA, AMP, and 11-COOH-THC. With the aid of *in silico* predictions and the employment of alternative *in vitro* systems, several new metabolites were found.

The synthetic MP and EC assay systems appeared to generate a wider variety of metabolites, including stable and potentially reactive derivatives such as HFA, HPA, an imine derivative, a quinone derivative, 11-CHO-THC, and methylidene-THC. Some of the novel metabolites were also found with the HLM assay, showing that there are still new metabolites that to be found with the most used *in vitro* system. Results indicate that the use of all three *in vitro* systems may provide a more complete profile of potential Phase I oxidative SM and RM for a variety of drugs that may be targeted for analysis in forensic toxicological studies and that reveal possible adduct forming species.

4.2. Task 2 – Assessment of adduct potential with peptides

A primary goal of this study was to use *in vitro* systems to produce reactive metabolites of drugs of abuse and assess the capability of these reactive species to form adducts with reactive biological thiols that could be measured as long-term biomarkers of exposure for drugs of abuse. In Task 2, the capability of reactive drug metabolites to form adducts with GSH and Hb $\beta^{93}\text{Cys}$ was investigated. Additionally, the effectiveness of the *in vitro* assays for semi-preparative synthesis of peptide standards for a QqQ based screening method was explored.

This part of the work was done using the HLM and the EC assays. It was decided to not move forward to this stage with the synthetic MPs, due to the harsh organic solvents present in the BMO kits. This study aimed to perform all metabolism in an aqueous ammonium bicarbonate buffer with physiological pH. The use of organic solvents in the trapping phase could cause the denaturing of the Hb $\beta^{93}\text{Cys}$ peptide which could impair its reactivity and use as a trapping agent.

4.2.1. GSH adduction studies

Among the known reactive sites within protein structure, cysteine, lysine, and histidine represent the most reactive nucleophiles. The free thiol within glutathione is one of the most reactive biological nucleophiles known, allowing the molecule to intercept potentially harmful reactive electrophiles *in vivo*. In the initial part of this Task, drug adducts with GSH were detected via HLM assay using positive mode ionization for APAP, COC, and MDMA. Table 7 summarizes the MS/MS data collected for these drugs, and their MS/MS data is shown in Appendix 3a-c. These results confirmed previous reported data using negative mode ionization, as indicated in Table 7.

Table 7: Summary table of the MS/MS data collected for glutathione adducts obtained with the HLM assay.

Drug	Composition	Adducted GSH [M+H]⁺	Mass error (ppm)	Previously Reported
APAP	APAP + GSH - 2H	457.1393	1.53	Zhu <i>et al.</i> (2007) ⁸⁸
COC	COC + GSH + O	627.2331	-1.75	Schneider and DeCaprio (2013) ⁸
MDMA	MDA + GSH	487.1863	-2.87	Meyer <i>et al.</i> (2014) ²

The objective of these experiments was to find additional GSH adducts that were not previously seen in the negative ionization mode studies. However, this

goal was not successful, as the adducts identified had already been previously reported in the literature. These experiments also showed that positive mode ionization is not ideal for the MS-based analysis of GSH adducts.

Adduction studies with GSH were also done with the EC assay, and the summary of the results obtained for APAP and THC are shown in Table 8. For this study, a new electrode with a higher surface area was employed; a mesh Pt WE. This was done in order to have a higher rate of conversion of drug to RM and to provide a higher yield of adducts as well. The bulk electrolysis potential for APAP was +600 mV and for THC it was +450 mV. The optimal duration of the bulk electrolysis was determined to be 10 min for both drugs.

Table 8: Summary table of the MS/MS data collected for GSH adducts obtained with the EC assay.

Drug	Composition	Adducted GSH [M+H]⁺	Mass error (ppm)
APAP	GSH + APAP - 2H	455.1220	-4.8
APAP	GSH + APAP + O - 2H	471.1229	8.1
THC	GSH + 11-OH-THC - 2H	634.2858	8.5
THC	GSH + 11-COOH-THC -2H	650.2733	-3.1
THC	GSH + 11-COOH-THC + OH - 2H	666.2747	6.8

Figure 52 shows the negative mode MS/MS obtained for the GSH adducts found with the EC assay. The fragment ions for the GSH + APAP - 2H adduct

included the molecular ion (m/z 455), five fragments specific to GSH (m/z 272, 254, 210, 143, and 128), and a fragment corresponding to the drug moiety bound to the sulfur of GSH (m/z 182). A second APAP adduct was also found, GSH + APAP + O - 2H (m/z 471), and four fragments consistent with GSH modification (m/z 272, 210, 143, and 128) in addition to a fragment corresponding to the drug moiety bound to the sulfur of GSH (m/z 198).

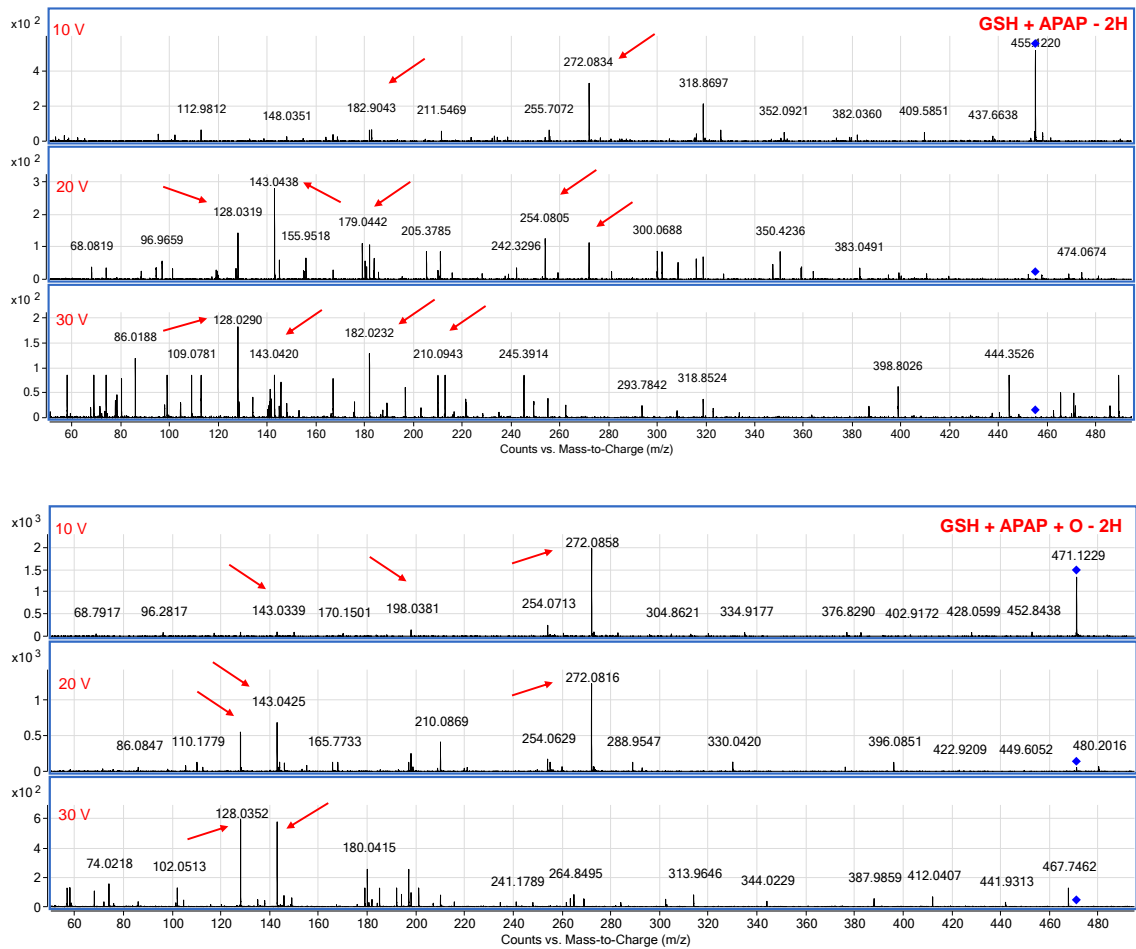


Figure 52: MS/MS data for the APAP GSH adducts obtained with the EC assay. The data are shown at 10 eV (top), 20 eV (middle), and 40 eV (bottom). Arrows point to relevant peaks.

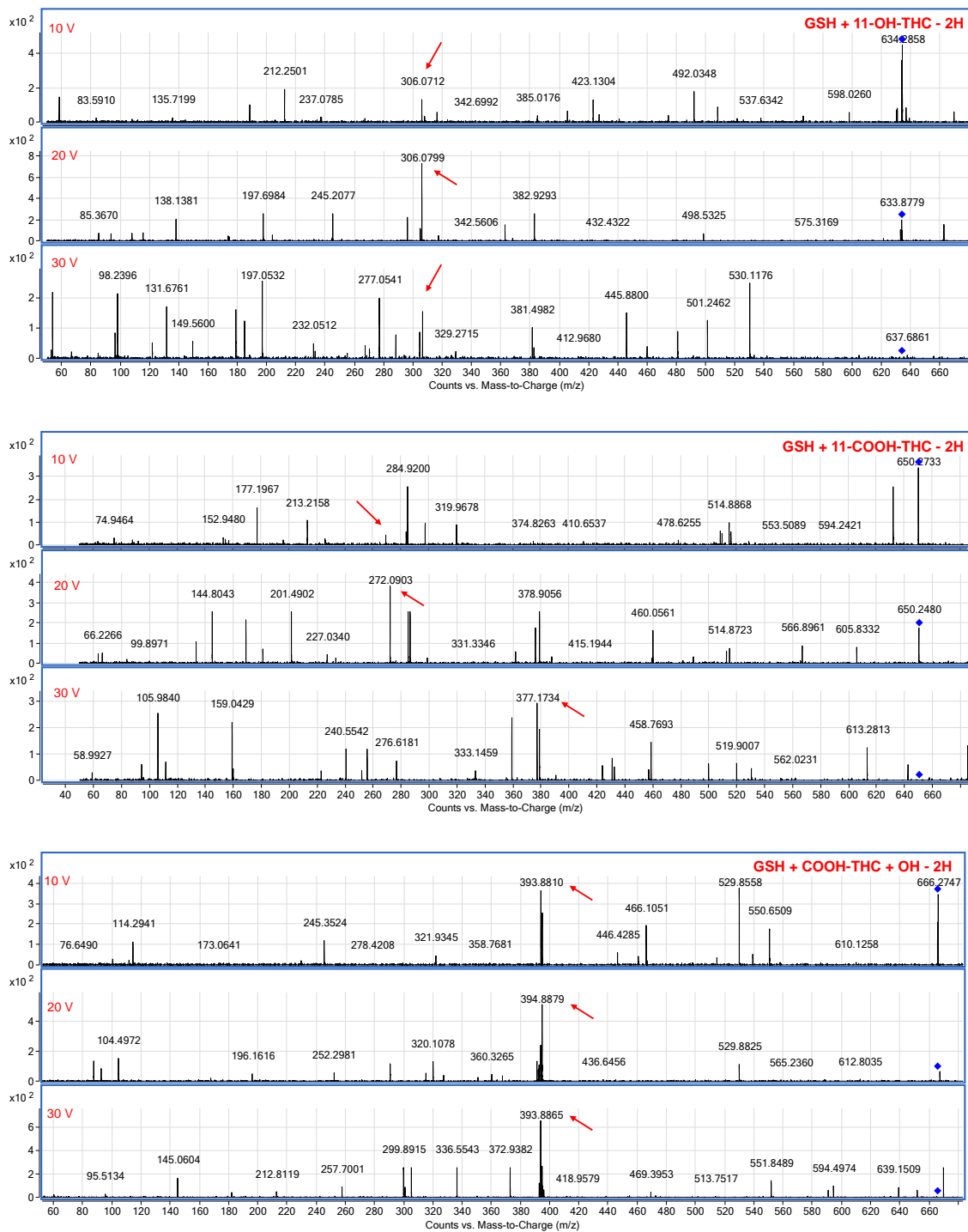


Figure 53: MS/MS data for the THC GSH adducts obtained with the EC assay. The data are shown at 10 eV (top), 20 eV (middle), and 40 eV (bottom). Arrows point to relevant peaks.

Three THC adducts were found as shown in Figure 53. The first showed a [M-H]⁻ ion at *m/z* 634, consistent with GSH + 11-OH-THC - 2H modification, a fragment specific to GSH was found at *m/z* 306. The second THC adduct had a [M-H]⁻ ion at *m/z* 650, which is consistent with GSH + 11-COOH-THC -2H modification; two fragments specific to GSH were found at *m/z* 377 and 272. Lastly, the adduct GSH + 11-COOH-THC + OH - 2H exhibited a [M-H]⁻ ion at *m/z* 666 and showed a drug-specific fragment at *m/z* 393.

The results found for the EC assay with GSH adduction were consistent with the previously published work done by Gilliland and DeCaprio using HLM assay.²⁴ These data demonstrate that the EC assay can be employed as an alternative to HLM assay for the generation of drug adducted peptides. However, the yields of such products are likely still too low to support use of EC to produce adducted GSH standards.

4.2.2. Preliminary IAM adduction study

In the next part of the study, the specific tryptic peptide containing the reactive ⁹³Cys residue of β-globin (*i.e.*, Hb β⁹³Cys peptide) was custom synthesized and used as trapping agent in the *in vitro* assays. As a positive control, Hb β⁹³Cys peptide with conversion of the thiol with a known alkylating agent was prepared by incubation with IAM, as described in the methodology section. This product was needed to confirm the ability of the data analysis to identify the exact location of an adduct within the peptide (*i.e.*, confirm modification of the β⁹³Cys). Samples were analyzed on the LC-QTOF-MS in FIA mode. Figure 54 shows the

MS spectrum of the control and adducted peptide. The observed mass differential of +91.4614 Da on the doubly charged peptide (at 802.8012 Da in Figure 54) is consistent with a single covalent modification of the $\beta^{93}\text{Cys}$ by IAM. However, the presence of unadducted peptide ion (at 771.3398 Da) indicates that the conversion by IAM was not stoichiometric.

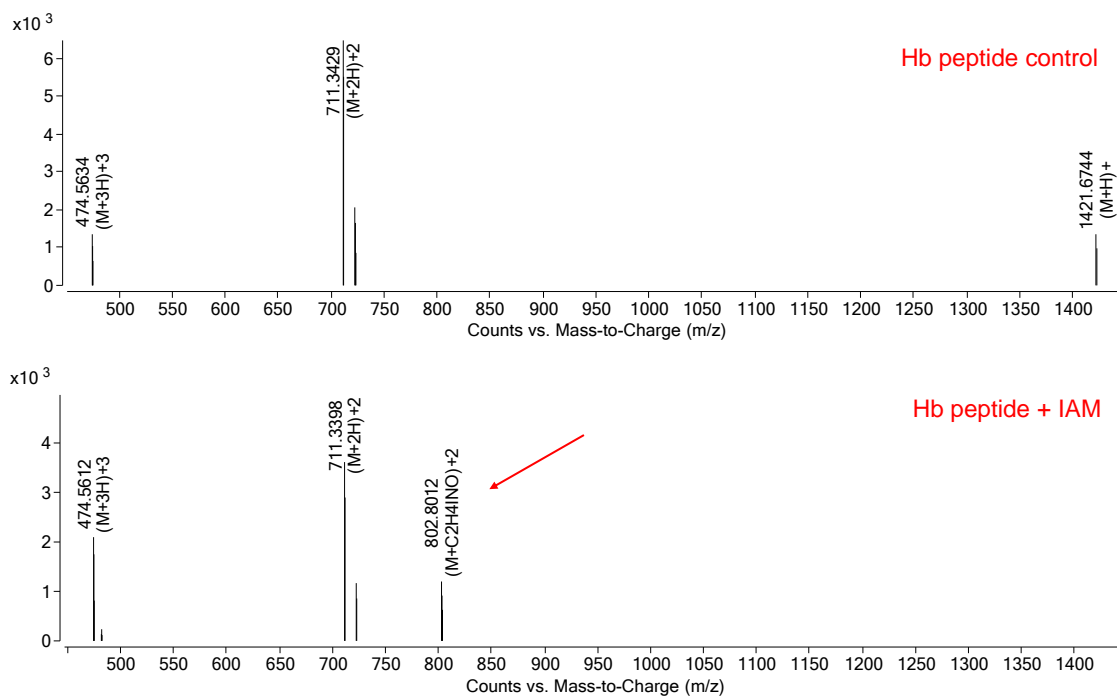


Figure 54: MS spectra of A) control and B) IAM adducted Hb $\beta^{93}\text{Cys}$ peptide.

4.2.3. Targeted MS/MS analysis of the drug-peptide adducts

The Hb $\beta^{93}\text{Cys}$ peptide was then utilized in the HLM assay as a trapping agent for RM of selected drugs. Theoretical covalent modifications for selected drugs and/or their metabolites were added as target ions to the BioConfirm software via Sequence Manager. MS/MS analysis was then performed to confirm

the location of the putative adducts at the Cys moiety. The summary of the results for APAP, cocaine, MDMA and METH are shown in Table 9.

Table 9: MS/MS results for HLM metabolism of APAP, cocaine, and MDMA.

Drug	Molecular Ion (m/z)	Composition	Fragment Ions (m/z)	Fragment Ions (ID)
APAP	1608.6776	Hb peptide + APAP + K	1412.6018, 1364.6195, 1220.5347, 615.3101	y ₁₁ -H ₂ O, c ₁₁ , z ₉ , y ₉ ⁺²
	799.8614	Hb peptide + NAPQI + OH + CH ₃	920.3594, 792.3422, 525.1634, 450.2489, 120.0797	b ₉ , y ₅ , y ₃ -NH ₃ , a ₅ , F
	515.9012	Hb peptide + 1,4-benzoquinone + OH	600.1768, 534.7370, 425.1125, 304.1009, 110.0708, 86.0956	x ₉ ⁺² , y ₈ ⁺² , y ₆ -H ₂ O ⁺² , y ₄ -H ₂ O ⁺² , H, L
COC	801.9225	Hb peptide + ecgonidine + CH ₃	681.3525, 516.2908, 403.2036, 221.1280, 120.0799	y ₄ , y ₁₂ ⁺³ , y ₉ -H ₂ O ⁺³ , y ₄ -H ₂ O ⁺³ , F
MDMA	1600.7676	Hb peptide + HHA + H + CH ₃	1263.6065, 1099.5070, 615.2769, 302.0356	x ₉ , y ₉ -H ₂ O, y ₉ ⁺² , y ₆ -NH ₃ ⁺³
	539.5802	Hb peptide + Aminochrome + O + OH	647.2571, 504.1562, 414.1393, 362.1625, 110.0708	y ₁₀ -NH ₃ ⁺² , y ₇ -H ₂ O ⁺² , y ₉ ⁺³ , x ₄ ⁺² , H
METH	784.8806	Hb peptide + methcathinone	718.3388, 641.2211, 544.6038, 479.2164, 348.0664, 129.0990	x ₁₁ ⁺² , a ₁₁ ⁺² , y ₈ ⁺² , x ₁₁ ⁺³ , a ₄ , K

Three peptide modifications were found for APAP and their MS/MS spectra can be seen in Figure 55. The first drug-peptide adduct found with APAP exhibited a mass differential of $m/z +188.0108$ and was consistent with the addition of APAP

at ^{93}Cys plus K^+ ion. With further analysis by Protein Prospector, four diagnostic fragment ions were found, being that $y_{11}\text{-H}_2\text{O}$, c_{11} , z_9 and y_9^{+2} contained the adducted thiol.

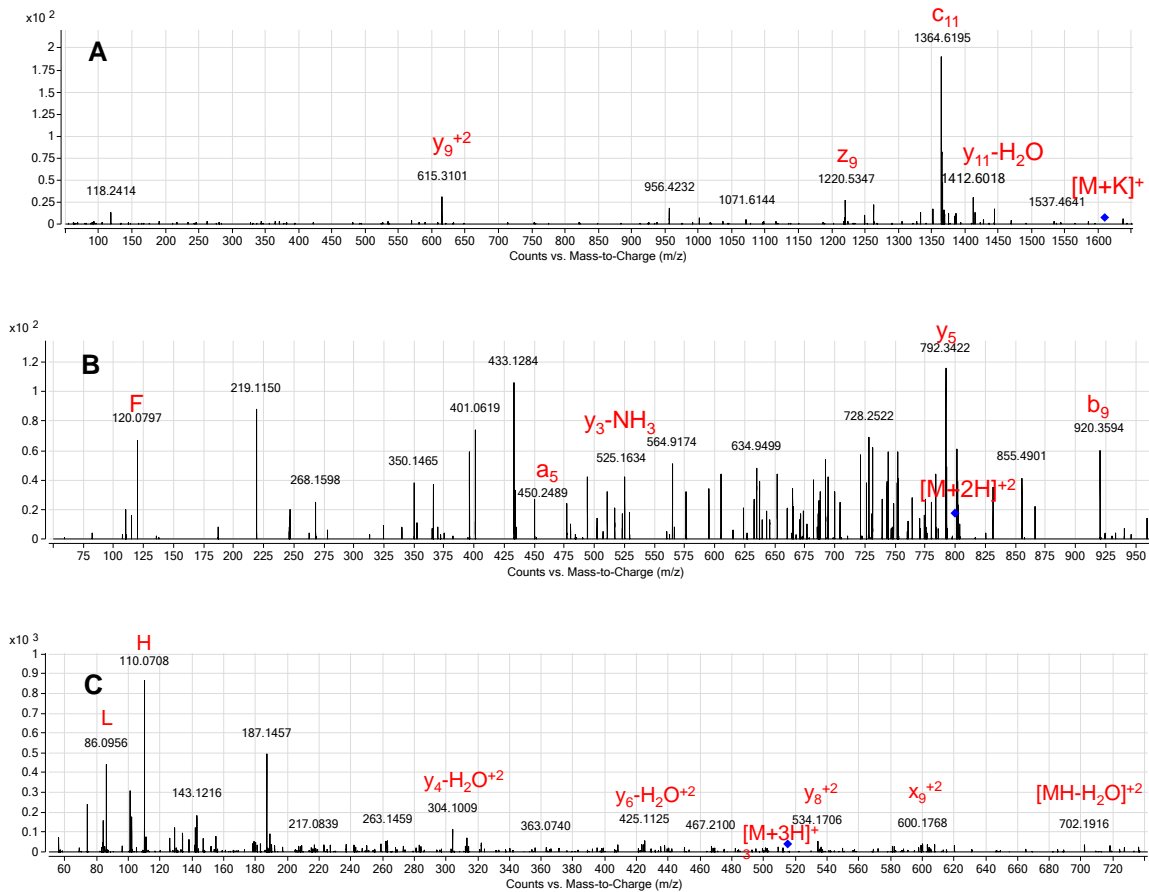


Figure 55: QTOF MS/MS spectra of Hb $\beta^{93}\text{Cys}$ peptide modified by APAP obtained with the HLM trapping assay, A) Hb peptide + APAP + K, B) Hb peptide + NAPQI + OH + CH_3 , and C) Hb peptide + 1,4-benzoquinone + OH.

The second modification exhibited a mass differential of $m/z +177.0426$, consistent with a NAPQI modification at ^{93}Cys , a hydroxylation at ^{95}Lys , and a methylation at ^{92}His . Two characteristic fragments were found (y_5 and $y_3\text{-H}_2\text{O}$) that contained the adducted thiol. The third adduct found with APAP exhibited a mass

differential of m/z +124.0160, identified as a 1,4-benzoquinone modification at ^{93}Cys and a hydroxylation at ^{95}Lys . Four diagnostic fragments were found (x_9^{+2} , y_8^{+2} , $y_6\text{-H}_2\text{O}$, and $y_4\text{-H}_2\text{O}$) that contained the adducted thiol.

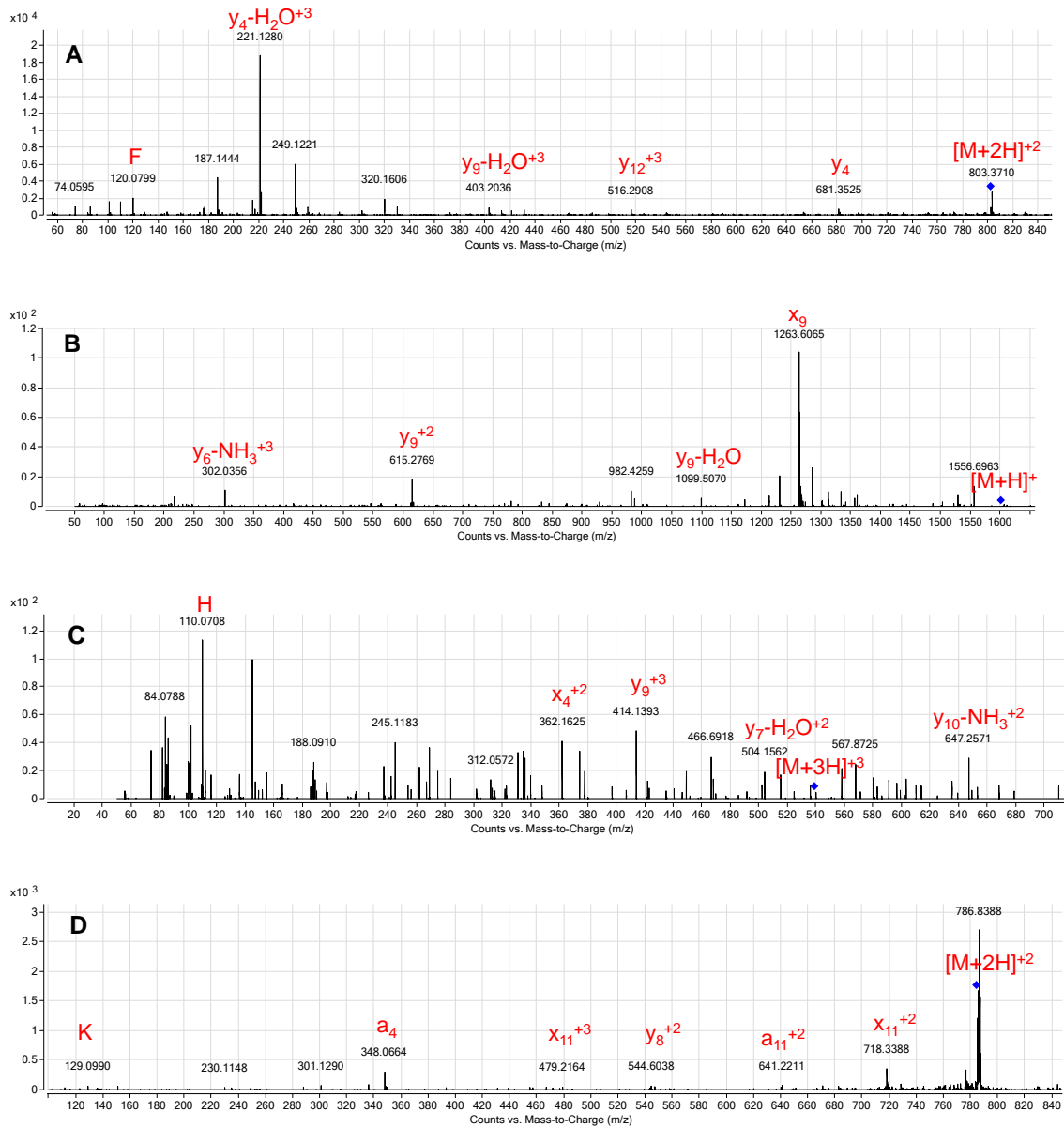


Figure 56: QTOF MS/MS spectra of Hb $\beta^{93}\text{Cys}$ peptide modified by APAP obtained with the HLM trapping assay, A) Hb peptide + ecgonidine + CH_3 , B) Hb peptide + HHA + H + CH_3 , C) Hb peptide + Aminochrome + O + OH, D) Hb peptide + methcathinone.

For cocaine, one drug-peptide adduct was found, with a mass differential of m/z +178.0868, consistent with an ecgonidine modification at ^{93}Cys and a methylation at ^{95}Lys . Three diagnostic fragments of the adducted Hb molecule were found (y_4 , $y_9\text{-H}_2\text{O}^{+3}$, $y_4\text{-H}_2\text{O}^{+3}$) that contained the adducted thiol as shown in Figure 56A.

For MDMA, two drug-peptide adducts were found, the first with a mass differential of m/z +179.0946 consisting of an HHA modification at ^{93}Cys and a methylation at ^{95}Lys as seen in Figure 56B. Four diagnostic fragments were found (x_9 , $y_9\text{-H}_2\text{O}$, y_9^{+2} , $y_6\text{-NH}_3^{+3}$) that contained the adducted thiol. The second peptide adduct exhibited a mass differential of m/z +195.0532 consistent with an aminochrome plus oxygen modification at ^{93}Cys and a hydroxylation at ^{95}Lys as seen in Figure 56C. Four diagnostic fragments were found ($y_{10}\text{-NH}_3^{+2}$, $y_7\text{-H}_2\text{O}^{+2}$, x_4^{+2} and y_9^{+3}) that contained the adducted thiol.

For METH, one drug-peptide adduct was found, with a mass differential of m/z +147.0809 consisting of a methcathinone modification at ^{93}Cys as seen in Figure 56D. Four diagnostic fragments were found, (x_{11}^{+2} , a_{11}^{+2} , y_8^{+2} , x_{11}^{+3}) that contained the adducted thiol. The *in vitro* enzymatic metabolism was also performed for THC; however, no peptide adducts were detected.

EC trapping assay MS/MS results for the Hb $\beta^{93}\text{Cys}$ peptide treated with APAP, COC, MDMA, METH, and THC are shown in Table 10. Three peptide adducts were found with APAP and their MS/MS spectra can be seen in Figure 57.

Table 10: MS/MS data for Hb $\beta^{93}\text{Cys}$ peptide adducts observed with the EC oxidation of APAP, cocaine, and THC.

Drug	Molecular Ion (m/z)	Composition	Fragment Ions (m/z)	Fragment Ions (ID)
APAP	1570.7206	Hb peptide + APAP	982.3930, 875.3585, 514.2050, 373.2259, 277.1282	y_7 , $y_6\text{-H}_2\text{O}$, y_3 , $y_5\text{-H}_2\text{O}$, a_3
	793.8614	Hb peptide + APAP + OH	706.8351, 573.3008, 460.2171, 377.1816, 288.1333, 262.1353, 147.1118	a_{12}^{+2} , $b_6\text{-H}_2\text{O}$, $b_5\text{-H}_2\text{O}$, b_4 , $b_3\text{-H}_2\text{O}$, y_2 , y_1
	1569.7128	Hb peptide + NAPQI	1425.6047, 1310.5825, 1058.5241, 765.3285, 390.1187, 288.1302	b_{12} , b_{11} , b_{10} , y_5 , $y_9\text{-H}_2\text{O}^{+3}$, $b_3\text{-H}_2\text{O}$
COC	534.9326	Hb peptide + ecgonidine + CH_3	1012.4773, 796.3858, 454.7086, 120.0796	y_7 , y_5 , $y_6\text{-NH}_3^{+2}$, F
MDMA	1614.7977	Hb peptide + MDMA	769.4709, 620.5840, 457.6662	$y_{12}\text{-H}_2\text{O}^{+2}$, y_9^{+2} , $b_5\text{-H}_2\text{O}$
METH	529.9148	Hb peptide + benzoic acid + OH + CH_3	488.9085, 393.1924, 344.0709	$y_7\text{-H}_2\text{O}^{+2}$, y_5^{+2} , x_4^{+2}
THC	882.4317	Hb peptide + 11-CHO-THC + OH	874.4270, 573.2977, 377.1789, 288.1344	$[\text{M}+2\text{H}]^{+2}$, $b_6\text{-H}_2\text{O}$, b_4 , $b_3\text{-H}_2\text{O}$

The first drug-peptide found for APAP exhibited a mass differential of m/z +149.0477, consistent with addition of APAP at ^{93}Cys . Protein Prospector analysis

indicated four diagnostic fragments (y_7 , y_6 -H₂O, y_3 , and y_5 -H₂O) that contained the adducted thiol. The second drug-peptide adduct found for APAP exhibited a mass differential of m/z +165.0426, characteristic of addition of APAP at ⁹³Cys, and hydroxylation at ⁹⁵Lys. A single diagnostic fragment (a_{12}^{+2}) that contained the adducted thiol was noted. The third adduct found with APAP exhibited a mass differential of m/z +164.0348, corresponding to a NAPQI modification at ⁹³Cys and a hydroxylation at ⁹⁵Lys. Four diagnostic fragments (b_{12} , b_{11} , y_5 and y_9 -H₂O⁺³) that contained the adducted thiol were identified.

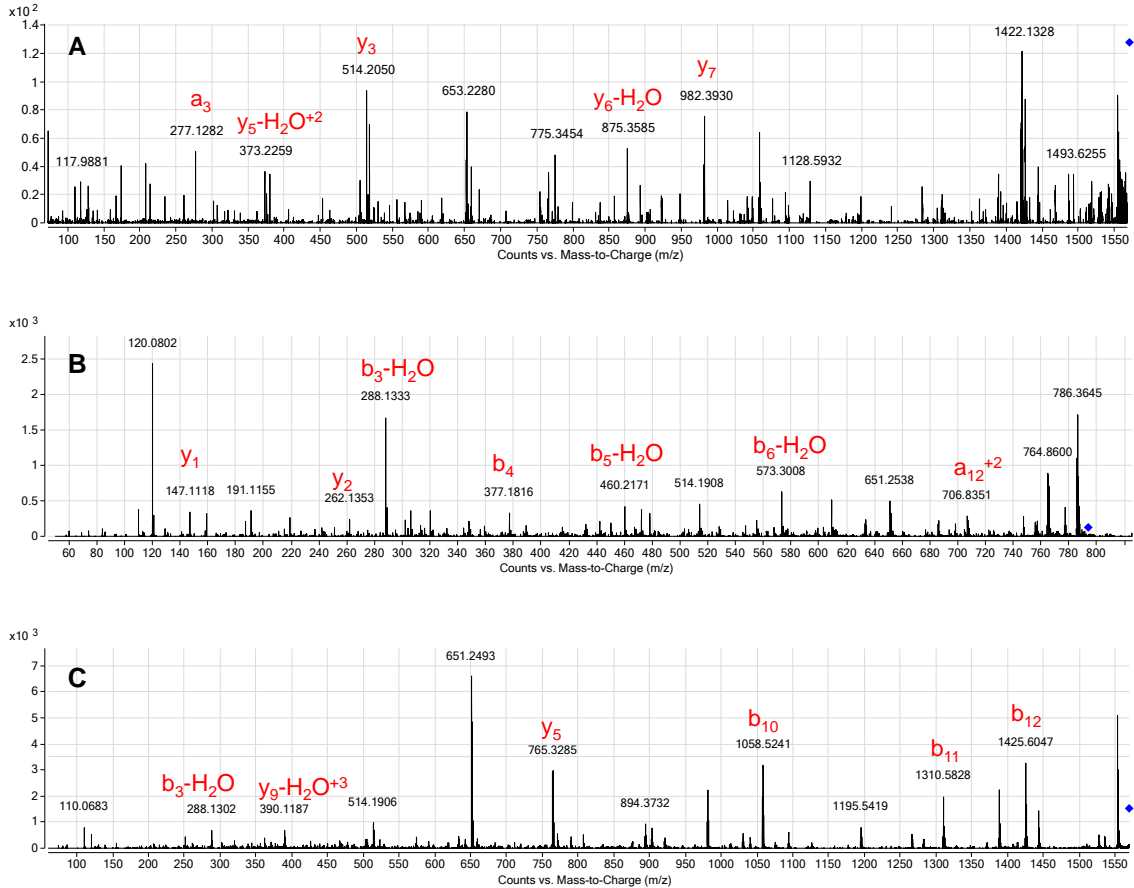


Figure 57: QTOF MS/MS spectra of Hb β^{93} Cys peptide modified by APAP obtained with the EC trapping assay, A) Hb peptide + APAP, B) Hb peptide + APAP + OH, and C) Hb peptide + NAPQI.

For cocaine, a single modified peptide species was found, with a mass differential of $m/z +193.1103$, consistent with addition of an ecgonidine moiety at ^{93}Cys and a methylation at ^{95}Lys . Three diagnostic fragments ($y_{12}-\text{H}_2\text{O}^{+2}$, y_9^{+2} , and $b_5-\text{H}_2\text{O}$) that contained the adducted thiol were identified.

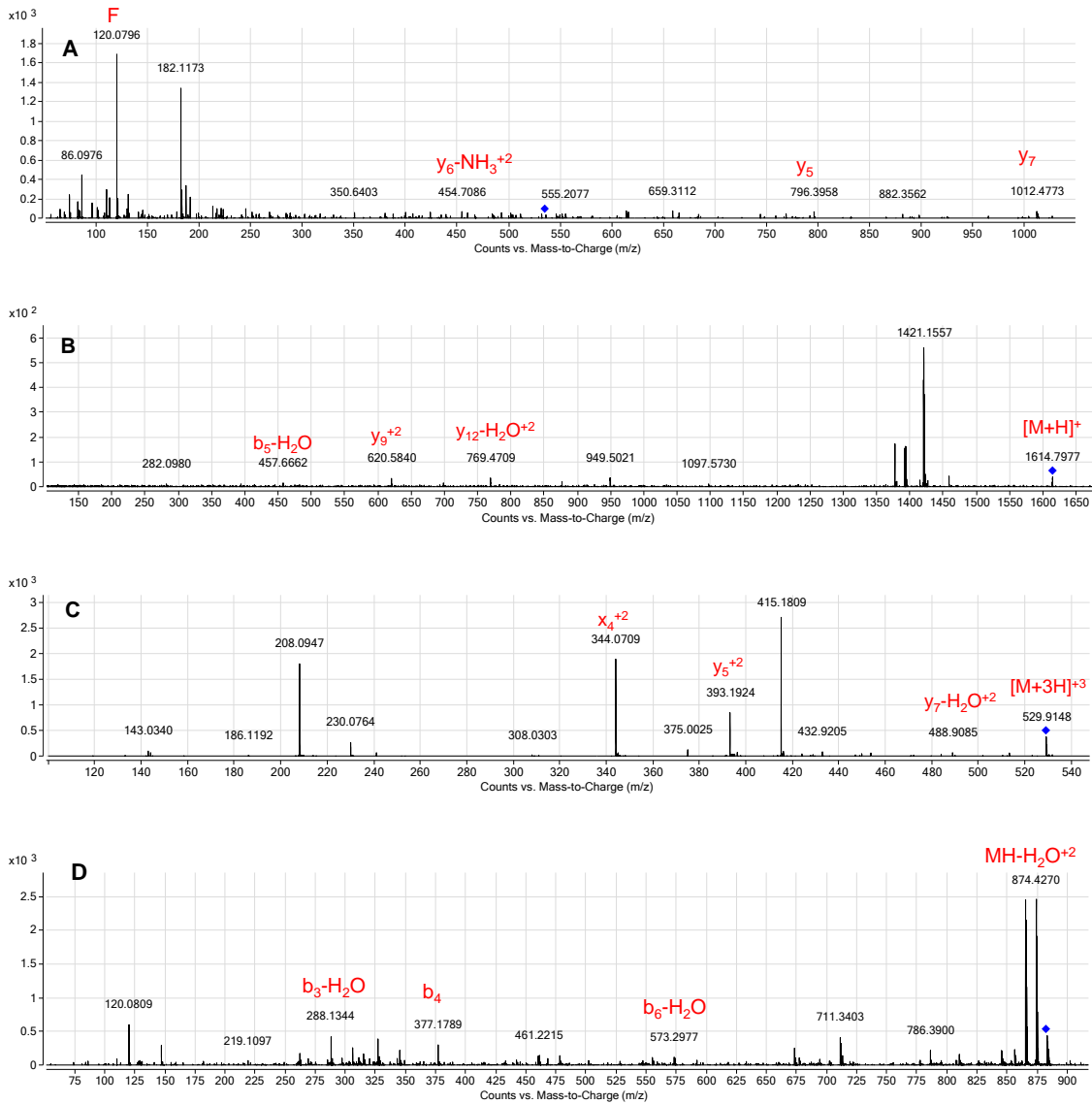


Figure 58: QTOF MS/MS spectra of Hb $\beta^{93}\text{Cys}$ peptide modified by COC, MDMA, METH and THC obtained with the EC trapping assay, A) Hb peptide + ecgonidine + CH_3 , B) Hb peptide + MDMA, C) Hb peptide + benzoic acid + OH + CH_3 and D) Hb peptide + 11-CHO-THC + OH .

A single modified peptide species was found for METH, with a mass differential of $m/z +150.0317$, consistent with addition of a benzoic acid moiety at ^{93}Cys , a hydroxylation at ^{95}Lys , and a methylation at ^{92}His . Three diagnostic fragments ($y_7\text{-H}_2\text{O}^{+2}$, y_5^{+2} , and x_4^{+2}) that contained the modified thiol were found.

For THC, a single modified peptide species was found, with a mass differential of $m/z +342.1831$, consistent with addition of a 11-CHO-THC moiety at ^{93}Cys and hydroxylation at ^{95}Lys . Three diagnostic fragments ($b_6\text{-H}_2\text{O}$, b_4 , $b_3\text{-H}_2\text{O}$) were found.

In both the HLM and EC studies, the yield of drug adducted Hb $\beta^{93}\text{Cys}$ peptide was generally low and inadequate for use as a semi-preparative method. This was surprising in view of the demonstrated high reactivity of the Hb $\beta^{93}\text{Cys}$ moiety in the intact protein. Consequently, a computer analysis was performed on the Hb $\beta^{93}\text{Cys}$ peptide using the VMD software developed by the University of Illinois at Urbana–Champaign. The VMD software is used to visualize, model, and analyze biological systems such as proteins, peptides, nucleic acids, lipid bilayer assemblies, and so on. It offers numerous methods for rendering and coloring a molecule, including simple points and lines, spheres and cylinders, licorice bonds, backbone tubes and ribbons, cartoon drawings, and others. VMD can be used to generate a molecule's 3D conformation and show the interactions within the molecule such as hydrogen bonds to determine its reactivity.

The Licorice representation of Hb $\beta^{93}\text{Cys}$ peptide is shown in Figure 57 and was to examine the intramolecular interactions present in the isolated peptide that

could influence the reactivity of the $\beta^{93}\text{Cys}$ thiol. The thiol moiety is represented by the color yellow in the Licorice representation, and as can be seen in the Figure, its spatial conformation is in close proximity to a neighboring serine hydroxyl group. This can help account for the relatively low reactivity observed for the isolated peptide, since the thiol could be tied up in intramolecular H-bonding with this serine and thus be less reactive to an exogenous electrophile. In contrast, the Hb $\beta^{93}\text{Cys}$ present in the native protein would have no such restriction to electrophilic attack.

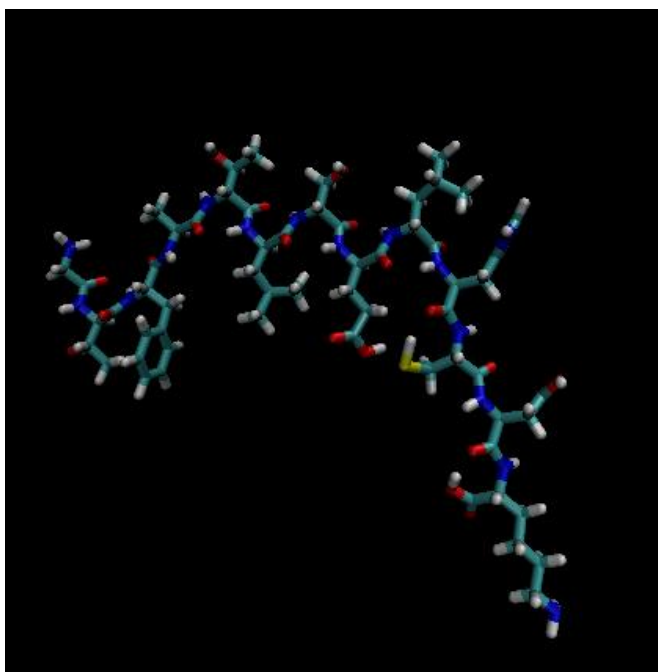


Figure 59: Licorice representation of Hb $\beta^{93}\text{Cys}$ peptide generated with the Visual Molecular Dynamics (VMD) software.

In summary, results of the Task 2 *in vitro* trapping assay studies with GSH and the Hb $\beta^{93}\text{Cys}$ peptide revealed that both HLM and EC oxidation assays can be effectively employed to identify thiol modifications formed by RM of drugs of abuse. However, yields of such products are too low to support use of these assays

for synthesis of adducted peptide standards, Nevertheless, the demonstrated ability of the selected drugs to covalently modify the β -Hb peptide containing the reactive $\beta^{93}\text{Cys}$ suggests that such modifications could be monitored as an alternative to clinical and forensic hair analysis for retrospective exposure assessment.

4.3. Task 3 – Development of an MRM method for adducted peptide screening

For screening of *in vitro* modified Hb ^{93}Cys peptide, and ultimately, proteins obtained from authentic blood specimens, an MRM LC-QqQ-MS method is needed. Several techniques for global profiling of Cys thiol adducts and for confirming specific protein modifications have been developed over the past decade^{32,33}. In this method, data generated during the *in vitro* trapping experiments and QTOF-MS analysis for each drug/peptide combination was utilized for preliminary studies on an MRM based detection method. For each identified drug/peptide adduct, two precursor/product ion pairs were selected as targeted MRM transitions for confirmation of a specific adduct in the Hb $\beta^{93}\text{Cys}$ peptide. Selection was done based on ion intensities and reproducibility in repeated experiments. Based on our proof-of-concept data and previous work with other reactive metabolites²⁵ and on other published studies³⁴, these included b_2 and y_2 type ions.

Agilent MassHunter Optimizer software was used in order to identify the transitions, associated collision energy, and optimal fragmentor voltage for each of the Hb $\beta^{93}\text{Cys}$ peptide adducts found in Task 2. The abundance of the data acquired from the HLM assay was insufficient to be seen in the LRMS instrument.

However, a few drug-Hb $\beta^{93}\text{Cys}$ peptide adducts obtained with the EC assay were successfully detected and two transitions were found with the dMRM method. The Optimizer summary table for the experimental conditions found for the detected adducts are shown in Appendix 4. Results for APAP, MDMA, and THC are shown in Table 11 and Figure 58.

Table 11: MRM data for Hb $\beta^{93}\text{Cys}$ peptide adducts observed with the electrochemical oxidation of APAP, MDMA, and THC.

Drug	Molecular Ion (m/z)	Composition	Fragments (m/z)	Fragments (ID)
APAP	785.9	Peptide + APAP - H	110.1; 807.4	H; b_8
	764.3	Peptide + 1,4-Benzoquinone - H	120.1; 789.4	F; $b_8\text{-H}_2\text{O}$
MDMA	801.9	Peptide + HHA + H + CH_2	721.8; 830.0	b_{12}^{+2} ; $y_8\text{-H}_2\text{O}^{+2}$
THC	588.6	Peptide + 11-CHO-THC - H + OH	573.3; 866.4	$b_6\text{-H}_2\text{O}$, $\text{MH-H}_2\text{O}^{+2}$

Two peptide adducts were found with APAP. The first exhibited a mass differential of $m/z +149$, consistent with addition of APAP and loss of H. Two transitions were found with the MRM study for this adduct (H and b_8). The second adduct found with APAP exhibited a mass differential of $m/z +109$, corresponding to a 1,4-benzoquinone modification on ^{93}Cys , and two diagnostic fragments (F and $b_8\text{-H}_2\text{O}$) were found.



Figure 60: MRM spectra of Hb $\beta^{93}\text{Cys}$ peptide modified by APAP (A-B), MDMA (B), and THC (D) obtained with the electrochemical trapping assay.

For MDMA, one peptide adduct was found, the first with a mass differential of $m/z + 179$ consistent with an HHA modification ^{93}Cys and a methylation on ^{95}Lys . Two diagnostic fragments were found (b_{12}^{+2} ; $y_8 - \text{H}_2\text{O}^{+2}$) and the y_8 fragment

contains the adducted thiol. Lastly, for THC, a single modified peptide species was found, with a mass differential of $m/z +342$, consistent with addition of a 11-CHO-THC moiety on ^{93}Cys and hydroxylation on ^{95}Lys . Two diagnostic fragments ($b_6\text{-H}_2\text{O}$, $\text{MH-H}_2\text{O}^{+2}$) were found.

In summary, results for Task 3 showed that the adducted peptide products formed in the EC assay can be detected using an LRMS LC-QqQ-MS MRM method. The original goal was to adapt a method developed by Osaki *et al.*¹¹, which consists of populating a master table of MS $\Delta m/z$ shift values associated with the peptide precursor ion (e.g., $[\text{Hb } \beta^{93}\text{Cys } \text{M}+\Delta+\text{nH}]^{n+}$ ion) and multiple corresponding product ions (e.g., $b_n+\Delta$ and $y_n+\Delta$ ions). However, to be able to use the Osaki method there needs to be an identification of the major adduct for each drug. While some adducts were detected, they were at low abundance and adducts were not detected for some drugs.

Consequently, additional work will be required to develop a reliable LRMS method for Hb adduct detection. Specifically, major Hb $\beta^{93}\text{Cys}$ adducts for each drug need to be identified, followed by synthesis of corresponding adducted peptide standards. This could be achieved by further development of the EC assay. Furthermore, an enrichment assay needs to be employed after the adduction has been performed to concentrate the adducted peptides and eliminate the unadducted forms. Such an enrichment assay is currently being developed in the DeCaprio Laboratory.

SUMMARY AND PROSPECT

The goal of this research was to investigate the metabolism of drugs of

abuse using three different *in vitro* systems, and to assess the potential for the metabolites generated to form adducts with thiol containing peptides. This was accomplished through a series of steps, the optimization and application of the three *in vitro* systems: HLM assay, EC assay and synthetic MP catalysts. This work successfully compiled a list of the metabolites obtained with each method and compared them. This work also identified and characterized 18 metabolites for the drugs of interest, five of which were novel. Although structural determination was not a focus of this research, plausible structures were proposed for the novel metabolites. By comparing all three *in vitro* systems, it is possible to have a more complete understanding of the metabolism that occurs *in vivo*.

This research was also able to successfully collect HRMS and MS/MS data for four GSH adducts and eleven Hb $\beta^{93}\text{Cys}$ adducts formed by the drugs of interest, thus confirming the adduction by APAP, COC, MDMA and THC. This work has a wide range of potential applications in the field of forensics. Hair analysis is currently the only method available for long-term detection of illicit drug use. However, hair analysis faces methodological and interpretive challenges, and the mechanisms by which most drugs incorporate into hair are not well understood. Furthermore, current blood and urine biomarkers are removed from the body after only a few days, limiting the detection window for many drugs of abuse. Peptide adducts derived from adducted Hb may be used as long-term biomarkers of exposure to supplement existing analytical methods to ensure complete detection of drugs of abuse. Because all of the identified peptide adducts are specific to

individual drugs, based on the MS/MS data collected for an individual's sample it may be possible to confirm not only the class of drugs consumed, but also the exact drug consumed. Long-term biomarkers of exposure are a favorable and effective application of protein adducts formed by drugs of abuse due to their specificity and overall stability.

REFERENCES

1. Moeller, M. R.; Steinmeyer, S.; Kraemer, T., Determination of drugs of abuse in blood. *Journal of Chromatography B: Biomedical Sciences and Applications* **1998**, 713 (1), 91-109.
2. Meyer, M. R.; Richter, L. H.; Maurer, H. H., Methylenedioxy designer drugs: mass spectrometric characterization of their glutathione conjugates by means of liquid chromatography-high-resolution mass spectrometry/mass spectrometry and studies on their glutathionyl transferase inhibition potency. *Analytica Chimica Acta* **2014**, 822, 37-50.
3. Dulaurent, S.; El Balkhi, S.; Poncelet, L.; Gaulier, J. M.; Marquet, P.; Saint-Marcoux, F., QuEChERS sample preparation prior to LC-MS/MS determination of opiates, amphetamines, and cocaine metabolites in whole blood. *Analytical and Bioanalytical Chemistry* **2016**, 408 (5), 1467-1474.
4. Wada, M.; Ikeda, R.; Kuroda, N.; Nakashima, K., Analytical methods for abused drugs in hair and their applications. *Analytical and Bioanalytical Chemistry* **2010**, 397 (3), 1039-1067.
5. Míguez-Framil, M.; Cocho, J. Á.; Tabernero, M. J.; Bermejo, A. M.; Moreda-Piñeiro, A.; Bermejo-Barrera, P., An improved method for the determination of D9-tetrahydrocannabinol, cannabinol and cannabidiol in hair by liquid chromatography–tandem mass spectrometry. *Microchemical Journal* **2014**, 117, 7-17.
6. Schaffer, M.; Cheng, C. C.; Chao, O.; Hill, V.; Matsui, P., Analysis of cocaine and metabolites in hair: validation and application of measurement of hydroxycocaine metabolites as evidence of cocaine ingestion. *Analytical and Bioanalytical Chemistry* **2016**, 408 (8), 2043-2054.
7. Wennig, R., Potential problems with the interpretation of hair analysis results. *Forensic Science International* **2000**, 107 (1-3), 5-12.
8. Schneider, K. J.; DeCaprio, A. P., Covalent thiol adducts arising from reactive intermediates of cocaine biotransformation. *Chemical Research in Toxicology* **2013**, 26 (11), 1755-1764.
9. Liebler, D. C.; Guengerich, F. P., Elucidating mechanisms of drug-induced toxicity. *Nature Reviews Drug Discovery* **2005**, 4 (5), 410.

10. Liebler, D. C., Protein damage by reactive electrophiles: targets and consequences. *Chemical Research in Toxicology* **2007**, 21 (1), 117-128.
11. Osaki, F.; Goto, T.; Lee, S. H.; Oe, T., Predicted multiple selected reaction monitoring to screen activated drug-mediated modifications on human serum albumin. *Analytical Biochemistry* **2014**, 449, 59-67.
12. Indriati, E.; Buikstra, J. E., Coca chewing in prehistoric coastal Peru: dental evidence. *American Journal of Physical Anthropology: The Official Publication of the American Association of Physical Anthropologists* **2001**, 114 (3), 242-257.
13. UNODC, *World Drug Report 2022*. United Nations publication: Vienna, Austria, 2022.
14. Zhang, Z.; Tang, W., Drug metabolism in drug discovery and development. *Acta Pharmaceutica Sinica B* **2018**, 8 (5), 721-732.
15. Kumar, A.; singla, C.; Singla, D., Drug metabolism. *International Journal of Advances in Engineering Sciences* **2011**, 1 (1), 67-68.
16. Estabrook, R. W., A passion for P450s (remembrances of the early history of research on cytochrome P450). *Drug metabolism and disposition* **2003**, 31 (12), 1461-1473.
17. Parkinson, A.; Ogilvie, B. W.; Buckley, D. B.; Kazmi, F.; Czerwinski, M.; Parkinson, O., Biotransformation of Xenobiotics. In *Casarett & Doull's Essentials of Toxicology, 3e*, Klaassen, C. D.; Watkins Iii, J. B., Eds. McGraw-Hill Education: New York, NY, 2015.
18. Pereira, M. M.; Dias, L. D.; Calvete, M. J. F., Metalloporphyrins: Bioinspired Oxidation Catalysts. *ACS Catalysis* **2018**, 8 (11), 10784-10808.
19. Huang, X.; Groves, J. T., Oxygen Activation and Radical Transformations in Heme Proteins and Metalloporphyrins. *Chemical Reviews* **2018**, 118 (5), 2491-2553.
20. Evans, D. C.; Watt, A. P.; Nicoll-Griffith, D. A.; Baillie, T. A., Drug-protein adducts: an industry perspective on minimizing the potential for drug bioactivation in drug discovery and development. *Chemical Research in Toxicology* **2004**, 17 (1), 3-16.

21. Shifman, M. A.; Graham, D. G.; Priest, J. W.; Bouldin, T. W., The neurotoxicity of 5-nonanone: preliminary report. *Toxicology Letters* **1981**, *8* (4-5), 283-288.
22. Zhou, S.; Chan, E.; Duan, W.; Huang, M.; Chen, Y. Z., Drug bioactivation covalent binding to target proteins and toxicity relevance. *Drug Metabolism Reviews* **2005**, *37* (1), 41-213.
23. Ma, J.; Zhang, W.; He, Y.; Zhu, L.; Zhang, C.; Liu, J.; Ye, Y.; Zhuge, Y.; Lin, G., Clinical application of pyrrole–hemoglobin adducts as a biomarker of pyrrolizidine alkaloid exposure in humans. *Archives of Toxicology* **2021**, *95* (2), 759-765.
24. Gilliland, R. A.; Möller, C.; DeCaprio, A. P., LC-MS/MS based detection and characterization of covalent glutathione modifications formed by reactive drug of abuse metabolites. *Xenobiotica* **2019**, *49* (7), 778-790.
25. Möller, C.; Davis, W. C.; R.Thompson, V.; Marí, F.; P.DeCaprio, A., Proteomic Analysis of Thiol Modifications and Assessment of Structural Changes in Hemoglobin Induced by the Aniline Metabolites N-Phenylhydroxylamine and Nitrosobenzene. *Scientific Reports* **2017**, *7*, 1-17.
26. Elkader, A.; Sproule, B., Buprenorphine: clinical pharmacokinetics in the treatment of opioid dependence. *Clin Pharmacokinet* **2005**, *44* (7), 661-80.
27. Kerns, E.; Di, L.; Properties, D.-I., Concepts, Structure Design and Methods: from ADME to Toxicity Optimization. Academic press San Diego, CA, USA:: 2008.
28. Schneider, K. J.; DeCaprio, A. P., Evaluation of in vitro metabolic systems for common drugs of abuse. 1. Cocaine. *Xenobiotica* **2013**, *43* (12), 1043-1054.
29. Rodríguez-Cid, L.; Sentellas, S.; Saurina, J., Voltammetric and electrogeneration approaches for the assessment of the oxidative drug metabolism. *Analytical and Bioanalytical Chemistry* **2018**, *410* (8), 2229-2239.
30. Lassila, T.; Mattila, S.; Turpeinen, M.; Tolonen, A., Glutathione trapping of reactive drug metabolites produced by biomimetic metalloporphyrin catalysts. *Rapid Communications in Mass Spectrometry* **2015**, *29* (6), 521-532.
31. Lohmann, W.; Karst, U., Biomimetic modeling of oxidative drug metabolism. *Analytical and Bioanalytical Chemistry* **2008**, *391* (1), 79-96.

32. Jurva, U.; Wikström, H. V.; Bruins, A. P., In vitro mimicry of metabolic oxidation reactions by electrochemistry/mass spectrometry. *Rapid Communications in Mass Spectrometry* **2000**, *14* (6), 529-533.
33. Madsen, K. G.; Olsen, J.; Skonberg, C.; Hansen, S. H.; Jurva, U., Development and evaluation of an electrochemical method for studying reactive phase-I metabolites: correlation to in vitro drug metabolism. *Chemical Research in Toxicology* **2007**, *20* (5), 821-831.
34. van Leeuwen, S. M.; Blankert, B.; Kauffmann, J.-M.; Karst, U., Prediction of clozapine metabolism by on-line electrochemistry/liquid chromatography/mass spectrometry. *Analytical and Bioanalytical Chemistry* **2005**, *382* (3), 742-750.
35. Baglia, R. A.; Zaragoza, J. P. T.; Goldberg, D. P., Biomimetic reactivity of oxygen-derived manganese and iron porphyrinoid complexes. *Chemical Reviews* **2017**, *117* (21), 13320-13352.
36. Chorghade, M. S.; Hill, D. R.; Lee, E. C.; Pariza, R. J.; Dolphin, D. H.; Hino, F.; Zhang, L. Y., Metalloporphyrins as chemical mimics of cytochrome P-450 systems. *Pure and Applied Chemistry* **1996**, *68* (3), 753-756.
37. Buzdygon, R. Introduction to the BMO Kit: An Alternative Metabolite Production Tool. [https://www.xenotech.com/webinar-slides/bmowebinar combined](https://www.xenotech.com/webinar-slides/bmowebinar%20combined).
38. Chapman, C. M.; Pruneau, J. M.; Laverack, C. A.; Dutton, A. S.; Jones, G. B., Biomimetic oxidation of acetaminophen prodrugs catalyzed by iron porphyrins: Effect of nitrogen and thiolate axial ligands on drug and metabolite formation. *Applied Catalysis A: General* **2016**, *510*, 204-215.
39. Getek, T.; McRae, T.; Hinson, J., Utility of solution electrochemistry mass spectrometry for investigation the formation and detection of biologically important conjugates of acetaminophen. *Journal of Chromatography A* **1989**, *474* (1), 245-256.
40. Elgrishi, N.; Rountree, K. J.; McCarthy, B. D.; Rountree, E. S.; Eisenhart, T. T.; Dempsey, J. L., A Practical Beginner's Guide to Cyclic Voltammetry. *Journal of Chemical Education* **2018**, *95* (2), 197-206.
41. Mielczarek, P.; Raouf, H.; Kotlinska, J. H.; Stefanowicz, P.; Szewczuk, Z.; Suder, P.; Silberring, J., Electrochemical simulation of cocaine metabolism—a step toward predictive toxicology for drugs of abuse. *European Journal of Mass Spectrometry* **2014**, *20* (4), 279-285.

42. de Bruyn Kops, C.; Stork, C.; Šícho, M.; Kochev, N.; Svozil, D.; Jeliaskova, N.; Kirchmair, J., GLORY: generator of the structures of likely cytochrome P450 metabolites based on predicted sites of metabolism. *Frontiers in Chemistry* **2019**, *7*, 402.
43. Kazmi, S. R.; Jun, R.; Yu, M.-S.; Jung, C.; Na, D., In silico approaches and tools for the prediction of drug metabolism and fate: A review. *Computers in Biology and Medicine* **2019**, *106*, 54-64.
44. <http://www.moldiscovery.com/software/metasite/>.
45. Ellefsen, K. N.; Wohlfarth, A.; Swortwood, M. J.; Diao, X.; Concheiro, M.; Huestis, M. A., 4-Methoxy- α -PVP: in silico prediction, metabolic stability, and metabolite identification by human hepatocyte incubation and high-resolution mass spectrometry. *Forensic Toxicology* **2016**, *34* (1), 61-75.
46. Frederick, D. L., Toxicology testing in alternative specimen matrices. *Clinics in Laboratory Medicine* **2012**, *32* (3), 467-92.
47. Hadland, S. E.; Levy, S., Objective testing: urine and other drug tests. *Child and Adolescent Psychiatric Clinics* **2016**, *25* (3), 549-565.
48. Barroso, M.; Gallardo, E.; Vieira, D. N.; López-Rivadulla, M.; Queiroz, J. A., Hair: a complementary source of bioanalytical information in forensic toxicology. *Bioanalysis* **2011**, *3* (1), 67-79.
49. Vincenti, M.; Salomone, A.; Gerace, E.; Pirro, V., Application of mass spectrometry to hair analysis for forensic toxicological investigations. *Mass Spectrometry Reviews* **2013**, *32* (4), 312-32.
50. Thompson, V. R.; DeCaprio, A. P., Covalent adduction of nitrogen mustards to model protein nucleophiles. *Chemical Research in Toxicology* **2013**, *26* (8), 1263-1271.
51. Grigoryan, H.; Edmands, W.; Lu, S. S.; Yano, Y.; Regazzoni, L.; Iavarone, A. T.; Williams, E. R.; Rappaport, S. M., Adductomics pipeline for untargeted analysis of modifications to Cys34 of human serum albumin. *Analytical Chemistry* **2016**, *88* (21), 10504-10512.
52. Kan, H.-I.; Chen, I. Y.; Zulfajri, M.; Wang, C. C., Subunit Disassembly Pathway of Human Hemoglobin Revealing the Site-Specific Role of Its Cysteine Residues. *The Journal of Physical Chemistry B* **2013**, *117* (34), 9831-9839.

53. Törnqvist, M.; Fred, C.; Haglund, J.; Helleberg, H.; Paulsson, B.; Rydberg, P., Protein adducts: quantitative and qualitative aspects of their formation, analysis and applications. *Journal of Chromatography. B, Analytical Technologies in the Biomedical and Life Sciences* **2002**, 778 (1-2), 279-308.
54. Funk, W. E.; Li, H.; Iavarone, A. T.; Williams, E. R.; Riby, J.; Rappaport, S. M., Enrichment of cysteinyl adducts of human serum albumin. *Analytical Biochemistry* **2010**, 400 (1), 61-68.
55. Fanali, G.; Di Masi, A.; Trezza, V.; Marino, M.; Fasano, M.; Ascenzi, P., Human serum albumin: from bench to bedside. *Molecular Aspects of Medicine* **2012**, 33 (3), 209-290.
56. Ahmed, M. H.; Ghatge, M. S.; Safo, M. K., Hemoglobin: Structure, Function and Allostery. In *Vertebrate and Invertebrate Respiratory Proteins, Lipoproteins and other Body Fluid Proteins*, Hoeger, U.; Harris, J. R., Eds. Springer International Publishing: Cham, 2020; pp 345-382.
57. Rubino, F. M.; Pitton, M.; Di Fabio, D.; Colombi, A., Toward an "omic" physiopathology of reactive chemicals: thirty years of mass spectrometric study of the protein adducts with endogenous and xenobiotic compounds. *Mass Spectrometry Reviews* **2009**, 28 (5), 725-84.
58. Sakatis, M. Z.; Reese, M. J.; Harrell, A. W.; Taylor, M. A.; Baines, I. A.; Chen, L.; Bloomer, J. C.; Yang, E. Y.; Ellens, H. M.; Ambroso, J. L., Preclinical strategy to reduce clinical hepatotoxicity using in vitro bioactivation data for > 200 compounds. *Chemical Research in Toxicology* **2012**, 25 (10), 2067-2082.
59. Toennes, S. W.; Wagner, M. G.; Kauert, G. F., Application of LC-TOF MS to analysis of hemoglobin acetaldehyde adducts in alcohol detoxification patients. *Analytical and Bioanalytical Chemistry* **2010**, 398 (2), 769-77.
60. Ishida, T.; Kumagai, Y.; Ikeda, Y.; Ito, K.; Yano, M.; Toki, S.; Mihashi, K.; Fujioka, T.; Iwase, Y.; Hachiyama, S., (8S)-(glutathion-S-yl)dihydromorphinone, a novel metabolite of morphine from guinea pig bile. *Drug Metabolism and Disposition* **1989**, 17 (1), 77-81.
61. Garadnay, S.; Gyulai, Z.; Makleit, S.; Sipos, A., First synthesis of important secondary oxidative metabolites of morphine and codeine with the Michael addition. *Central European Journal of Chemistry* **2013**, 11 (3), 430-437.

62. Todaka, T.; Ishida, T.; Kita, H.; Narimatsu, S.; Yamano, S., Bioactivation of morphine in human liver: isolation and identification of morphinone, a toxic metabolite. *Biological and Pharmaceutical Bulletin* **2005**, *28* (7), 1275-80.
63. Kovacic, P., Role of oxidative metabolites of cocaine in toxicity and addiction: oxidative stress and electron transfer. *Medical Hypotheses* **2005**, *64* (2), 350-6.
64. Bouis, P.; Boelsterli, U. A., Modulation of cocaine metabolism in primary rat hepatocyte cultures: Effects on irreversible binding and protein biosynthesis. *Toxicology and Applied Pharmacology* **1990**, *104* (3), 429-439.
65. Ndikum-Moffor, F. M.; Roberts, S. M., Cocaine-protein targets in mouse liver. *Biochemical Pharmacology* **2003**, *66* (1), 105-13.
66. Lloyd R. Snyder, J. J. K., John W. Dolan, Introduction. In *Introduction to Modern Liquid Chromatography*, 3rd edition ed.; John Wiley & Sons, Inc.: 2009; pp 1-17.
67. Brown, M. A., Liquid chromatography/mass spectrometry : applications in agricultural, pharmaceutical, and environmental chemistry. **1990**.
68. Watson, J. T.; Sparkman, O. D., *Introduction to mass spectrometry: instrumentation, applications, and strategies for data interpretation*. John Wiley & Sons: 2007.
69. Kebarle, P.; Verkerk, U. H., Electrospray: from ions in solution to ions in the gas phase, what we know now. *Mass Spectrometry Reviews* **2009**, *28* (6), 898-917.
70. Hendrickson, C. Electrospray ionization (ESI). <https://nationalmaglab.org/user-facilities/icr/techniques/esi>.
71. Stephens, W.; Serin, B.; Meyerhof, W., A method for measuring effective contact emf between a metal and a semi-conductor. *Physical Review* **1946**, *69* (1-2), 42.
72. Agilent Technologies, I. Agilent 6200 Series TOF and 6500 Series Q-TOF LC/MS System. https://www.agilent.com/cs/library/usermanuals/public/G3335-90231_TOF_Q-TOF_Concepts.pdf.

73. Xie, C.; Zhong, D.; Yu, K.; Chen, X., Recent advances in metabolite identification and quantitative bioanalysis by LC–Q-TOF MS. *Bioanalysis* **2012**, *4* (8), 937-959.
74. Silva, A. M.; Vitorino, R.; Domingues, M. R.; Spickett, C. M.; Domingues, P., Post-translational modifications and mass spectrometry detection. *Free Radical Biology and Medicine* **2013**, *65*, 925-941.
75. Spickett, C. M.; Reis, A.; Pitt, A. R., Use of narrow mass-window, high-resolution extracted product ion chromatograms for the sensitive and selective identification of protein modifications. *Analytical Chemistry* **2013**, *85* (9), 4621-4627.
76. Roepstorff, P.; Fohlman, J., Proposal for a common nomenclature for sequence ions in mass spectra of peptides. *Biomedical Mass Spectrometry* **1984**, *11* (11), 601.
77. Bertolini, A.; Ferrari, A.; Ottani, A.; Guerzoni, S.; Tacchi, R.; Leone, S., Paracetamol: new vistas of an old drug. *CNS Drug Reviews* **2006**, *12* (3-4), 250-275.
78. Bernadou, J.; Bonnafous, M.; Labat, G.; Loiseau, P.; Meunier, B., Model systems for metabolism studies. Biomimetic oxidation of acetaminophen and ellipticine derivatives with water-soluble metalloporphyrins associated to potassium monopersulfate. *Drug Metabolism and Disposition* **1991**, *19* (2), 360-365.
79. de la Torre, R.; Yubero-Lahoz, S.; Pardo-Lozano, R.; Farré, M., MDMA, methamphetamine, and CYP2D6 pharmacogenetics: what is clinically relevant? *Front Genet* **2012**, *3*, 235-235.
80. Carvalho, M.; Remião, F.; Milhazes, N.; Borges, F.; Fernandes, E.; Carvalho, F.; Bastos, M. L., The toxicity of N-methyl- α -methyldopamine to freshly isolated rat hepatocytes is prevented by ascorbic acid and N-acetylcysteine. *Toxicology* **2004**, *200* (2), 193-203.
81. Garrido, E. M.; Garrido, J. M.; Milhazes, N.; Borges, F.; Oliveira-Brett, A. M., Electrochemical oxidation of amphetamine-like drugs and application to electroanalysis of ecstasy in human serum. *Bioelectrochemistry* **2010**, *79* (1), 77-83.

82. de la Torre, R.; Farré, M., Neurotoxicity of MDMA (ecstasy): the limitations of scaling from animals to humans. *Trends in Pharmacological Sciences* **2004**, *25* (10), 505-508.
83. Li, L.; Everhart, T.; Jacobson, P.; Jones, R.; Mendelson, J., Stereoselectivity in the human metabolism of methamphetamine. *Br J Clin Pharmacol* **2010**, *69* (2), 187-192.
84. Palazzoli, F.; Citti, C.; Licata, M.; Vilella, A.; Manca, L.; Zoli, M.; Vandelli, M. A.; Forni, F.; Cannazza, G., Development of a simple and sensitive liquid chromatography triple quadrupole mass spectrometry (LC–MS/MS) method for the determination of cannabidiol (CBD), Δ^9 -tetrahydrocannabinol (THC) and its metabolites in rat whole blood after oral administration of a single high dose of CBD. *Journal of Pharmaceutical and Biomedical Analysis* **2018**, *150*, 25-32.
85. Watanabe, K.; Yamaori, S.; Funahashi, T.; Kimura, T.; Yamamoto, I., Cytochrome P450 enzymes involved in the metabolism of tetrahydrocannabinols and cannabinol by human hepatic microsomes. *Life Sciences* **2007**, *80* (15), 1415-1419.
86. Darzi, E. R.; Garg, N. K., Electrochemical Oxidation of Δ^9 -Tetrahydrocannabinol: A Simple Strategy for Marijuana Detection. *Organic Letters* **2020**, *22* (10), 3951-3955.
87. Wall, M. E., The in vitro and in vivo metabolism of tetrahydrocannabinol (THC). *Annals of the New York Academy of Sciences* **1971**, *191* (1), 23-39.
88. Zhu, M.; Ma, L.; Zhang, H.; Humphreys, W. G., Detection and Structural Characterization of Glutathione-Trapped Reactive Metabolites Using Liquid Chromatography–High-Resolution Mass Spectrometry and Mass Defect Filtering. *Analytical Chemistry* **2007**, *79* (21), 8333-8341.

APPENDICES

Appendix 1. Summary of the FIA data obtained for the synthetic MP assay using the screening and optimization BMO kits.

a) FIA data for the screening BMO kit with APAP; best condition is shown in red.

Solvent 1 - APAP		Solvent 2 - APAP	
Condition	Positive mode <i>m/z</i>	Condition	Positive mode <i>m/z</i>
A1	152.0712	A1	152.0710; 301.1191
A2	152.0709	A2	152.0705; 301.1180
A3	152.0707; 301.1181	A3	152.0707; 301.1185
A4	152.0707	A4	152.071
A5	152.0708	A5	152.0710; 301.1189
A6	150.0551; 301.1186	A6	152.0709
B1	152.0712	B1	152.0705; 301.1188
B2	-	B2	152.0710; 301.1178
B3	-	B3	152.0704; 301.1175
B4	152.0707	B4	152.071
B5	-	B5	152.071
B6	-	B6	-
C1	152.0705; 301.1195	C1	152.0710; 301.1177
C2	-	C2	150.0551
C3	-	C3	-
D1	152.0710; 301.1190	D1	152.0708; 301.1185
D2	152.0712; 301.1178	D2	152.0712; 301.1186
D3	152.0706; 301.1186	D3	152.0705; 301.1177
D4	152.0711	D4	152.0707; 301.1185
E1	152.0707; 301.1184	E1	152.0710; 301.1187
E2	152.0710; 301.1185	E2	152.0709; 301.1185
E3	152.0706	E3	152.0702
F1	152.0712	F1	152.0709
F2	152.0713	F2	152.0706
F3	152.0711	F3	152.0708

b) FIA data for the screening BMO kit with MDMA; best condition is shown in red.

Solvent 1		Solvent 2	
Condition	Positive mode <i>m/z</i>	Condition	Positive mode <i>m/z</i>
A1	194.1170; 196.1233	A1	194.1172; 196.1235
A2	179.0883; 180.0984; 182.1165; 194.1163; 196.1209	A2	194.1171; 196.1229
A3	194.1169; 196.1228	A3	194.117; 196.1229
A4	194.1170; 196.1234	A4	194.1170; 196.1232
A5	168.1019; 179.0892; 180.1005; 182.1175; 194.1175; 196.1228	A5	168.1015; 194.1169; 196.1230
A6	168.1010; 194.1169; 196.1195	A6	194.1169; 196.1231
B1	194.1171; 196.1229	B1	194.1170; 196.1231
B2	168.1012; 182.1166; 194.1169; 196.0967	B2	168.1011; 180.0980; 182.1168; 194.1169; 196.1214
B3	194.1171; 196.1194	B3	182.1170; 194.1168; 196.1226
B4	194.1170; 196.1230	B4	194.1167; 196.1227
B5	179.0911; 180.1035; 182.1188; 194.1192; 196.1218	B5	168.1018; 180.1018; 182.1181; 194.1177; 196.1209
B6	194.1169; 196.1107	B6	180.1013; 182.1161; 194.1168; 196.1219
C1	194.1170; 196.1233	C1	194.1171; 196.1230
C2	168.1018; 182.1179; 194.1175; 196.0983	C2	168.1013; 194.1168; 196.1205
C3	182.1188; 194.1170; 196.1220	C3	194.1169; 196.1225
D1	166.1075; 196.1171; 196.1233	D1	180.1011; 194.1164; 196.1106
D2	180.1015; 182.1172; 194.1170; 196.0987	D2	180.1011; 194.1160; 196.1209
D3	180.1022; 182.1185; 194.1181; 196.1240	D3	180.0994; 194.1151; 196.1210
D4	166.1065; 194.1170; 196.1234	D4	166.1064; 180.1007; 194.1165; 196.1224
E1	194.1167; 196.1228	E1	194.1171; 196.1238
E2	194.1167; 196.1228	E2	194.1168; 196.1227
E3	194.1167; 196.1229	E3	194.1166; 196.1225
F1	194.1169; 196.1229	F1	194.1182; 196.1241
F2	194.1169; 196.1228	F2	194.1185; 196.1246
F3	194.1170; 196.1233	F3	194.1181; 196.1243

c) FIA data for the screening BMO kit with METH; best condition is shown in red.

Solvent 1		Solvent 2	
Condition	Positive mode <i>m/z</i>	Condition	Positive mode <i>m/z</i>
A1	136.1119; 150.1277; 152.1346	A1	136.1125; 150.1277; 152. 1343; 166.1246
A2	136.1117; 150.1276; 152.1344	A2	136.1117; 150.1276; 152.1341; 166.1232
A3	150.1278; 152.1343	A3	136.1129; 150.1276; 152.1344; 166.1236
A4	136.1111; 150.1277; 152.1349	A4	136.1131; 150.1275; 152.1342
A5	136.112828; 150.1278; 152.1347	A5	136.1132; 150.1275; 152.1343; 166.1233
A6	150.1278; 152.1347	A6	136.1121; 150.1274; 152.1345; 166.1224
B1	136.1113; 150.1278; 152.1344	B1	136.1118; 150.1276; 152.1344
B2	150.1277; 152.1348; 166.1498	B2	136.1113; 150.1276; 152.1342; 166.1219
B3	150.1280; 152.1348; 166.1460	B3	136.1115; 150.1276; 152.1343
B4	136.1125; 150.1278; 152.1347	B4	136.1124; 150.1276; 152.1343
B5	150.1278; 152.1344; 166.1503	B5	136.1119; 150.1275; 152.1342
B6	166.1500; 150.1278; 152.1347	B6	136.1110; 150.1273; 152.1338
C1	136.1106; 150.1279; 152.1346	C1	136.1117; 150.1276; 152.1344
C2	136.1121; 150.1278; 152. 1344	C2	136.1123; 150.1274; 152.1345
C3	136.1138; 150.1278; 152.1346	C3	150.1274; 152.1341
D1	136.1124; 150.1278; 152.1346; 166.1217	D1	136.1119; 150.1275; 152.1343
D2	150.1278; 152.1344	D2	136.1120; 150.1275; 152.2478
D3	150.1277; 152.1345; 166.1234	D3	136.1121; 150.1275; 152.1340
D4	150.1278; 152.1347; 166.1240	D4	136.1111; 150.1276; 152.1345
E1	136.1126; 150.1274; 152.1346	E1	136.1121; 150.1272; 152.1338; 168.0211
E2	136.1116; 150.1275; 152.1340	E2	136.1121; 150.1273; 152.1338

E3	136.1128; 150.1274; 152.1350	E3	136.1118; 150.1273; 152.1333; 168.0207
F1	150.1275; 152.1338; 168.0197	F1	150.1274; 152.1338; 168.0202
F2	150.1276; 168.0197	F2	150.1274; 152.1347; 168.0201
F3	150.1274; 152. 1339; 168.0197	F3	150.1277; 168.0196

d) FIA data for the screening BMO kit with THC; best condition is shown in red.

Solvent 1 - METH		Solvent 2 - METH	
Condition	Positive mode <i>m/z</i>	Condition	Positive mode <i>m/z</i>
A1	-	A1	313.2156; 329.2099
A2	329.2117	A2	315.2314; 329.2126
A3	329.2113	A3	313.2165; 315.2316; 329.2119
A4	313.2150; 315.2310; 329.2111; 345.2044	A4	313.2140; 315.2290; 329.2095; 345.2052
A5	329.2092; 345.2046	A5	329.2109
A6	329.2111	A6	329.2129
B1	313.2165	B1	313.2147; 315.2290; 329.2092; 345.2043
B2	345.2037	B2	313.2167; 329.2116
B3	329.2078	B3	313.2158; 329.2108
B4	313.2167	B4	313.2170; 315.2328; 329.2122; 345.2053
B5	329.2091	B5	345.2049
B6	329.2085	B6	345.2038
C1	313.2150; 315.2321; 329.2123; 345.2049	C1	313.2133; 315.2286; 329.2094
C2	313.2171; 329.2123	C2	329.2091; 345.2046
C3	313.2178; 329.2138	C3	329.2115; 345.2055
D1	329.2108; 331.2247; 345.2059	D1	329.2092; 331.2237; 345.2036
D2	329.2141	D2	329.2119; 331.2254; 345.2060
D3	-	D3	329.2111; 345.2057
D4	313.2152; 329.2102; 331.2256; 345.2055	D4	313.2157; 329.2106; 331.2261; 345.2252
E1	313.2185; 315.2362; 329.2155; 345.2127	E1	313.2125; 315.2295; 329.2077; 345.2028
E2	313.2114	E2	313.2151; 315.2309; 329.2094
E3	313.2137; 315.2292	E3	313.2144; 315.2312; 329.2095
F1	315.2313; 329.2112	F1	315.2297; 329.2092; 345.2036
F2	313.2141; 315.2317; 329.2110	F2	315.2296; 329.2102
F3	315.2312; 329.2115	F3	315.2324; 329.2118; 345.2063

e) FIA data for the optimization BMO kit with APAP; best condition is shown in red.

Optimization kit	
Condition	Positive mode <i>m/z</i>
A1	110.0599; 150.0543; 301.1180
A2	150.0549; 301.1181
A3	150.0550; 301.1181
A4	150.0553; 301.1177
A5	110.0531; 150.0550; 301.1185
A6	150.0553; 301.1173
A7	150.0548; 301.1187
A8	150.0551; 301.1174
A9	150.0547; 301.1187
A10	150.0547; 301.1182
A11	150.0553; 301.1175
A12	150.0550; 301.1184

f) FIA data for the optimization BMO kit with MDMA; best condition is shown in red.

Optimization kit	
Condition	Positive mode <i>m/z</i>
A1	181.0132; 194.1170; 196.1227
A2	182.1168; 194.1190; 210.1125; 226.1090
A3	179.0887; 182.1172; 194.1194; 210.1121; 226.1081
A4	182.1171; 194.1192; 210.1115; 226.1072
A5	168.1023; 182.1182; 194.1192; 210.1121; 226.1094
A6	168.1017; 182.1175; 194.1193; 210.1118; 226.1079
A7	168.1009; 182.1172; 194.1192; 210.1111; 226.1077
A8	182.1184; 194.0965; 210.1124; 226.1084
A9	182.1166; 194.1193; 210.1123; 226.1087
A10	194.1191; 210.1135
A11	194.1191
A12	168.1028; 182.1181; 194.1195; 210.1123

g) FIA data for the optimization BMO kit with METH; best condition is shown in red.

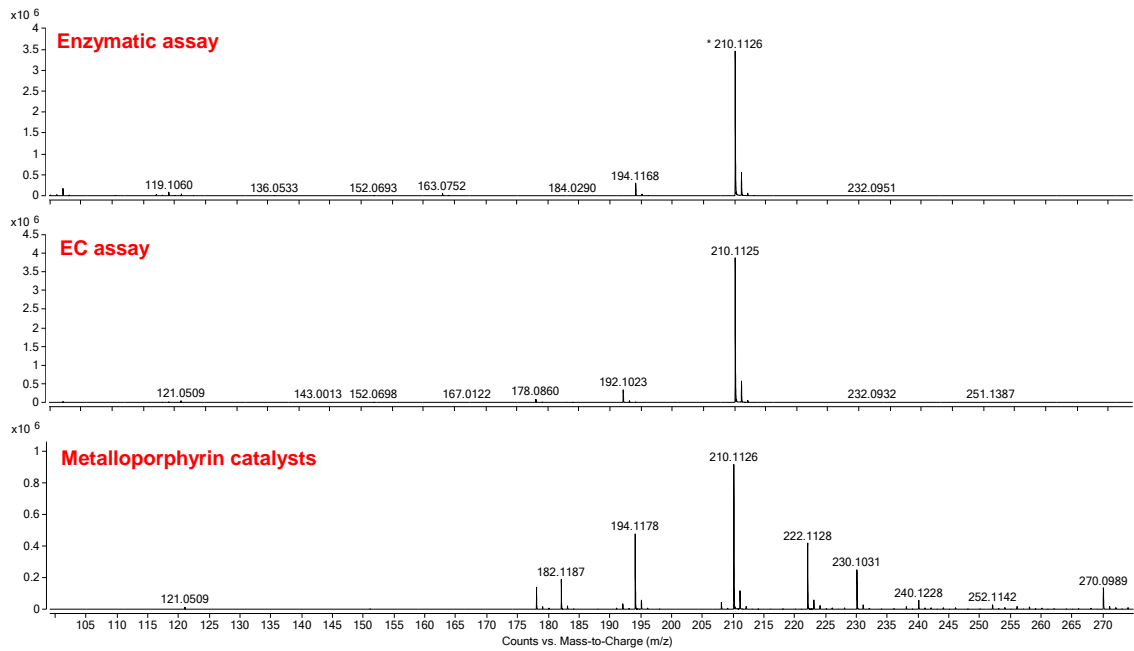
Optimization kit	
Condition	Positive mode <i>m/z</i>
A1	150.1284
A2	150.1276; 166.1252
A3	150.1278; 164.1072; 166.1222
A4	150.1277; 166.1220
A5	150.1278; 166.1230
A6	150.1278; 166.1212
A7	136.1105; 150.1278; 164.1065; 166.1220
A8	150.1277; 166.1245
A9	150.1280; 166.1232
A10	136.1137; 150.1278; 164.1057; 166.1221
A11	136.1118; 150.1278; 164.1064; 166.1219
A12	150.1278; 166.1226

h) FIA data for the optimization BMO kit with THC; best condition is shown in red.

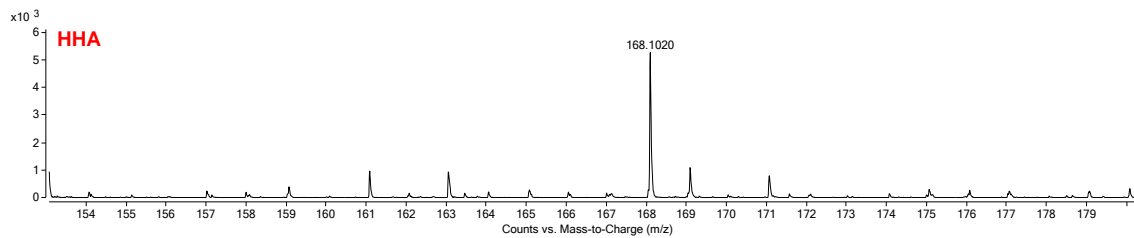
Optimization kit	
Condition	Positive mode <i>m/z</i>
A1	313.2175; 329.2109; 331.2261; 345.2067; 347.2213
A2	313.2166; 329.2112; 331.2268; 345.2067; 347.2219
A3	313.2160; 329.2107; 331.2267; 345.2062; 347.2209; 373.2377
A4	313.2166; 329.2103; 331.2261; 345.2055; 347.2215; 373.2375
A5	313.2168; 329.2109; 331.2260; 345.2064; 347.2211
A6	313.2169; 329.2113; 331.2265; 345.2074; 347.2218
A7	313.2173; 329.2104; 331.2283; 345.2062; 347.2214; 373.2357
A8	313.2164; 329.2101; 331.2254; 345.2066; 347.2211; 373.2344
A9	313.2167; 329.2100; 331.2265; 345.2065; 347.2211
A10	313.2166; 329.2106; 331.2263; 345.2070; 347.2210; 373.2271
A11	313.2158; 329.2114; 331.2270; 345.2061; 347.2211
A12	313.2159; 329.2104; 345.2067; 347.2212

Appendix 2. XIC data for the minor metabolites of MDMA, METH and THC generated with the three *in vitro* methods.

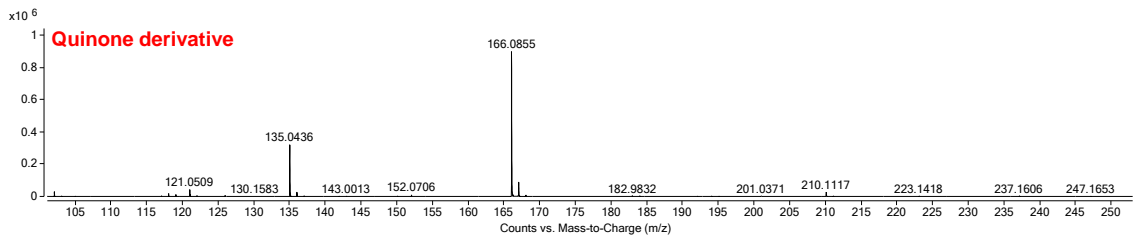
a) XIC spectra for HFA obtained with the three methods.



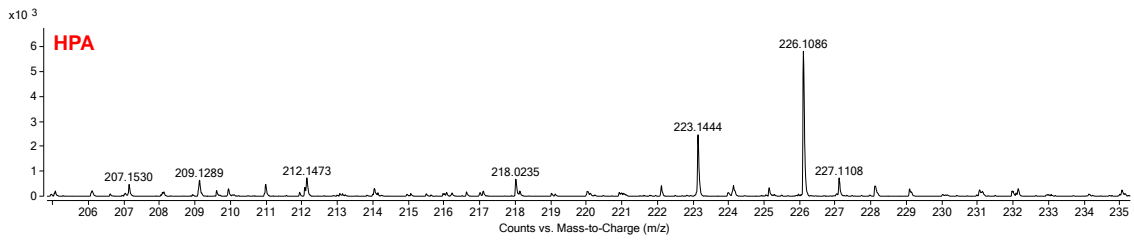
b) XIC spectra for HHA obtained with the HLM assay.



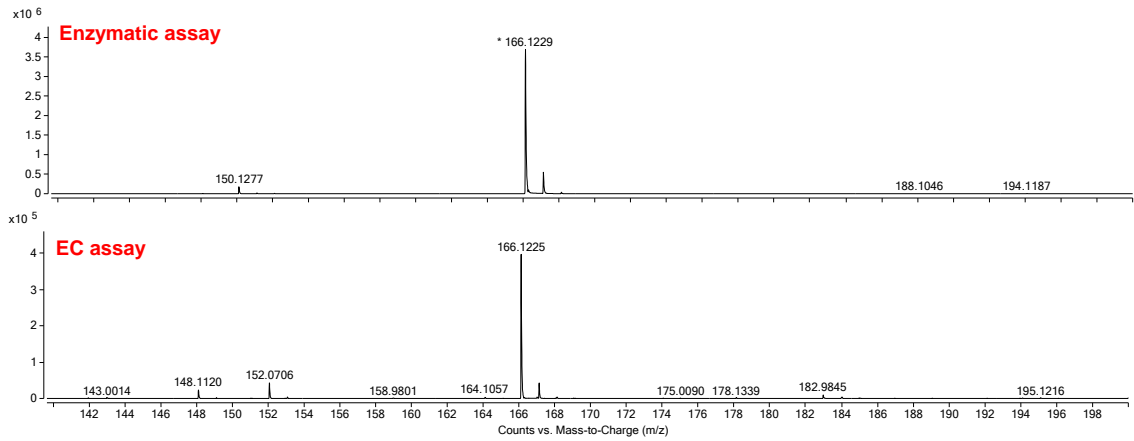
c) XIC spectra for the quinone derivative obtained with the EC assay.



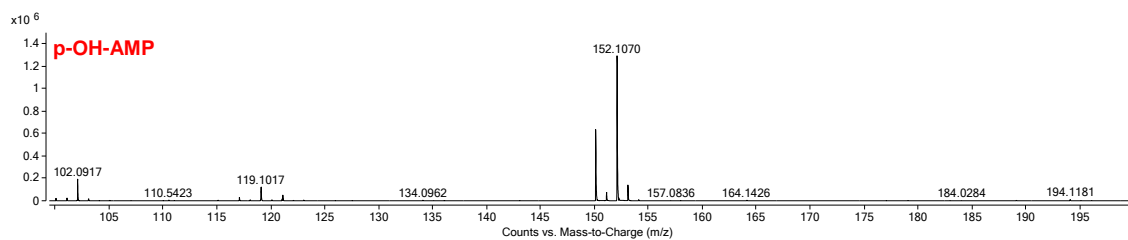
d) XIC spectra for HPA obtained with the synthetic metalloporphyrin catalysts.



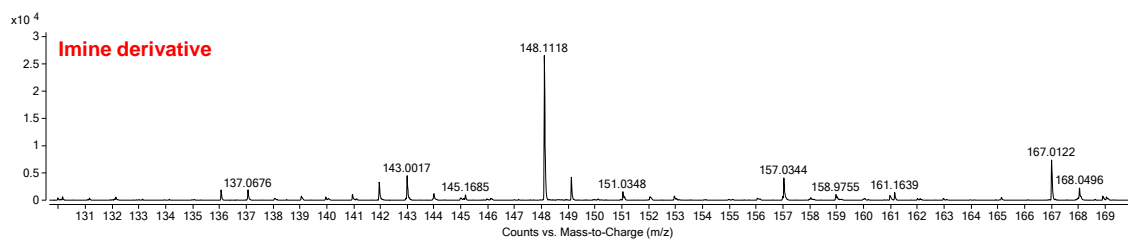
e) XIC spectra for N-OH-METH obtained with the HLM assay and EC assay.



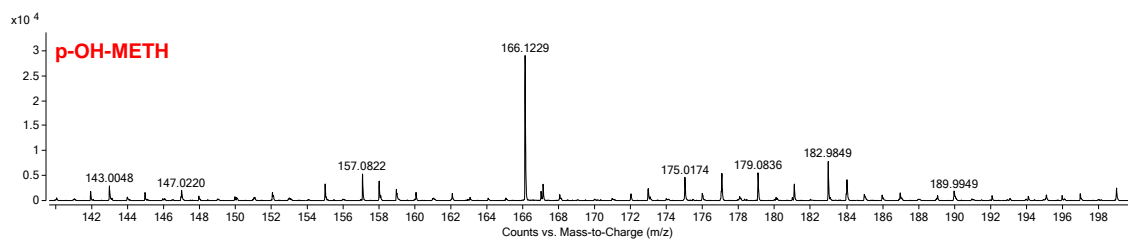
f) XIC spectra for N-OH-AMP obtained with the *in vitro* enzymatic assay.



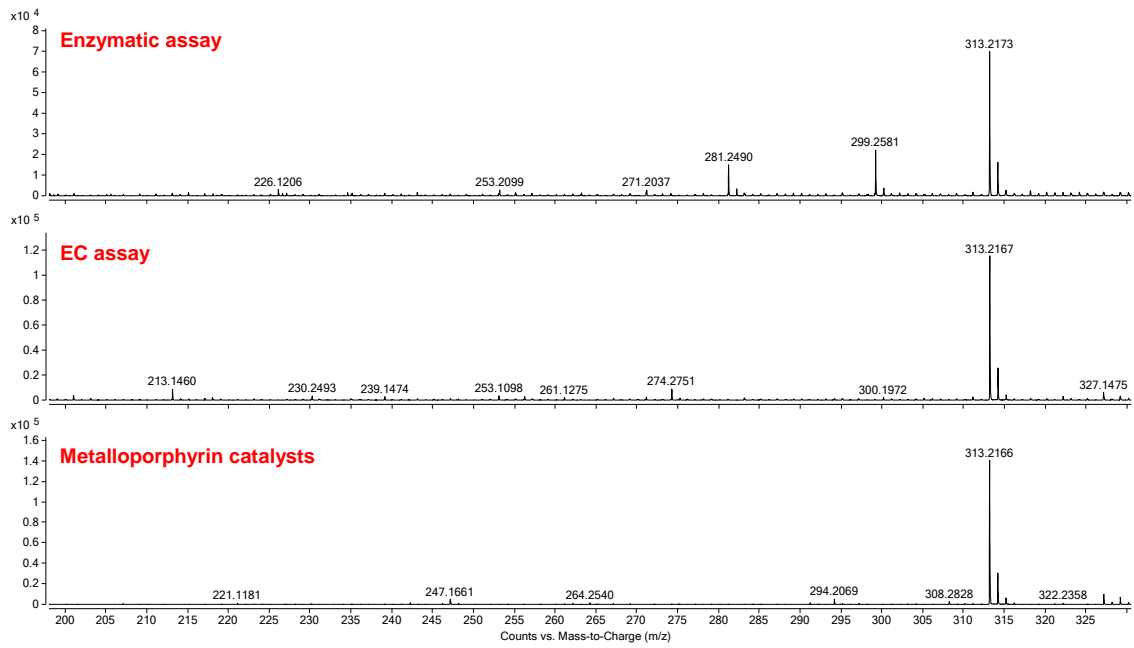
g) XIC spectra for the imine derivative obtained with the EC assay.



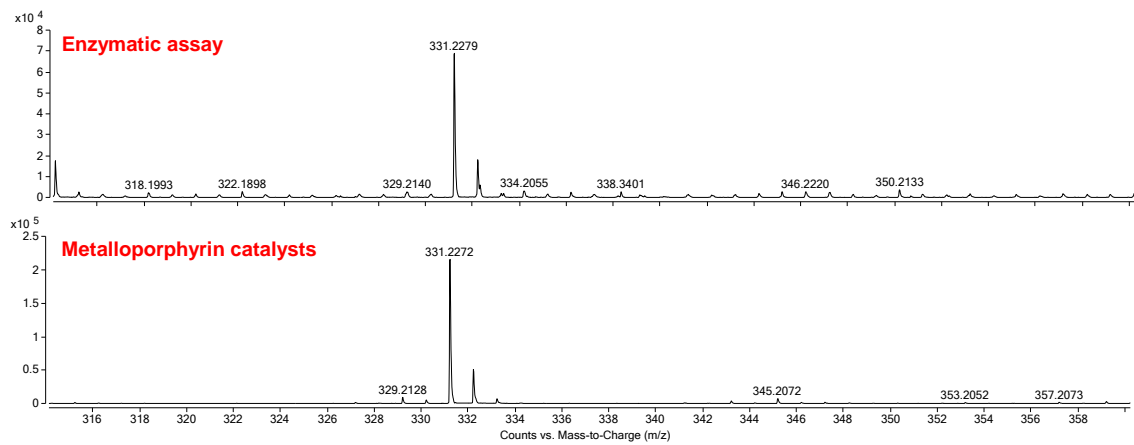
h) XIC spectra for p-OH-METH obtained with the synthetic metalloporphyrin catalysts.



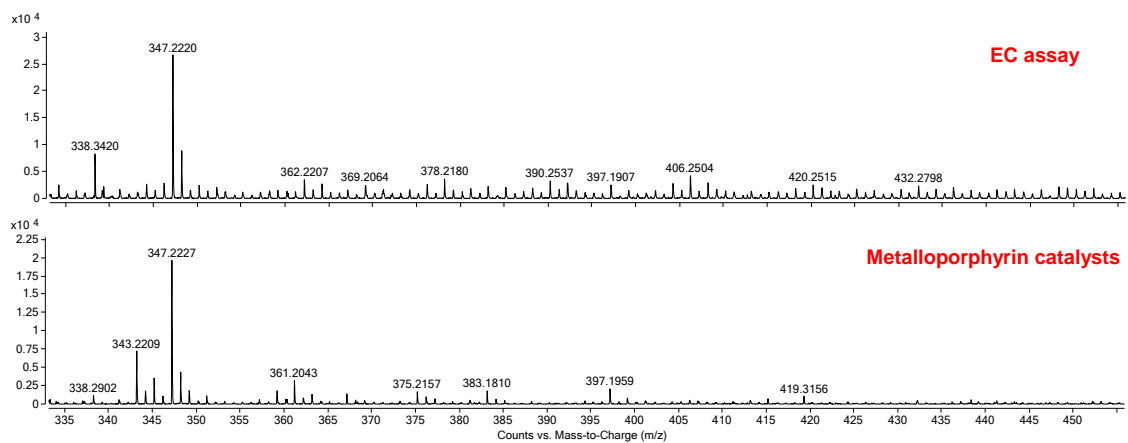
i) XIC spectra for methylidene-THC obtained with the three methods.



j) XIC spectra for 11-OH-THC obtained with the HLM assay and synthetic metalloporphyrin catalysts.

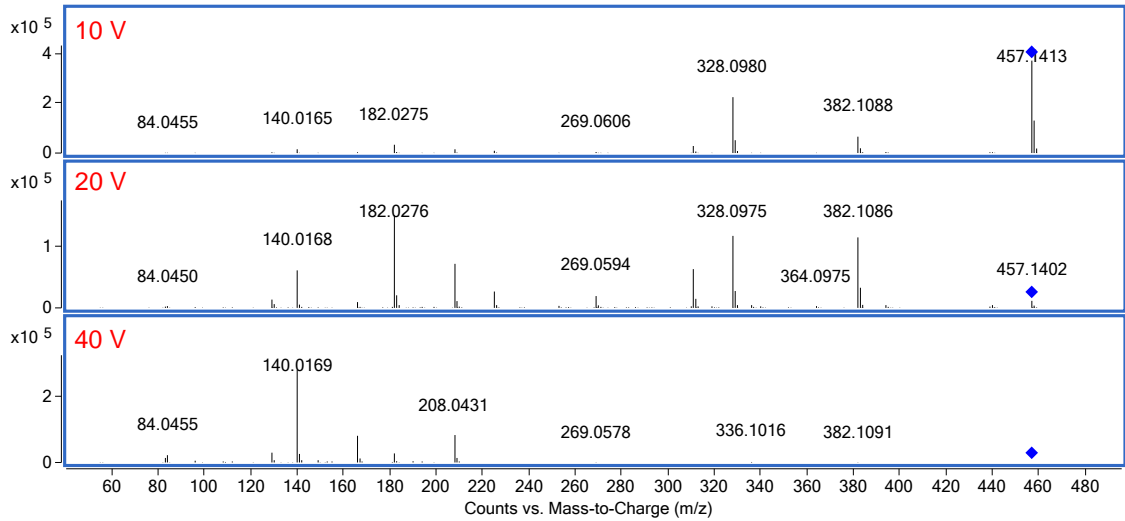


k) XIC spectra for dihydroxy-THC obtained with the synthetic metalloporphyrin catalysts and EC assay.

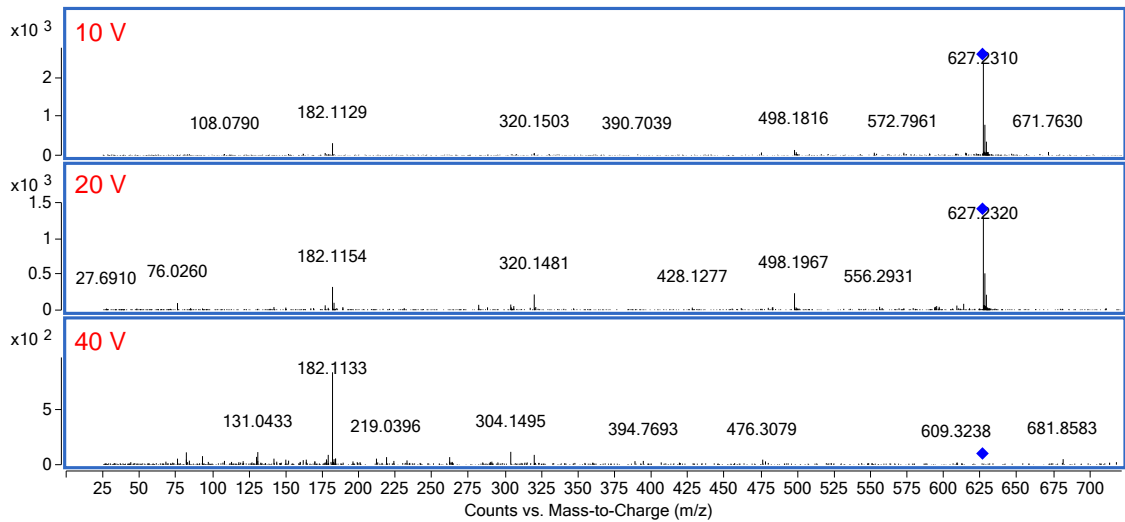


Appendix 3: MS/MS data for the found GSH adducts with the CID shown at 10 eV (top), 20 eV (middle), and 40 eV (bottom) for each drug.

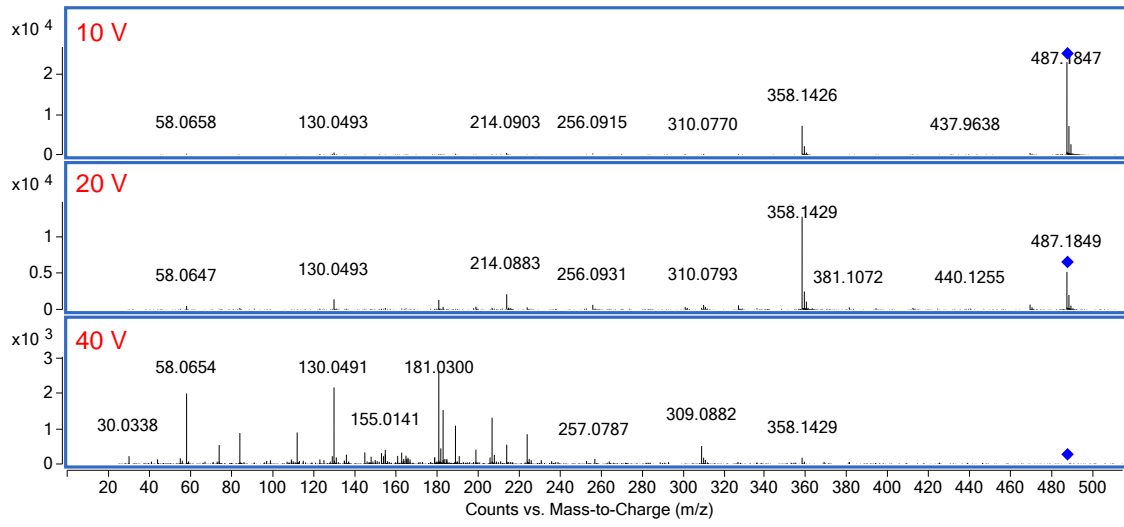
a) MS/MS data for the GSH adduct found with APAP.



b) MS/MS data for the GSH adduct found with COC.



c) MS/MS data for the GSH adduct found with MDMA.



Appendix 4: Summary of Optimizer experimental conditions found for the detected adducts with the EC assay.

Adduct	Precursor Ion	Product Ion	Fragmentor	CE	Abundance
Peptide + APAP - H	785.9	110.1	205	68	14161
Peptide + APAP - H	785.9	807.4	205	68	7645
Peptide + 1,4-Benzoquinone - H	764.3	120.1	192	60	771
Peptide + 1,4-Benzoquinone - H	764.3	789.4	192	60	72
Peptide + HHA + H + CH ₂	801.9	721.8	99	12	107
Peptide + HHA + H + CH ₂	801.9	330.0	99	8	69
Peptide + 11-CHO-THC - H + OH	588.6	573.3	129	8	247
Peptide + 11-CHO-THC - H + OH	588.6	866.4	129	12	53

VITA

LUDMYLA SANTOS TAVARES

- 2010-2014 B.S., Industrial Chemistry
Federal University of Goiás
Goiânia, Goiás, Brazil
- 2013-2014 Study Abroad
University of East Anglia
Norwich, Norfolk. U.K.
- 2015-2017 M.S., Chemistry
Federal University of Goiás
Advisor: Andréa Rodrigues Chaves
Goiânia, Goiás, Brazil
- 2017-2020 M.S., Forensic Science
Florida International University
Advisor: Anthony DeCaprio
Miami, Florida, U.S.
- 2020-2022 Doctoral Candidate
Florida International University
Advisor: Anthony DeCaprio
Miami, Florida, U.S.
- 2020-2022 National Institute of Justice Graduate Fellow
Florida International University
Miami, Florida, U.S.
- 2021 Winner of the Leo dal Cortivo Best Poster Award
2021 SOFT annual meeting
Nashville, Tennessee, U.S.

PUBLICATIONS AND PRESENTATIONS

Tavares, L. S., Vaz, B. G. (December, 2016). *New developments in paper spray mass spectrometry*. Oral presentation given at the 6th BrMASS Conference on Mass spectrometry, Rio de Janeiro, Rio de Janeiro, Brazil.

Gasparotto, G., Tavares, L. S., Silva, T.C., Maia, L.J.Q., Carvalho, J.F. (2018). *Structural and spectroscopic properties of Eu³⁺ doped Y₄A₁₂O₉ compounds through a soft chemical process*. Journal of Luminescence, 204: 513–519.

Tavares, L. S., Carvalho, T. C., Romão, W., Vaz, B. G., Chaves, A. R. (2018). *Paper Spray Tandem Mass Spectrometry Based on Molecularly Imprinted Polymer Substrate for Cocaine Analysis in Oral Fluid*. Journal of The American Society for Mass Spectrometry, 29: 566-572.

Tavares, L. S., Bernardo, R. A., de Oliveira, A. E., Vaz, B. G., Chaves, A. R. (2021). *Novel Method for the Extraction of Cocaine from Oral Fluid by Means of Disposable Pipette Modified with Restricted Access*. Journal of the Brazilian Chemical Society, 32 (12): 2235-2244.

Tavares, L. S., DeCaprio, A. P., (September, 2021). *Comparison of In vitro Systems for the Generation of Drug Metabolites in Forensic Toxicology*. Poster presented at the 2021 annual meeting of the Society of Forensic Toxicologists, Nashville, TN.

Tavares, L. S., DeCaprio, A. P., (March, 2022). *In vitro Generation of Reactive Drug Metabolites and Trapping by a Thiol-Containing Hemoglobin Peptide*. Poster presented at the Society of Toxicology 61st Annual Meeting and ToxExpo, San Diego, CA.

Tavares, L. S., DeCaprio, A. P., (October, 2022). *In vitro Systems for the Generation of Drug Metabolites*. Invited oral presentation given at the 2022 SOFT Young Forensic Toxicologists Symposium, Cleveland, OH.

Tavares, L. S., DeCaprio, A. P., (November, 2022). *Generation and Trapping of Reactive Drug Metabolites by a Thiol-Containing Hemoglobin Peptide*. Poster presented at the 2022 Annual Meeting of the Society of Forensic Toxicologists, Cleveland, OH.

Tavares, L. S., Dares, C. J., DeCaprio, A. P. *Comparison of In Vitro Systems for the Identification of Abused Drug Metabolites*, Drug Testing and Analysis (final draft).

Tavares, L. S., DeCaprio, A. P. *In vitro Generation of Reactive Drug Metabolites and Trapping by Thiol-Containing Peptides*, Xenobiotica (in preparation).

Tavares, L. S., DeCaprio, A. P., (March, 2023). *In vitro Systems for the Generation of Drug Metabolites and Trapping by a Thiol-Containing Hemoglobin Peptide*. Invited oral presentation to be given at the 2023 Pittcon Conference and Exposition, Philadelphia, PA.